2016

Study of Electron Transfer through the Reductase Domain of Neuronal Nitric Oxide Synthase and Development of Bacterial Nitric Oxide Synthase Inhibitors

Yue Dai

STUDY OF ELECTRON TRANSFER THROUGH THE REDUCTASE DOMAIN OF NEURONAL NITRIC OXIDE SYNTHASE AND DEVELOPMENT OF BACTERIAL NITRIC OXIDE SYNTHASE INHIBITORS

YUE DAI

Bachelor of Science in Chemistry

Wuhan University

June 2008

submitted in partial fulfillment of requirements for the degree

DOCTOR OF PHILOSOPHY IN CLINICAL AND BIOANALYTICAL CHEMISTRY

at the

CLEVELAND STATE UNIVERSITY

July 2016

We hereby approve this dissertation

for

Yue Dai

Candidate for the Doctor of Philosophy in Clinical-Bioanalytical Chemistry Degree

for the

Department of Chemistry

and

CLEVELAND STATE UNIVERSITY'S

College of Graduate Studies by

Dennis J. Stuehr. PhD.

Department of Pathobiology, Cleveland Clinic / July 8th 2016

Mekki Bayachou. PhD.

Department of Chemistry / July 8th 2016

Thomas M. McIntyre. PhD.

Department of Cellular and Molecular Medicine, Cleveland Clinic / July 8th 2016

Bin Su. PhD.

Department of Chemistry / July 8th 2016

Jun Qin. PhD.

Department of Molecular Cardiology, Cleveland Clinic / July 8th 2016

Student's Date of Defense: July 8th 2016

ACKNOWLEDGEMENT

First I would like to express my special appreciation and thanks to my Ph. D. mentor, Dr. Dennis Stuehr. You have been a tremendous mentor for me. It is your constant patience, encouraging and support that guided me on the road of becoming a research scientist. Your advices on both research and life have been priceless for me. I would like to thank my committee members - Professor Mekki Bayachou, Professor Bin Su, Dr. Thomas McIntyre, Dr. Jun Qin and my previous committee members - Dr. Donald Jacobsen and Dr. Saurav Misra for sharing brilliant comments and suggestions with me. I would like to thank all our lab members for their help ever since I joint our lab. I also would like to thank our Chemistry Department and College of Science for the course works and administrative matters.

Special thanks to my family. Words cannot express how grateful I am. At the end I would like to express appreciation to my beloved fiancée Yufan Zheng who spent many difficult days with me and who is always my support.

STUDY OF ELECTRON TRANSFER THROUGH THE REDUCTASE DOMAIN OF NEURONAL NITRIC OXIDE SYNTHASE AND DEVELOPMENT OF BACTERIAL NITRIC OXIDE SYNTHASE INHIBITORS

YUE DAI

ABSTRACT

Crystal structure of neuronal Nitric Oxide Synthase reductase (nNOSr) implies that large-scale domain motion is essential for electron transfer. However, the details are not well understood. To address this, we generated a functioning "Cys-lite" version of nNOSr and then replaced the nNOSr Glu^{816} and Arg^{1229} residues with Cys in the FMN and FAD domains (CL5SS) in order to allow cross-domain disulfide bond formation under pH 9 or to cross-linking using bis-maleimides. Cross-linked CL5SS exhibited a ≥95% decrease in cytochrome *c* reductase activity and reduction of the disulfide bond restored the activities. The results demonstrate that a conformational equilibrium involving FMN domains motion is essential for the electron transfer. A graded lengthening of the bis-maleimide cross-linkers was associated with an increase in activity, thus helping to define the distance constraints for domain opening. Stopped-flow kinetic

studies showed cross-linking did not negatively affect the hydride transfer and inter-flavin electron but severally impaired the electron efflux from the FMN domain to its redox partner. How these findings impact our understanding of the nNOS catalytic cycle and details are discussed.

Staphylococcus aureus nitric oxide synthase (saNOS) helps *S. aureus* to maintain its antibiotics resistance, making saNOS a drug target. However, *in vitro* determination of saNOS inhibitor potency by activity assay is challenging because saNOS lacks an attached reductase. Herein, we employ the following approaches to optimize the *in vitro* assessment of NO synthesis by saNOS (1) *B. subtillis* flavodoxin YkuN and *B. subtillis* flavodoxin reductase FLDR were adopted as reductase partners for saNOS; (2) PEGylated-oxyhemoglobin was used for the direct capture of NO; (3) a 96-well plate format was used to increase the assay throughput. Our results showed that PEGylation of oxyHb minimizes the futile redox cycling within the flavoprotein and ensured effective electron transfer from produced NO to oxyHb. Nitric oxide produced by saNOS and cell cytosol was successfully detected by our assays. We also tested the inhibitory potency of six compounds derived from trimethoprim. They were confirmed to be H_4F competitor with IC50 varying from 1 μM to 1 mM. The most potent inhibitor UCP111F26M is very specific to saNOS. Details of this inhibitor are discussed.

TABLE OF CONTENTS

LIST OF TABLES

LIST OF FIGURES

NOMENCLATURE

Abbreviation	Expansion
4-amino-H4B	4-Amino-(6R)-5,6,7,8-tetrahydro-L-biopterin dihydrochloride
7-NI	7-Nitroindazole
Ab	Amyloid b-peptide
ACR	Acriflavine
AI	Autoinhibitory insert
Akt	Protine Kinase B
BM	Bis-maleimide
bNOS	Bacterial nitric oxide synthase
bsNOS	*Bacillus subtilis* nitric oxide synthase
CaM	Calmodulin
CAPON	Carboxy-terminal PDZ ligand of nNOS
cGMP	Cyclic guanosine monophosphate
ChDHFR	Cryptosporidium hominis DHFR
CL5	Cys-lite nNOSr

CL5SS	Cys-lite nNOSr E816C R1229C
CMS	Chronic mild stress
CPYOR	Cytochrome P450 reductase
CT	C-terminal tail of nitric oxide synthase
DAF-2	Diaminofluoroscein-2
dALA	d-Aminolevulinic acid
DAN	2,3-Diaminonaphthalene
deoxyHb	Deoxyhemoglobin
DETA-NA	Diethylenetriamine-nitric oxide adduct
DG	Dentate gyrus
DHFR	Dihydrofolate reductase
drNOS	*Deinococcus radiodurans* nitric oxide synthase
DTT	Dithoreitol
EGF	Epidermal growth factor
eNOS	Endothelial nitric oxide synthase
ERF	Endothelium relaxing factor
FAD	Flavin adenine dinucleotide

FLDR	*E. coli* flavodoxins NADP+ oxidoreductase
FMN	Flavin mono nucleotide
FNR	Ferredoxin $NADP^+$ reductase domain
GTP	Guanosine triphosphate
H_4B	(6R)-5,6,7,8-Tetrahydrobiopterin
H_4F	Tetrahydrofolate
HBOC	Hemoglobin (Hb) based O_2 carrier
Heme	Iron protoporphyrin IX
IFN- γ	Interferon-γ
IM	Imipramine
iNOS	Inducible nitric oxide synthase
IPTG	Isopropyl-b-D-thiogalactopyranoside
L-Arg	L-arginine
LB	Lysogeny broth
L-NAME	N^{ω}-nitro-L-arginine methyl ester
LPS	Lipopolysaccharide
MDD	Major Depressive disorder

metHb	Methemoglobin
metHb-PEG	PEGylated methemoglobin
MP4	Methoxypolyethylene glycol 5000 conjugated hemoglobin
MPTP	1-Methyl-4-phenyl-1,2,3,6-tetrahydropyridine
NADPH	Nicotinamide adenine dinucleotide phosphate
NEM	N-Ethylmaleimide
NMDA	N-Methyl-D-aspartate receptor
nNOS	Neuronal nitric oxide synthase
NO	Nitric oxide
NOHA	N^{ω}-hydroxy-L-arginine
NOS	Nitric oxide synthase
NOSoxy	Oxygenase domain of nitric oxide synthase
NOSr	Reductase domain of nitric oxide synthase
OB	Olfactory bulb
oxyHb	Oxyhemoglobin
oxyHb-PEG	PEGylated oxyhemoglobin
pABA	Glutamyl p-amino benzoic acid side chain

PD	Parkinson's disease
PDB	Protein Data Bank
PDZ domain	Post synaptic density protein, Drosophila disc large tumor suppressor and zonula occludens-1 protein similar domain
PEG	Polyethylene glycol
PMSF	Phenylmethanesulfonylfluoride
PSD 93	Post-synaptic density protein 93
PSD 95	Post-synaptic density protein 95
PYR	Pyrimethamine
RBC	Red blood cell
RMS	Rostal migratory stream
RNS	Reactive nitrogen species
saNOS	*Staphylococcal aureus* nitric oxide synthase
SAP90	Synapse associated protein 90
scNOS	Sorangium cellulosum nitric oxide synthase
SFD	*Staphylococcal* foodborne diseases
sGC	Soluble guanylyl cyclases

stNOS	*Streptomyces turgidiscabies* nitric oxide synthase
SVZ	Subventricular zone
TB	Terrific Broth
TMP	Trimethoprim
TrpRS II	Tryptophanyl tRNA synthetase protein II
YkuN	*B. subtilis* flavodoxins YkuN

CHAPTER I

GENERAL INTRODUCTION

1.1 Nitric oxide

Nitric oxide (NO) is a colorless gaseous molecule under standard condition and has been long known as air pollutant[1, 2]. Surprisingly, in mid-1980s, studies showed this short-lived simple inorganic molecule could be endogenously produced and could act as an endothelium relaxing factor (ERF), a cytotoxic agent triggering immune response and a signaling molecule[2-10]. By that time the concept that an inorganic gas, which penetrates membranes and regulates the function of other cells in human organism was entirely new. This discovery was rewarded Nobel Prize for physiology and medicine in 1998 and that was just the beginning of the story about NO.

With several decades' study of NO's physiological roles, now we know that NO is a signaling molecule activating soluble guanylyl cyclase (sGC), which is the primary

NO receptor, by binding to its heme moiety[11-13]. The binding between sGC and NO induces the production of the second messenger cyclic guanosine monophosphate (cGMP) from guanosine triphosphate (GTP) and triggers downstream signaling cascades [11, 13, 14]. Besides being a signaling molecule, NO is also capable of post-translationally modifying proteins, DNA and lipids[4, 6, 15-17]. Although NO is an important biological molecule, NO accumulation in cells rises the risk of reactive nitrogen species (RNS) production and nitrosative stress, which is a pathological condition causing detrimental effects to host cell including apoptosis, proliferation, mutagenesis and invasiveness[2, 7, 15]. So the NO detoxification by reducing or antioxidant chemicals in cell is essential for the cell homeostasis[17].

1.2 Nitric Oxide Synthase (NOS)

Although NO can be produced by cellular respiration, the majority of NO in cell is produced by an enzyme called nitric oxide synthase (NOS)[3, 18]. NOS coverts L-arginine (L-Arg) into L-citrulline and NO in a NADPH and (6R)-5,6,7,8-tetrahydrobiopterin (H_4B) dependent manner via the intermediate N^{ω}-hydroxy-L-arginine (NOHA)[3, 18, 19]. Three NOS isoforms have been identified in animals[18]. Neuronal nitric oxide synthase (nNOS, NOS type I or NOS-I) is constitutively expressed in neurons and produces nM level of NO as signaling molecule in the nervous system[20]. Inducible nitric oxide synthase (iNOS, NOS type II or NOS-II) is expressed primarily in macrophages upon pathogen recognition and produces μM level of NO as part of immune response[21]. Endothelial nitric oxide synthase (eNOS, NOS type III or NOS-III) is

generally expressed in endothelial cells constitutively producing μM level NO for endothelial cell relaxation[22, 23]. The genes of these three different isoforms are located on different chromosomes and they share a 51-57% amino acid homology[24]. Although they differ in expression levels and catalytic activities, these three NOS isoforms share general structural features and catalytic mechanism[18, 24].

1.3 Structure of NOS

NOSs are multidomain metalloenzymes[25, 26]. NOS is usually referred to homodimer but in fact the active form of NOS is a tetramer consisted of two NOS monomers and two calmodulin (CaM) monomers[26]. The active form of NOS also binds a series of cofactors including nicotinamide adenine dinuleotide phosphate (NADPH/ $NADP^+$), flavin adenine dinucleotide (FAD), flavin mono nucleotide (FMN), H_4B and iron protoporphyrin IX (heme) [26]. An NOS molecule contains an N-terminal oxygenase domain (NOSoxy) and a C-terminal reductase domain (NOSr) [26]. They are covalently linked by a peptide hinge, which contains a CaM/Ca^{2+} binding sequence[26, 27]. The NOSoxy domain contains binding sites for heme, H_4B and L-Arg[26]. The reductase domain contains binding sites for NADPH, FAD and FMN[3, 26]. The separate domains are catalytically active and has been successfully over-expressed and purified in a variety of expression systems for structural and functional studies[28, 29].

Comparison of oxygenase domain of different isoforms shows that they have almost identical catalytic sites except for the L-Arg binding site (Asp in iNOS and Asn in eNOS)[3]. Generally, the NOSoxy is a heme protein with the heme iron axially

coordinated to a proximal Cys [30-32]. This pentacoordination pattern of heme allows the heme iron to axially coordinate an oxygen molecule [30-32]. The heme is buried interiorly in the NOSoxy and anchored stably by van der Waals interaction with surrounding hydrophobic residues [30-32]. The porphyrin ring in heme is also sandwiched by a Trp and a Phe by stacking interaction [30-32]. Dimerization of NOSoxy generates a cavity close to the dimer interface allowing diffusion of L-Arg and citrulline [30-32]. The L-Arg binding site locates in the narrow part of the cavity [30-32]. Such structure features make the guanidino group of L-Arg lay coplanar with heme and also forms hydrogen bonds with surrounding residues [30-32]. NOHA binds the same way as L-Arg with NOS [33]. The binding cavity of H_4B is also located close to the dimer interface [30-32]. The H_4B interacts with NOSoxy primarily through stacking interaction between the pterin ring and a surrounding Trp residue[30]. Hydrogen bonding networks between H_4B side chains and the N-terminal hook also helps to anchor H_4B on its binding site[30, 34]. Interestingly, a zinc finger has also been identified on the bottom of the dimer interface and it is generally believed to be important for the NOS dimer stability[30].

NOSr belongs to the dual-flavin reductase family and consisted of a covalently attached FMN binding domain, a FAD binding domain and a NADPH binding domain [35]. The FAD binding domain and NADPH binding domain together function as a ferredoxin-$NADP^+$ reductase (FNR) module and FMN module functions as ferredoxin [35]. These domains are part of the electron transfer chain during NOS catalysis and the details about electron transfer though NOSr are discussed in chapter II.

1.4 NOS Catalysis

NOS is a unique enzyme that has attracted tremendous interest over decades due to its high biological importance and chemical complexity. It uses flavins as electron transfer component and heme as catalytic center, which distinguishes NOS from most of other heme proteins[36]. The structural components of NOS co-operate to make NO biosynthesis efficient and allow NOS to be specifically regulated by multiple regulatory factors[35]. The intricate structure-function relationship of NOS is still one center topics of NOS research.

The biosynthesis of NO by NOS has been studied extensively and the general scheme of NO production by NOS is shown in Fig. 1[35]. Briefly, oxygen first oxidizes the guanidine nitrogen on L-Arg, producing the stable intermediate NOHA that then oxidizes NOHA, producing NO and L-citruline under the catalysis by NOS. Although the scheme in Fig 1 looks straight forward, the stepwise electron transfer on heme center of NOS is very complex (Fig. 2)[37]. NADPH first binds to NOS reductase domain and transfer one electron to NOSr as hydride[37]. This electron is then transferred to the ferric heme center in NOS oxygenase domain and reduces the ferric heme to ferrous heme[37]. This allows oxygen to bind the ferrous iron center on heme to form a superoxy species (species I) [37]. Species I is not reactive toward L-Arg but it can receive another electron from H_4B or NOSr (in absence of H_4B) to form an intermediate heme-peroxo species (species II)[37]. Species II can be further protonated and converted to a reactive iron-oxo species (species III)[37]. Species III is capable of hydroxylating L-Arg into NOHA or hydroxylating NOHA into citrulline and NO[37]. The produced NO is initially

bounded to the ferric heme center and released afterwards[37]. In the overall biosynthesis of NO, the reduction of ferric heme into ferrous heme is the slowest step[37]. The H_4B radical formed after H_4B provide an electron to the heme center is recycled by downstream reaction[37]. The electron must be transferred to NOSoxy at precise time and rate to achieve optimal NO synthesis and to minimize the reactive oxygen species formation[37]. Details about the reactivity of these related species have been discussed [38].

Besides NO production, the NO release from heme-NO complex also limits the NOS catalysis[37]. In one hand, the produced NO needs to get off the heme binding site so the heme can bind another oxygen molecule to start another round of catalysis[37]. In the other hand, the heme-NO complex can be oxidized and ultimately resulting in nitrate formation without NO release[37]. The cycle that releases the NO is referred to as "productive cycle" and the cycle in which the heme-NO complex is reduced into nitrite without free NO production is referred to as the "futile cycle"[37]. The heme-NO complex can also be reduced by NOSr and forms a ferrous-NO complex[37], which releases NO at a very slow rate[37]. These processes together create a global mechanism for NOS catalysis (Fig 3) and give a general idea about how both NO production and NO release affect NOS biosynthesis [37].

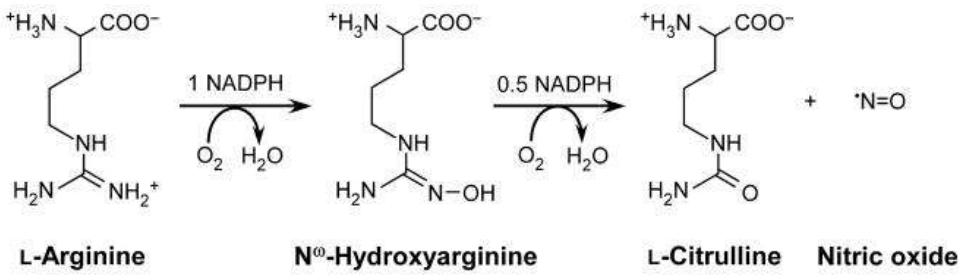

Fig. 1. **Scheme of NO production catalyzed by NOS from L-Arg**

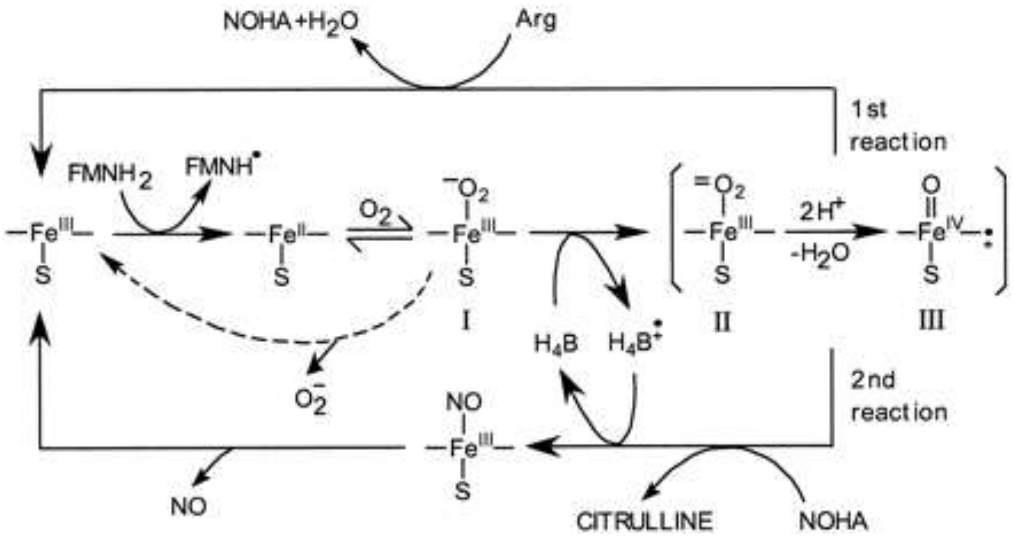

Fig. 2. **L-Arg and NOHA oxidation on the heme center of NOSoxy**. The ferric heme receives an electron from NOSr and is reduced to ferrous heme. The ferrous heme binds oxygen and forms a superoxy species I. Species I receives another electron to form intermediate heme-peroxo species II, which can be further convert to iron-oxo species III. Species III is capable of hydroxylating both L-Arg and NOHA.

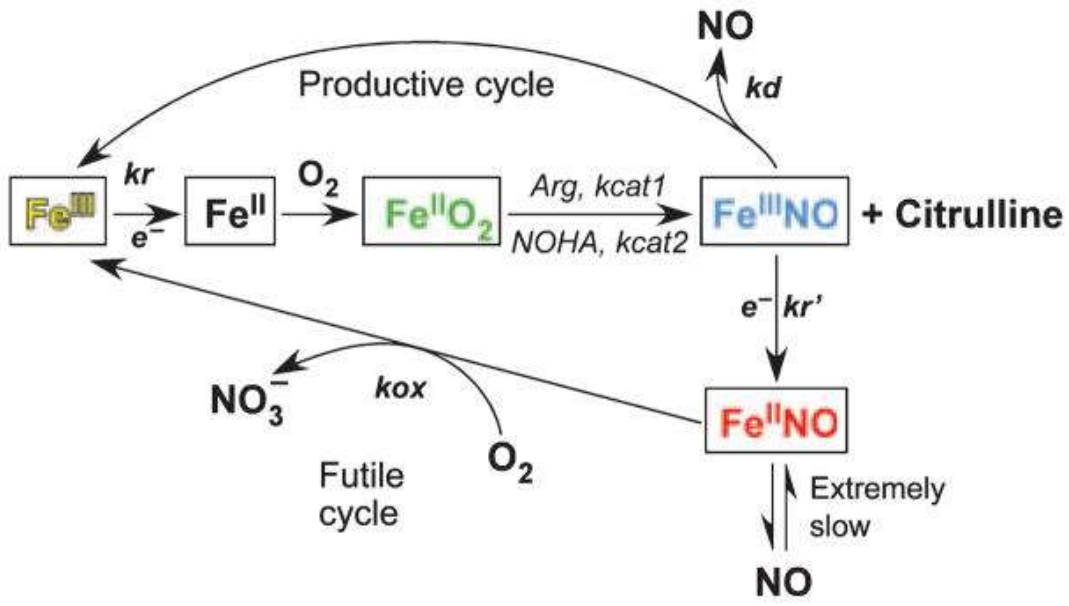

Fig. 3. **Global model of NO biosynthesis.** The heme reduction rate (k_r) is the rate-limiting step of the NO biosynthesis by NOS. The k_{cat1} and k_{cat2} represent the conversion rates of $Fe^{II}O_2$ species to $Fe^{III}NO$ species. The $Fe^{III}NO$ species can either release NO with a rate k_d or be reduced into $Fe^{II}NO$ species with a rate k_r'. The $Fe^{II}NO$ species can be oxidized by O_2 and convert back to the ferric heme with a rate k_{ox}.

1.5 nNOS Physiology

nNOS, which can be expressed in immature and mature neurons, is responsible for majority NO production in nervous system and exists in both particulate and soluble forms [20]. However, studies show nNOS can also be expressed in rat cardiac myocytes and rat brain blood vessels[39]. nNOS is either bond to plasma membrane directly or indirectly anchored to the plasma membrane by adapter proteins to exert its function[20]. Adaptor proteins including post-synaptic density protein 93 (PSD93), post-synaptic density protein 95 (PSD95), synapse associated protein 90 (SAP90) and CAPON (carboxy-terminal PDZ ligand of nNOS) also help to delivery nNOS to its discrete site[20]. Interestingly, many studies indicated that the PDZ domain of nNOS can interact with a variety of proteins which also contain a PDZ domain and these interactions play a regulatory role in nNOS distribution in cells and nNOS activity[20].

Function of nNOS-derived NO is concentration dependent. It is a physiological neuromodulator mediating synaptic plasticity at low concentrations (nM), but a neurotoxic factor at higher concentrations (μM)[20]. NO produced by nNOS involves in a variety of physiological and pathological conditions and several selected nNOS related conditions are listed below.

1.5.1 Neurogenesis

Two major observations support the hypothesis that nNOS is related with neurogenesis. First, subventricular zone (SVZ, a neurogenesis site) is surrounded by

neurons, which contain nNOS[40, 41]. Second, neuronal precursors in dentate gyrus (DG, another neurogenesis site) are capable of expressing nNOS [42]. Several studies have been done trying to reveal the function of nNOS in neurogenesis. The majority of publications in last ten years suggest an inhibitory role of nNOS in neurogenesis, but excitatory effects are also been reported[20].

Previous studies imply that NO is related with neuronal tissue formation processes and has antiporoliferative effects by inhibiting the epidermal growth factor (EGF) receptor [20]. Studies show that NOS inhibitor N^{ω}-nitro-L-arginine methyl ester (L-NAME) increases the percentage of BrdU-immunoreactive cells, which is an indication of cell proliferation, cultured in vitro in presence of EGF and NO donor diethylenetriamine-nitric oxide adduct (DETA-NA) leads to a decrease in cell proliferation in mouse SVZ cultured in vitro [43]. Mouse model studies show NOS inhibition by 7-nitroindazole (7-NI) or nNOS gene knockout is capable of raising the number of mitotic cells in SVZ and the olfactory bulb (OB, an olfactory related neural structure). It also increases the number of progenitor cells in DG[44]. Moreover, it has been showed that in mice model the number of cells generated in DG and olfactory subependyma can be increased by both intracerebroventricular infusion of a NOS inhibitor or nNOS gene knockout[44]. Although most evidences so far imply that nNOS derived NO inhibits SVZ neurogensis, there are a few studies show that nNOS-derived NO can promotes neurogensis in hippocampal[45]. The cause of such controversy still remains unclear and requires further study.

1.5.2 Memory and Learning

Both learning and memory are complicated multi-step processes[46]. Although their mechanism is still not entirely clear, there are evidences showing that NO plays an important role in these processes[47]. Previous animal model studies show that inhibition of nNOS impairs hippocampal long-term potentiation, synaptic plasticity and long-term memory formation[48, 49]. It has been shown that pharmacological inhibition of nNOS by 7-NI, at the doses that do not affect blood pressure, could induce amnesic effects in animals in both water maze and the a-arm radial maze[50]. The routes which animal was treated by 7-NI also affect the experiment outcome, implying nNOS was involved in different phase of memory[50]. Similarly, studies show that genetic inhibition of nNOS caused by nNOS gene knockout impaired the cognitive performance and spatial memory of mice[51]. Further study implies that nNOS gene removal induces an abnormal expression of a series of exocytotic machinery-related proteins including glycolytic enzymes and T-complex protein 1, resulting an impaired spatial memory [52]. Although such observations show clear relationship between nNOS and memory/learning, details about how nNOS regulates or affects these processes remain large unknown and require further study.

1.5.3 Excitotoxicity and Ischemia

Studies have shown that nNOS is particularly related with excitotoxicity, which is a pathological process resulting neuronal injury or death by an excessive synaptic release

of neurotransmitter such as glutamate[53]. During excitotoxicity process, excitotoxins binds their receptors such as N-methyl-D-aspartate receptor (NMDA) receptor and allows Ca^{2+} influx into the neural cells, which activates a series of enzymes including NOS [54-56]. Excitotoxicity breaks the homeostasis of neurons, damages the cell structures and eventually cause cell death[55, 56]. Previous in vitro studies indicate that nNOS is one major cause of NMDA neurotoxicity[55, 56]. In vitro experiments show primary cortical neuronal cultures from nNOS null transgentic mice are more resistant to NMDA toxicity, indicating NO produced by nNOS it one major source of neurotoxiciy [57].

1.5.4 Depression

Major Depressive disorder (MDD, clinical depression or unipolar depression) is a chronic recurring and potential life threatening mental illness characterized by consistent depressive mood and a loss of interest in normal relationship and activities[58]. World Health Organization estimated that MDD would the primary cause of disability by 2020[58]. Although little is known about the exact mechanism of its pathophysiology, research shows nNOS plays an important role in the pathogenesis of MDD [59, 60]. It has been shown that plasma nitration concentration in depressed patients is significantly elevated and commonly used antidepressant paroxetien and imipramine (IMI) are capable of inhibiting NOS activity in animals and humans[60]. Studies also show that 7-NI (a NOS inhibitor mentioned earlier) could induce antidepressant-like effect and this effect could be reversed by L-Arg pretreatment but not D-Arg[61]. Study with chronic mild stress (CMS) model also shows the importance of nNOS in pathophysiology of

depression [62]. It has been shown that nNOS expression level is increased in hypocampus with CMS and inhibition of nNOS could prevent CMS-induced depression[62]. Similarly, nNOS gene knockout mice is also found to be resist to CMS-induced depression[62]. However, why nNOS could induce depression and whether nNOS is a common target of antidepressants still requires further study.

1.5.5 Parkinson's Disease

Parkinson's disease (PD), featuring muscle rigidity, tremor, bradykinesia, changes in speech and gait, is a central nervous system dysfunction mainly affecting the motor system [63, 64]. It caused by progressive loss of dopamine-generating cells in the substantia nigra[64]. The relation between PD and nNOS was studied using nNOS knockout mice with a nNOS inhibitor 1-methyl-4-phenyl-1,2,3,6-tetrahydropyridine (MPTP) [65]. MPTP is a drug that induces PD similar symptoms in both human and rodents[65]. Comparing the behavior of nNOS knockout mice and wild type littermates after treated with MPTP showed that nNOS knockout mice were more resistant to MPTP neurotoxicity [65]. Moreover, study shows that 7-NI can protect wild type mice from MPTP neurotoxicity, implying that nNOS is related with PD pathogenesis[66]. In the meantime, increased level of nNOS expression, NO production and nitrated protein amount were found in basal ganglia and circulating neutrophils of PD patients[67]. These observations suggest that nNOS plays a role in the pathogenesis of Parkinson's disease but the details are still poorly understood and require further study.

1.5.6 Alzheimer's Disease

Alzheimer's disease (AD,) is a chronic neurodegenerative disease featuring short-term memory loss, mood swing, speaking and orientation problems and other behavioral issues[68]. Symptoms get worse overtime and eventually lead to death within three to nine year[68]. AD is associated with two critical processes in brain: neuritic plaque formation caused by amyloid b-peptide (Ab) aggregation and tau protein hyperphosphorylation that leads to neurofibrillary tangles[68-70]. Previous study shows chronic intracerebroventricular infusion of Ab1-40, an Ab isoforms, causes RNS formation and protein nitration on their tyrosine[70]. Moreover, study shows nitrated proteins in AD patient are highly co-localized with nNOS in cortical pyramidal cells, implying the protein nitration is regulated through nNOS related processes[71, 72] . Also, expression level of all three NOS isoforms is elevated in AD patients[72, 73]. These observations suggest that NO and NOS plays important roles in AD. Study of the effect of NO on AD and pathological details of NO and nNOS on AD would ultimately benefit its treatment.

1.6 Bacterial Nitric Oxide Synthase History

The history of NO being a biological product begins at 1967, when NO was identified as marine bacterium *Pseudomonas perfectomarinus* denitrification product[74]. Soon after that more bacteria including *Thiobacillus denitrificans*, *Micrococcus denitrificans* and *Paracoccus denitrificans* were identified belonging to the

denitirification bacteria family[75-77]. These bacteria utilize nitrite primarily for energy generation with the help of a copper-containing nitrite reductase[25]. This process also helps these bacteria balancing their redox state during the anaerobic respiration[25].

Although NO as biological compound was first identified in bacteria, whether prokaryotes contain nitric oxide synthase remains controversy until late 1990s. With the help of sequencing technology it has been identified that the open reading frame of *Bacillus subtilis* encodes an mNOSoxy similar protein[78]. This protein conserves all the key catalytic residues for NO synthesis, suggesting it is capable of producing NO from L-Arg[78]. Soon mNOSoxy similar proteins were identified in *Deinococcus radiodurans* by genomic sequencing as well[79].

The enzymatic validation of these bacterial nitric oxide synthases (bNOS) started in 2002. Adak. S *et al.* cloned the gene of the mNOS similar protein in *Deinococcus radiodurans* (drNOS) into a bacterial protein expression vector and successfully overexpressed and purified the drNOS from *E. coli*[80]. This drNOS is revealed to be a stable homer dimer, containing heme and maintaining all the spectroscopic features of mNOSoxy[80]. drNOS is capable of producing citrulline and nitrite from L-Arg in presence of a nNOS reductase in a H_4B dependent way with a rate much slower than mNOS[80]. For the first time it has been shown that prokaryotes encode a protein, which has NOS activity. Later, study on the NOS similar protein identified in *Bacillus subtilis* (bsNOS) revealed the bsNOS is capable of producing NOHA and NO sequentially, which is the same as mNOS[81]. Furthermore, both *in vivo* and *in vitro* studies prove that NO is a bona fide produce of other bNOSs[82-86]. To date, bNOS has been identified in a few

other bacteria species including *Staphylococcus aureus, Bacillus anthrasis, Streptomyces turgidiscabies and Geobacillus stearothermophilus* [80-86].

1.7 Structure of Bacterial Nitric Oxide Synthase

Interest about bNOS structure had been raised immediately after the discovery of bNOS. The first bNOS crystal structure was published in 2002 for bsNOS[87]. Its crystal structure suggests that the bsNOS is highly structurally similar with mNOSoxy[87]. As mNOXoxy, the bsNOS is a homer dimer and each monomer contains a heme and the heme is buried deeply in a "catcher's mitt" fold [87]. The heme of bsNOS is axially coordinated with a Cys and interacts with Tyr325 by hydrogen bond and stack interaction [87]. Similar to mNOS, the substrate and pterin binding sites of bsNOS locate on the dimer interface[87]. However, bsNOS also notably differs from mNOSoxy in the ways that bsNOS lacks the N-terminal hook and tetrahedral zinc finger, which is important for H_4B binding and H_4B specificity[87]. More importantly, the bsNOS lacks the covalently attached reductase domain, which implies it can only accept electrons from surrounding electron donors and is not regulated by CaM[87]. Until now, crystal structures of several other bNOS including gsNOS and saNOS has been resolved and they are all strongly assemble the structure of bsNOS[88, 89]. Interestingly, there is a unique member in bNOS family. The NOS similar protein in a gram-negative bacterium *Sorangium cellulosum* (scNOS) has a covalently attached reductase module[90, 91]. Unlike the mNOS, the reductase domain of scNOS is consisted of a Fe_2S_2 cluster rather than flavin

containing domains[91]. Also, the reductase domain of scNOS locates on the N-terminal domain, which differs from the domain assemble pattern of mNOS[91].

1.8 Catalysis of Bacterial Nitric Oxide Synthase

NOS is one of the most substantially studied enzymes, this provides a solid foundation of understanding bNOS catalysis[25]. From a structural point of view, the catalytic center of bNOSs is almost identical to mNOS except that a conserved Val near heme iron in mNOS is substituted by IIe[25]. Based on the structure similarities between mNOS and bNOS, it is rational to predict that they have similar reactivity, which has already proven by later studies[25]. Besides converting L-Arg or NOHA together with an external reductase partner, bNOSs are capable of producing nitrate/nitrite from L-Arg in presence of peroxide species with a rate similar to H_4B free mNOS[25]. The catalytic mechanism on the heme iron center in bNOS has been proven almost the same with mNOS[25].

Such similarities between bNOS and mNOS imply that our knowledge about mNOS catalytic mechanism can apply to bNOS and vice versa. This can be very useful for NOS mechanism and kinetic studies since bNOSs offer several advantages. Many identified bNOSs can be well expressed and readily purified from *E. coli*[25]. They can form a stable dimer without pterin cofactors, which can be a simplification for experiment design. The bNOS from special species allow us to study the NOS kinetics under very different condition than mNOS. For example, we can study the kinetics of NOS from thermophilic organisms under relatively high temperature. Moreover, their

kinetics at ambient temperatures will be slow and that may help us to identify more reaction intermediate.

1.9 Biological Functions of Bacterial Nitric Oxide Synthase

What bacterial NOS do has been one of the most intriguing questions ever since the discovery of bNOS. It is obvious that the functions of bNOS significantly differ from that of the mNOS since a single cell organism do not have a multi-cell immune system, a nervous system or smooth muscle cells. By merging the findings of previous studies, it is clear that functions of bNOS vary considerably depending on the species[25]. Here we briefly summarized the functions of several bNOSs.

1.9.1 *Streptomyces turgidiscabies* NOS (stNOS)

The first function study on bNOS function came out on 2008 about *Streptomyces turgidiscabies* nitric oxide synthase (stNOS). *Streptomyces turgidiscabies* is a bacterial pathogen causing scab in potatoes[92]. stNOS is capable of producing NO *in vivo*, confirmed by LC with chemiluminescence detection and *in situ* spin-trapping[83]. The study was inspired by the discovery that the open reading frame of the stNOS gene is located in a pathogenicity island, which confers thaxtomins (a class of plant toxin, derived from cyclo-[L-tryptophanyl-L-phenylananyl] dipeptides) biosynthesis[93]. Moreover, the NOS gene also locates closely to two genes of nonribosomal peptide synthases, which are involved directly in the thaxtomin biosynthesis[92]. The results of

this study show 1) the thaxtomin production in *S. turgidiscabies* is sharply decreased by NOS gene knockout; 2) the thaxtomin production in NOS knockout strains can be greatly restored by NOS complementation and 3) the thaxtomin production can be inhibited by mNOS inhibitors[92]. These results directly show stNOS relates with the virulence of *Streptomyces turgidiscabies* via thaxtomins biosynthesis[92]. Surprisingly, result from a ^{15}N feeding experiment proves the NOS derived NO could nitrate the tryptophanyl moiety of thaxtomins, which is very rarely seem in nature[92]. Taken together the fact that NO relates with thaxtomin pathogenicity and NOS is the only known enzyme to oxidize guanidinium group on Arg, it is clear that NOS is involved in the thaxtomin pathogenicity by causing nitration of the thaxtomin Trp moiety[92]. Another interesting finding is that *S. turgidiscabies* hyphae produces more NO than what is needed for toxin biosynthesis in response to cellobiose (plant cell wall component) [92]. In the mean time, NO is known as a signaling molecule stimulates plants growth and extension of root tips[25]. That implies that stNOS is bi-functional. In one hand it facilitates the bacterial infection, in the other hand it promote the growth of infected plant tissue[25].

However, several questions still remain unanswered. The function of nitration is puzzling since thaxtomin itself is an active toxin without nitration. It is unlikely that the thaxtomin get produced before it is nitrated because stNOS affect the production of thaxtomin[25]. This implies that the nitration may affect the production of thaxtomin precursor[25]. Also, so far biosynthetic nitration reaction directly by NO is still unprecedented. Other enzyme(s) may be required for downstream enzymatic reactions with NO to create more reactive nitrogen species such as nitrosonium (NO^+) and peroxynitrite (ONOO). Identities of such enzyme(s) and their role in NO oxidation still

remain unknown. Much more works are needed to understand the roles of stNOS in the biosynthesis of thaxtomin[25].

1.9.2 *Deinococcus radiodurans* NOS (drNOS)

Deinococcus radiodurans is an extremophilic bacterium[94]. It is famous for its resistance to several extreme environmental conditions including radiation, dehydration, oxidative damage, coldness and even vacuum and known as one of world's toughest bacterium[94].

As one of the earliest identified bNOS, functions of drNOS have been studied soon after its discovery by comparing the behaviors of wild type *D. radiodurans* and nos gene deleted (Δnos) strain under different conditions[86, 94, 95]. Results show that although Δnos strain only has a small growth defect in rich media, it is no longer able to recover after UV radiation exposure[86]. Dramatic growth defect of Δnos strain under UV radiation exposure has also been observed[86]. Moreover, providing exogenous NOS by transformation a NOS expression plasmid or adding exogenous NO can complement such growth defect of Δnos strain[86]. These facts clearly show that drNOS is a critical factor for *D. radiodurans* survival under stressed conditions.

However, the mechanism of such protecting effect of drNOS is not entirely clear. One proposed mechanism is that UV radiation induces drNOS expression, resulting in production of NO[86]. The produced NO then acts as signaling molecule to upregulate transcription of other growth factor, which is involved in cell proliferation[86]. Several clues support such mechanism. First, NO addition triggers recovery of Δnos strain despite

whether NO is added before, during or after UV exposure[86]. This shows NO does not directly protect *D. radiodurans* from radiation damage, otherwise the cell would not recover after the damage had already been done[86]. Second, previous studies show that UV radiation can induce NOS expression of *D. radioduran* and the intracellular NO level positively correlates with NOS expression level in *D. radiodurans*, which implies UV radiation increases the intracellular NO level[86]. Third, transcriptional profiling experiments reveal that UV radiation upregulates the gene expression of the general growth regulator Obg in wild type *D. radiodurans* but not the Δnos construct[86]. Interestingly, although drNOS potentially involved in radiation resistance, Δnos strain is still resistant to oxidative damage[86]. This implys the oxidative stress resistance of *D. radiodurans* may be unrelated with NOS[86].

Similar to stNOS, drNOS is surprisingly involved in nitration of Tpr residues [96]. Previous Pull-down experiments imply that drNOS interacts with a tryptophanyl tRNA synthetase protein (TrpRS II), which is a tryptophanyl tRNA synthetases identified in *D. radiodurans*[96]. TrpRS II is known for its ability to adenylate Trp and charging tRNA Trp[25]. Study shows that drNOS interacts with TrpRS II and also destabilizes the interaction between fluorescent ATP analogs and TrpRS II[25]. In the other hand, TrpRS II increases the affinity between drNOS and Arg[25]. More importantly, drNOS is found to catalyze formation of a small amount of 4-nitro-Trp alone together with a mammalian reductase[25]. TrpRS II and ATP significantly increase the yield of 4-nitro-Trp while H_4B inhibits the production of 4-nitro-Trp[25]. This implies that drNOS and TrpRS II may work together to produce 4-nitro-TrptRNATrp rather than producing NO [25]. The produced 4-nitro-Trp tRNA may act as substrate for downstream reactions[25]. However,

the reactivity, detailed mechanism and kinetics of drNOS and TrpRS II are still unclear. Overall, many questions about drNOS still remains unanswered.

1.9.3 NOS in *Bacillus anthracis, Bacillus subtilis* and *Staphylococcus aureus*

Nudler group in NYU medical school has studied functions of NOSs in several *Bacillus* and *Staphylococcus* strains by comparing the behavior of NOS gene deleted strains (Δnos) with the wild type strains under a series of stressed conditions[97, 98]. Results show that 1) endogenous NO could be produced by the NOS in the tested bacteria; 2) wild type strains are more resistant to ROS; 3) significant growth defect of Δnos strain in presence of ROS was observed and such growth defect can be eased by providing external NO or NO donor; 4) survival percentage of Δnos strains under high dose of ROS can be greatly increased by exposing bacteria to NO for short time (5 seconds) before adding reactive oxygen species (ROS)[97]. These results clear show that the NO protects these bacteria against oxidative stress[97]. Three mechanisms of such protective effect of NO have also been proposed based on the results. (1) NO reacts directly with ROS including acriflavine (ACR) and convert them into less toxic reagents[97]. 2) NO suppresses the Fenton reactions (a reaction which generates ROS)[97]. The reduced thiol in *B. subtilis* can reduce ferric iron thus promote Fenton reactions[97]. NO is capable of interrupting the thioredoxin system thus blocking the formation of free thiol to protect *B. subtilis from* oxidative damage[97]. 3) NO induces the expression of superoxide dismutase (SOD), which can convert superoxide species into oxygen and water thus protect *B. subtilis*[97].

Such NO-mediated protection mechanism from ROS is important for pathogens to infect their host since hosts often generate ROS to defend the infection[97]. Mouse model studies show that spores of the nos gene deleted *B. anthracis* do not have virulence, and its survival rate in response to macrophages is significantly lower than the wild[85]. These findings suggest that NO plays a complex role in the infections by bacterial pathogens because NO protects bacterial pathogens and triggers host defense system at the same time[25]. More insight of such paradox requires further study.

CHAPTER II

FMN DOMAIN MOTION IS ESSENTIAL FOR CATALYSIS OF NEURONAL NITRIC OXIDE SYNTHASE

2.1 Introduction

2.1.1 Crystal Structure of nNOSr

Crystal structure of rat nNOSr has been resolved in 2004 by Garin *et al*. (Fig. 4.)[99]. It greatly improved our understanding about nNOSr structure and set up solid basis for the structure-function study of nNOSr[99]. In the crystal structure, the nNOSr is dimeric itself even without the oxygenase domain[99]. The flavin-containing face of FMN domain is buried into the deep cup-shape surface formed by the FNR and an α-helical connecting domain (CD)[99]. The CD connects the FMN and FAD domain and orients them in a conformation that their flavins align. In this conformation, the xylene

ring methyl group of FMN is only 4.8 Å away from the xylene ring methyl group of FAD, which makes the direct electron transfer between these flavins possible[99].

The FMN and FAD domain interact with each other in several ways[99]. They interact directly through a double salt bridge located in the center of the FAD/FMN domain interface formed by the residue pair Glu816 and Arg1229[99]. They also interact through the hydrogen bonds, hydrophobic contacts and electrostatic interactions[29, 99]. The Autoinhibitory insert (AI) on the FMN domain inserts into the space between the FMN domain and NADPH binding domain, which physically separates these two domains[99]. Interestingly, the two resolved crystal structures that have been reported so far exhibited a 4° rotation relative to each other, suggesting some flexibility of nNOSr[99]. The weakly defined electron density on some parts of CD also implies the conformational diversity of nNOSr [99].

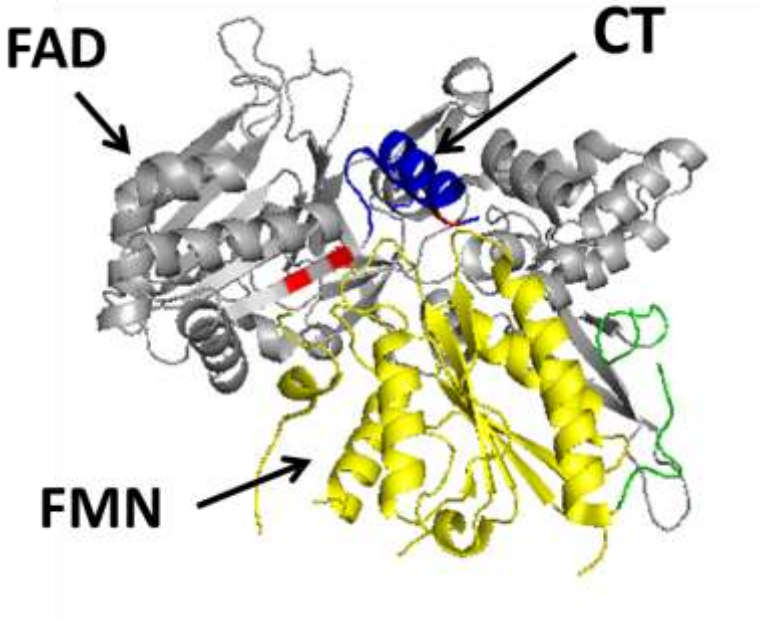

Fig. 4. **Crystal structure of nNOSr**

2.1.2 nNOSr Regulatory Elements

Previous studies reveal that nNOSr shares several common and unique regulation elements with other dual flavin enzymes[35]. How these control elements function and cooperate is a central topic in the area. Several control elements are listed below.

2.1.2.1 CaM Binding

CaM binding is a unique feature of NOS comparing to other flavin enzymes[35]. The CaM binding site locates upstream to FMN domain[99]. CaM binds to nNOS in presence of Calcium boosts the electron transfer within the reductase domain[35, 100]. Previous studies imply CaM interacts with nNOS through nNOS Arg752-CaM Glu47 bridging interaction and such interaction triggers a conformational change on nNOSr and removes the self-repression of nNOS[27]. More recently FRET study clear shows CaM binding changes the distance distribution between FAD and FMN binding domains and makes both FMN and FNR domains more dynamic[100].

2.1.2.2 Autoinhibitory Insert

Autoinhibitory insert (AI) amino acids locate within the FMN domain sequence[99]. However, the crystal structure shows that the α-helix of AI from residue 840 to 848 sequesters into the hydrophobic cave between FMN domain and NADPH-binding domain in the tertiary structure of nNOSr[99]. This structural element is believed

to inhibit the electron transfer from FNR module to FMN module[99].

2.1.2.3 C-terminal Tail

C-terminal tail (CT) is another unique structural element of NOS. The crystal structure of nNOSr indicates the CT contains an ordered α-helix structure(residues 1401–1412) and an unstructured part, which is invisible in the crystal structure[99]. The ordered part of CT inserts into the FAD/FMN domain interface and shielding both FAD and FMN from solvent, suggesting a regulatory role of CT[99]. CT hydrogen bonds with residue Tyr899 on FMN and Asp1351 on the FAD domain respectively[99]. It also has ionic interaction with NADPH and hydrophobic interactions with surrounding hydrophobic residues on FAD and FMN domain[99]. Kinetic studies on CT truncated nNOS proteins proved that the α-helix of CT represses the electron transfer through nNOSr and it also inhibits the $NADP^+$ releasing [101, 102]. In comparison, the unstructured part on CT has little effect on the activity of nNOSr and only a small effect on the NPADH-binding[101].

2.1.2.4 Other Key Residues

Phosphorylation and residue Ser1412

Ser1412 in rat nNOS is an Akt-dependent phosphorylation site[103]. The crystal structure of nNOSr showed Ser1412 locates on the end of CT[103]. The oxygen atom in Ser1412, which forms a phosphate bond after phosphorylation, points directly towards

the negative charged Glu916 and Asp918 on the FMN domain[103]. This suggests phosphorylation on this site would induce an electrostatic repulsion between CT and FMN thus may change the overall conformation of nNOSr[103]. Kinetics study on S1412D nNOSr proves a negative charge on residue 1412 does fasten the electron transfer through nNOSr and suggests such activation is conformation related[103].

FAD shielding residue F1395

The Phe1395 locates upstream to the CT and stacks with the isoalloxazine ring of FAD in the nNOSr crystal structure[104]. Following kinetics studies on F1395S of nNOSr reveal important regulatory roles of F1395 for nNOSr electron transfer and catalysis[104]. F1395 weakens the interaction between $NADP^+$ with nNOSr thus facilitate $NADP^+$ releasing to allow nNOSr bind NADPH[104]. More importantly, it relates with the conformational equilibrium involving the FMN domain, which is likely to be controlled by NADP(H) binding[104].

Hydride transfer and residue D1393

D1393 is a widely conserved residue among NOS[105]. In the crystal structure of nNOS, the carboxyl group of D1393 is direct on top of the isoalloxazine ring of FAD and it is thought to regulate the hydride transfer from NADPH to FAD[105, 106]. Kinetics studies show mutation on D1393 significantly slows hydride transfer, implying D1393 facilitates the hydride transfer from NADPH to FAD[105]. However, the mechanism of this excitatory effect of D1393 remains unclear.

2.1.3 nNOSr Conformational Model

Crystal structure of nNOSr shows the isoalloxazine rings of FAD and FMN cofactors are close enough for direct electron transfer[99]. However, the FMN cofactor is deeply buried within the cave generated by FAD domain and CD, preventing electron transfer from FMN to its redox partners[99]. The structure assemble study with NOSoxy, NOSred modules and a CaM-NOS-peptide complex implies the shortest distance between the FMN and heme cofactor is approximately 70 Å, which is too long for direct electron transfer[36, 99]. At the meantime, kinetics study of nNOS suggested that nNOS exists in different conformations during its catalysis[35, 100].

Based on these studies, we proposed a three-state, two-equilibrium model describing the electron transfer mechanism on NOS (Fig.5)[35]. In this model, the entire FMN domain swings back forth between FNR domain and NOS oxy, shuttling electrons between these two domains[35]. The NADPH-derived electron transfer from FNR domain to FMN domain in the equilibrium K_A, which is the equilibrium between FNR-FMN domain attached conformation (defined as "closed" or "FAD-shielded" form) and the FNR-FMN domain unattached conformation (defined as "open" form)[35]. The electrons transfer to NOSoxy in equilibrium K_B. Such large-scale movement of FMN domain has already been identified in the catalysis of other dual flavin enzymes including methionine synthase and CPR[107, 108].

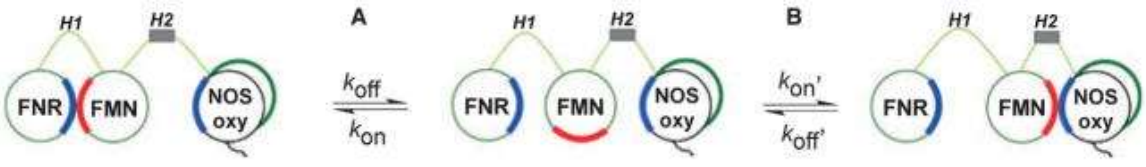

Fig. 5. **NOS conformational equilibrium model**

2.1.4 nNOSr Electron Transfer Model

Flavins are cofactors for a variety of enzymes including NOS and they can act as part of their electron transfer chain[36]. Flavins have three different oxidation states, fully oxidized, semiquinone(sq) and hydroguinone(hq) as shown in Fig 6[109]. In the electron transfer through nNOSr, only the hydroguinone(hq) is capable of donating electrons to an acceptor since nNOSr thermodynamically stabilizes the semiquinone[109]. During catalysis by nNOSr, FADhq donates an electron to FMNsq to produce FMNhq[109]. The FMNhq can donate one electron to an electron acceptor[109]. The overall electron flux pathway is shown in Fig 7[35].

Although Fig 6 looks quite straight forward, the actually electron transfer mechanism may be complicated because the electron transfer happens simultaneously with conformational motion in nNOSr and it is likely the electron transfer is regulated by such conformational motions[35]. Based on our current understanding of nNOSr, we proposed a simplified four state model to describe how conformational motions affect the electron transfer through nNOSr (Fig. 8)[35, 109]. This model includes a conformational opening equilibrium that allows FMNhq to donate one electron to its substrate and a conformational closing equilibrium that allows FMNsq to receive one electron from FADhq.

Here we define $K_{sq} = k_{-1} / k_1$ and $K_{hq} = k_{-3} / k_3$ so that higher K values reflect a higher percentage of nNOSr in open conformations[109]. This model has been used to compute the cytochrome *c* reduction results of nNOS, eNOS, cytochrome P450 reductase and methionine synthase reductase[109].

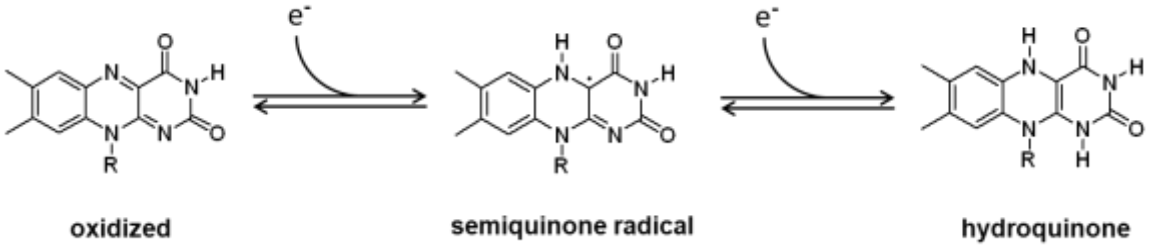

Fig. 6. **Oxidation state of FAD and FMN**. Oxidized FAD or FMN receives one electron through hydride transfer and becomes into a semiquinone radical, which can further accept another electron and becomes into hydroquinone.

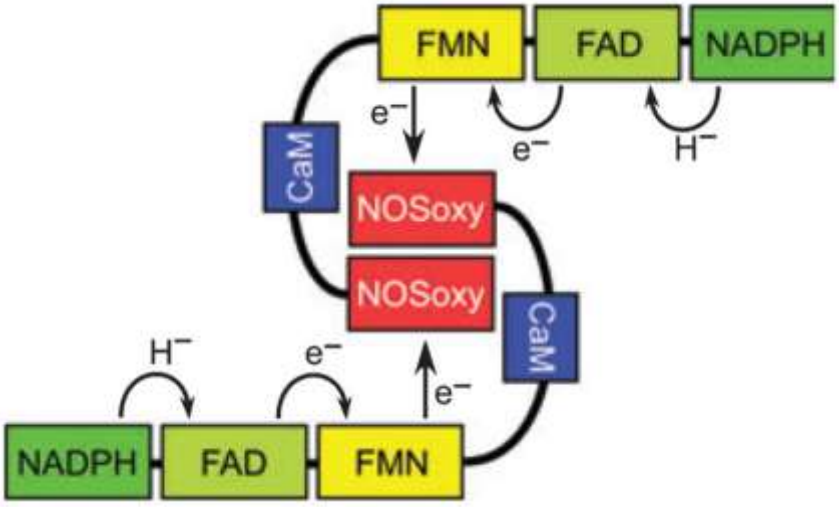

Fig. 7. **Electron transfer path of NOS.** NADPH donates one electron to FAD as hydride. The electron is then transferred to FMN and finial to the oxygenase domain on the other NOS monomer.

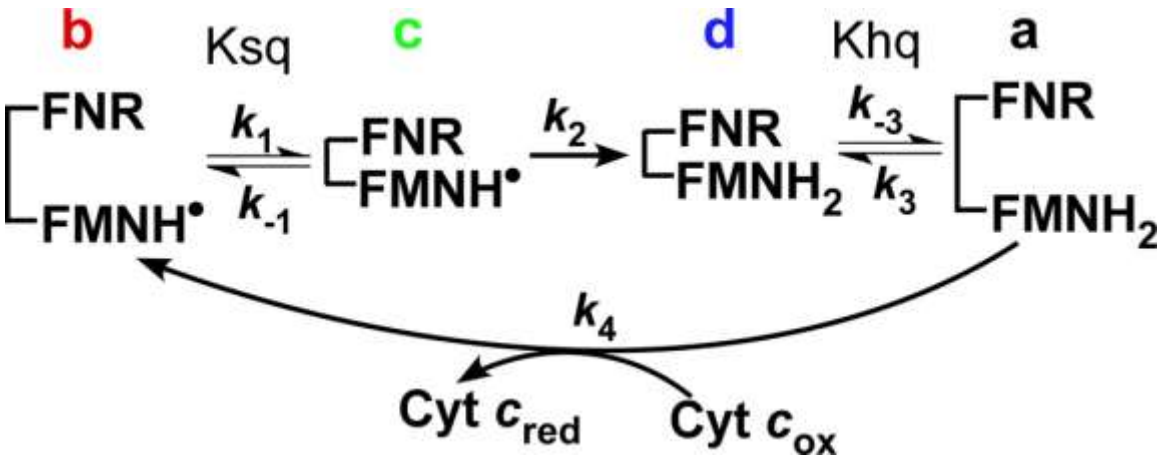

Fig. 8. **Electron transfer model of NOS reductase.** In this model, k_1 and k_3 represent the association rate of FNR and FMN. Similarly, k_{-1} and k_{-3} represent the dissociation rate of FNR and FMN. The rate k_2 is the FMNsq reduction rate. The rate k_4 is the cytochrome c reduction rate.

2.1.5 Conformation Study of a Mutated Cytochrome P450 Reductase

Cytochrome P450 reductase (CYPOR) is a related dual flavin enzyme that has an attached FMN binding domain and a FAD binding domain[108]. It has been proposed that its FMN binding domain undergoes large-scale movement during its catalysis[108]. And recent studies of CYPOR using biophysical and kinetic tools successfully proved

this hypothesis[108]. The CYPOR mutant CYPOR N147C R514C is one of the key components for these studies[108].

Similar to nNOSr, crystal structure of wild type CYPOR reveals a salt bridge between its FAD binding domain and FMN binding domain between the residue Asp147 and Arg514[108]. The authors first engineered a CYPOR mutant having C136A, C228A, C363T, C445L and C472T point mutations to delete the nonessential cysteine residues on CYPOR[108]. They then engineered a disulfide bond between the FMN and FAD binding domains of this CYPOR mutant by introducing the D147C and the R514C mutations. This mutant is referred to as CYPOR 147CC514[108]. The disulfide bond presumably prevents the movement of the FMN domain and was therefore expected to drastically change the electron transfer and catalysis of CYPOR[108]. The crystal structure of CYPOR 147CC514 revealed that the engineered disulfide bond successfully cross-linked the FAD and FMN domains[108]. The cross-linked enzyme exhibited a significantly lower steady-state activity and electron transfer rate from FMN to its redox partners[108]. Breaking the disulfide bond in CYPOR 147CC514 with DTT restored its normal catalytic activity[108]. These results directly showed that the FMN domain of CYPOR is involved in a conformational equilibrium, that is essential for catalysis[108]. Unrelated NMR and small-angle x-ray scattering studies on CYPOR revealed that the oxidized CYPOR does have open and closed conformations in solution and the ratio of open and closed conformations in solution is approximately 1:1[107].

2.1.6 Aims

Based on previous studies that suggest electron transfer through nNOSr is conformationally regulated and inspired by the above studies of cross-linked CYPOR, we created and utilized similar variants of the nNOSr protein (Cys-lite nNOSr and locked-down nNOSr) that allow us to specifically link different domains by disulfide bonds and by chemical crosslinkers. That allowed us to study the importance of domain motions on nNOSr electron transfer and to test if FMN domain motion is essential for nNOSr electron transfer.

2.2 Experiments

2.2.1 Reagents and Materials

Bis(maleimide)ethane (BMOE), bis(maleimide)butane (BMB), Bis(maleimide)-hexane (BMH), bis(maleimide)diethylene glycol ($BM(PEG)_2$), bis(maleimide)triethylene glycol, ($BM(PEG)_3$) were purchased from Thermo. Bis-Mal-PEG6 ($BM(PEG)_6$) and Bis-Mal-PEG11 ($BM(PEG)_{11}$) were purchased from BROADPHARM. All other reagents and materials were obtained from sources reported elsewhere[109, 110].

2.2.2 Molecular Biology

pCWori vector containing rat nNOSr DNA was constructed by previous lab members[109]. Rat nNOSr DNA with S774C, S823C, S921C, S945C and S1275C mutations was made and subcloned into pCWori vector (Custom DNA Constructs, OH, US). This mutant is called cys-lite nNOSr or CL5 since it has 5 Cys to Ser mutation. CL5 nNOSr DNA with E816C and R1229C mutations was also made and subcloned into pCWori vector (Custom DNA Constructs, OH, US). This mutant is referred to as CL5-SS. Sequences of all mutant DNA were confirmed by Cleveland Clinic sequencing facilities.

2.2.3 Expression and Purification of wild type and mutant nNOSr

pCWori vector containing DNA of wild type or mutant nNOSr were each transformed in to *E. coli* stand BL21 (DE3) for over-expression[110]. Transformed *E. coli* cells were inoculated in 500 mL LB media at 37°C in the presence of 100 mg/mL ampicillin with vigorous shaking (250 rpm) overnight. Eight 2 L flasks each containing 50 mL of overnight culture, 450 mL TB and the same antibiotics were used for nNOSr expression. The cultures were grown at 37 °C with vigorous shaking. 1 mM isopropyl-β-D-thiogalactopyranoside (IPTG) was added to induce nNOSr expression when the cultures OD_{600} reached 0.8~1.0. Cultures were then transferred to room temperature and grown for another 48 hrs with vigorous shaking (250 rpm). The cells were harvested by centrifuging at 5000 rpm for 30 min. The cell pellets were resuspended with minimum volume of 40 mM Epps, 150 mM NaCl, 10% glycerol, pH 7.6 containing protease

inhibitors, phenylmethanesulfonylfluoride (PMSF) and lysosome. The resuspended cells were sonicated using a Branson digital sonifier (3 × 35 s bursts on 35% power, interspaced by 1min) on ice. All of the following procedures were done at 4 °C unless indicated specifically. The lysates were centrifuged at 13000 rpm for 1 hr and the clear supernatant was loaded onto a gravity 2'5' ADP-sepharose column pre-equilibrated with 40 mM Epps, 150 mM NaCl, 10% glycerol, pH 7.6. The column was washed with 200 ml of 40 mM Epps, 500 mM NaCl, 10% glycerol, pH 7.6 containing 1 mM EDTA and eluted with 40 ml of 40 mM Epps, 150 mM NaCl, 10% glycerol, pH 7.6 containing 1 mM NADPH and 3 mM 2'(3')-AMP. $CaCl_2$ was added to make its final concentration 2 mM in the elute. The elute was loaded onto a CaM-sepharose affinity column pre-equilibrated with 40 mM Epps, 150 mM NaCl, 10% glycerol, pH 7.6 containing 1 mM $CaCl_2$. The column was washed with 100 ml of 150 mM NaCl, 10% glycerol, pH 7.6 containing 1 mM $CaCl_2$ and the bound nNOSr protein was eluted with 50 ml of 150 mM NaCl, 10% glycerol, pH 7.6 containing 3 mM EDTA. Eluted nNOSr was concentrated using a 50 ml Millipore concentration unit with 50 kD cut off (EMD Millipore, MA). Concentrated nNOSr wild type was dialyzed in 40 mM Epps, 150 mM NaCl, 10% glycerol, pH 7.6 with 1 mM DTT. nNOSr CL5 and CL5SS were dialyzed in 40 mM Epps, 150 mM NaCl, 10% glycerol, pH 7.6. Protein was aliquoted and stored in -70°C. Concentration of nNOSr and mutants were determined using an extinction coefficient of 22.9 mM^{-1} cm^{-1} at 457 nm[111].

2.2.4 Preparation of Bis-maleimide Cross-linked nNOSr

10 mM Bis-maleimide cross-linker (BM) stock solutions were made in DMSO immediately before use. Scheme of maleimide conjugation is shown in Fig. 9. BM cross-linking was carried out on ice by incubating protein pre-treated with 10 equivalents of TCEP and 5 equivalents of $NADP^+$ with 2 equivalents of BM for 40 min on ice in 40 mM EPPS, 150 mM NaCl, 10% glycerol pH 7.0 buffer. The reaction mixture was further incubated with Glutathione sepharose 4B resin (GSH resion) for another 40 min on ice to remove any double BM reacted CL5SS as shown in Fig. 10. The reaction mixture was centrifuged at 10000 rpm for 3 min at 4°C to remove the beads and the supernatant was loaded onto a desalting PD10 column (GE healthcare Lifescience) to remove excessed TCEP, $NADP^+$ and BMs.

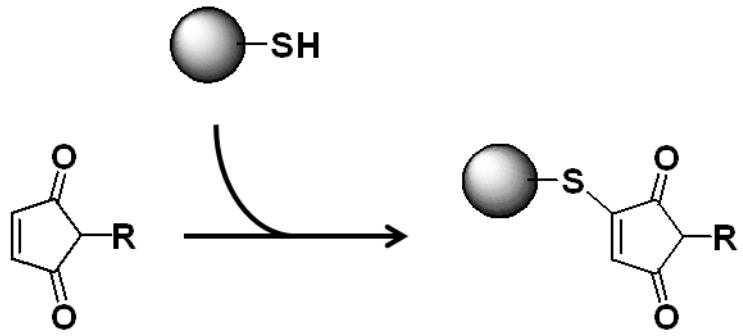

Cross-linkers	Arm Space	Structure
BMOE	8Å	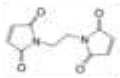
BMB	10.9Å	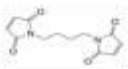
BMH	13Å	
$BM(PEG)_2$	14.7Å	
$BM(PEG)_3$	17.8Å	
$BM(PEG)_6$	41.1Å	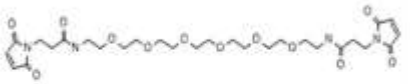
$BM(PEG)_{11}$	53.5 Å	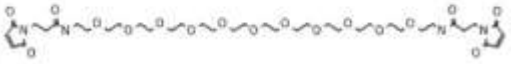

Fig.9. **Scheme of maleimide conjugation with thiol group and structure of selected cross-linkers**. The thiol group conjugates with the maleimide group on the carbon-carbon double bond.

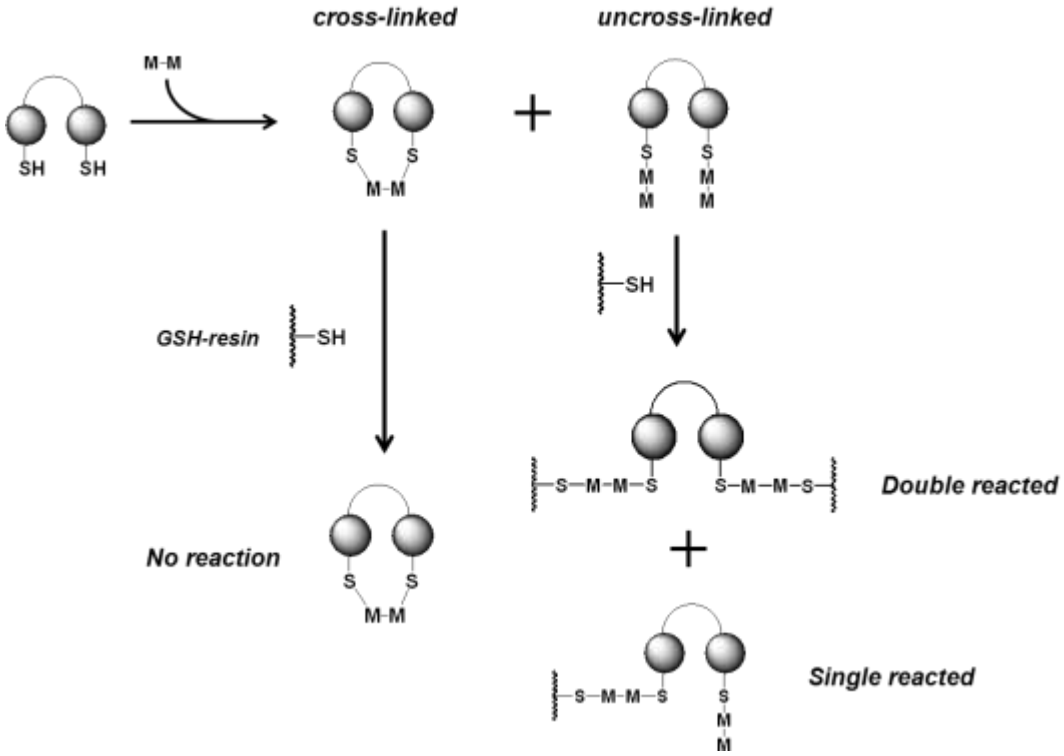

Fig. 10. **Side reaction of cross-linking and separation by GSH-resin.** The bis-maleimide cross-linking reaction with excess of cross-linker results in a mixture of cross-linked protein and uncross-linked protein. The uncross-linked protein can be pulled down by GSH resin, leaving only the cross-linked protein in the reaction solution.

2.2.5 Preparation of N-ethylmaleimide Conjugated CL5SS, Dithoreitol Reduced CL5SS and pH 9 Treated CL5SS

20 mM N-ethylmaleimide (NEM) stock solution was made in ultrapure water immediately before use. NEM conjugation was carried out at room temperature by incubating protein pre-treated with 10 equivalents of TCEP and 5 equivalents of $NADP^+$ with 10 equivalents of NEM for 1 hr in 40 mM EPPS, 150 mM NaCl, 10% glycerol pH 7.0 buffer. The reaction was stopped by passing the reaction mixture through a desalting PD10 column (GE healthcare Lifescience). Dithoreitol (DTT) reduced CL5SS was prepared by incubating CL5SS in 40 mM EPPS, 150 mM NaCl, 10% glycerol, pH 7.6 buffer containing 0.5 mM DTT for 1 hr on ice. The pH 9 treated CL5SS was prepared by incubating CL5SS in 50 mM Tris-HCl, 150 mM NaCl, pH 9.0 buffer for 1 hr on ice then passing a PD10 desalting column.

2.2.6 UV-Vis Spectroscopy

UV-Vis spectra of nNOSr wild type and mutants ranging from 250 nm to 700 nm before or after cross-linking were obtained in 40 mM Epps, 150 mM NaCl, 10% glycerol pH 7.6 using a Shimadzu UV-2401 PC UV-Vis spectrophotometer.

2.2.7 Reactive Thiol Group Quantification

The number of remaining thiol groups on BM cross-linked CL5SS (CL5SS-BMs) or CL5 was quantified using the Alexa Fluor 555 maleimide dye (A555, Thermo). CL5SS-BMs were incubated with 1 equivalent A555 at room temperature for 10 min. The reaction mixture was further incubated with CaM-sepharose affinity resin and 1 mM $CaCl_2$ for another 10 min at 4 °C. The CaM resin was then washed with 40 mM Epps, 150 mM NaCl, 1 mM $CaCl_2$, 10% glycerol, pH 7.6 containing 1 mM $CaCl_2$ until no apparent absorption at 555 nm was detected in the wash buffer by the UV-Vis spectrophotometer. The bound CL5SS-BMs was eluted using 40 mM Epps, 150 mM NaCl, 10% glycerol, pH 7.6 with 2 mM EDTA. Concentration of nNOSr and mutants were determined using an extinction coefficient 22.9 mM^{-1} cm^{-1} at 457 nm[111]. Concentration of A555 bound on the protein was determined using an extinction coefficient 150.0 mM^{-1} cm^{-1} at 555 nm.

2.2.8 Reactive Mal Group Quantification

The number of maleimide groups remaining in the CL5SS- BM was quantified using Amplite Flourimetric Maleimide Quantitation Kit (AAT Bioquest, CA) with a standard curve obtained with NEM standards provided in the kit.

2.2.9 Steady-state Cytochrome *C* Reductase Activity

Cytochrome *c* is a universal electron acceptor for dual flavin reductases[109]. Reduction of the cytochrome *c* by dual flavin reductase can be much faster than electron transfer through the reductase, thus it not typically the rate limiting step[109]. The steady-state cytochrome *c* reductase activity is widely used as an indication of enzyme activity[109]. In this assay, a reaction mixture containing ~10 nM nNOSr proteins, 100 μM cytochrome *c*, 40 mM EPPS, 150 mM NaCl and 10% glycerol, pH 7.6 with 1 mM EDTA or 100 μM CaM and 1 mM $CaCl_2$ was placed in a cuvette. The reactions were initiated by adding 100 μM NADPH. Absorbance at 550 nm versus time was record by a UV-Vis spectrophotometer (Shimadzu UV2401PC) and the slope was calculated by the built-in program of Shimadzu spectrophotometer software UVProble 2.32. The pseudo-zero order rate constant was calculated by dividing the slope value by the extinction coefficient of 21 mM^{-1} cm^{-1}[111]. The steady-state turnover number (*kcat*) was calculated by dividing the pseudo-first order rate constant by the concentration of enzyme used in the assay. Experiments were done at room temperature or 10°C and performed in triplicate. The results were shown as mean ± standard deviation.

2.2.10 Flavin Reduction Kinetics

Full oxidized nNOSr proteins (10~15 μM nNOSr protein in 40 mM Epps, 150 mM NaCl, 10% glycerol, pH 7.6, with 1 mM EDTA or 1 mM $CaCl_2$, 30 μM CaM and an NADPH solution (100 μM in 40 mM Epps, 150 mM NaCl, 10% glycerol, pH 7.6) were

made anaerobic by alternatively applying negative pressure created by a vacuum pump and nitrogen gas to sample solutions in an anaerobic cuvette for 90 min on ice. Anaerobic samples were transferred to two syringes in Stopped-flow camber, which was made oxygen free by flushing with nitrogen gas as shown in Fig. 11. (copied form TgK website). Measurements were initiated by rapidly mixing 100 µl solution from each syringe in the by Stopped-flow instrument at 10 °C. The full spectrum in the range 400 nm to 700 nm and the absorbance change at 457 nm or 600nm were recorded by SF-61DX2 or SF-61. The maximum absorbance value at 457 nm for individual nNOSr protein was obtained by mixing the protein sample with 40 mM Epps, 150 mM NaCl, 10% glycerol pH 7.6 buffer (no NADPH) in stopped-flow instrument. The minimum absorbance value at 457 nm was obtained by mixing buffer (40 mM Epps, 150 mM NaCl, 10% glycerol pH 7.6) with the same buffer in stopped-flow instrument.

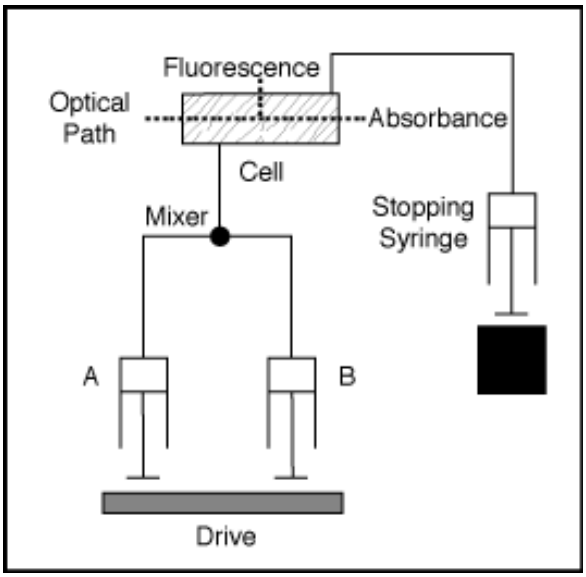

Fig. 11. **Stopped-flow instrument setup**

2.2.11 Data Analysis of Flavin Reduction Kinetic Traces

The signal to noise ratio of flavin reduction time course was improved by averaging 8-10 individual scans. A double exponential equation was used to fit the recorded traces at 457 nm to get the rate constants using OriginLab 8.0 (OriginLab Co. MA) with the constraint that the phase ratio of first and second phase is 1:1. This constraint was applied because in the end of flavin reduction both FAD and FMN are reduced and they contribute equally to the absorbance change at 457 nm[111]. A double exponential equation was also used to fit the recorded traces at 600 nm to get the rate constants. Percentage absorbance changes were determined using the maximum and minimum absorbance value at 457 nm as 100% and 0%.

2.2.12 Pre-steady-state Cytochrome *C* Reduction Kinetics

A solution containing 10~15 μM nNOSr protein and 1 mM EDTA in 40 mM Epps, 150 mM NaCl, 10% glycerol, pH 7.6 was made anaerobic by alternatively applying negative pressure created by a vacuum pump and nitrogen gas to sample solutions in an anaerobic cuvette for 90 min on ice. The concentration of nNOSr proteins was determined using an extinction coefficient 22.9 mM^{-1} cm^{-1} at 457 nm[111]. This solution was first reduced by adding 200 μM anaerobic NADPH then fully photo reduced by adding 1 μM 5-deazariboflavin then irradiating using a slide projector bulb until no further decrease in UV-Vis absorbance was observed with further irradiation. A solution containing 100 μM cytochrome *c* was made anaerobic with the same procedures. The

anaerobic samples were transferred to two syringes in stopped-flow instrument then rapidly mixed at 10 °C. Absorbance change at 550 nm was monitored. Initial cytochrome *c* absorbance at 550 nm ($A_{550, Initial}$) was obtained by rapidly mixing the same cytochrome *c* solution with an anaerobic buffer containing 40 mM Epps, 150 mM NaCl, 10% glycerol, 200 μM NADPH, pH 7.6 in the stopped-flow instrument.

2.2.13 Data Analysis of Pre-steady-state Cytochrome *C* Reduction Traces

The absorbance at 550 nm when 1 equivalent cytochrome *c* was reduced ($A_{550, Final}$) by nNOSr was determined by using the equation:

$$A_{550, Final} = A_{550, Initial} + \varepsilon * L * [nNOSr] * 0.5$$

Unit of nNOSr protein concentration is μM in this equation. ε is the extinction coefficient of cytochrome *c* at 550 nm, which is 21 μM^{-1} cm^{-1}[111]. L is the path length of SF51 Stopped-flow instrument, which is 1 cm. 0.5 was used because same volume of nNOSr protein and cytochrome were mixed in the stopped-flow instrument. The time it took to achieve 1 equivalent cytochrome *c* reduction was obtained by correlated $A_{500, Final}$ with time in the absorbance trace monitored at 550 nm. The zero time absorbance at 550 nm recorded when mixing fully reduced nNOSr protein with cytochrome *c* is written as $A_{550.}$ In this case, the K_{hq} of nNOSr proteins, which represents the ratio of the open conformation and closed conformation, is approximately equal to (A_{550} - $A_{550, initial}$) : ($A_{550, final}$ - A_{550}) [111].

2.2.14 $NADP^+$ Titration

$NADP^+$ binds nNOS and forms a charge transfer complex with the FAD isoalloxazine ring, which results in a shift on its UV-Vis spectrum[104]. The spectrum of 20 μM nNOSr proteins before and after adding 100 μM $NADP^+$ were recorded by a Shimdazu UV-2401PC UV-Vis spectrophotometer and subtracted to obtain the spectral shift. In a separate experiment, 20 μM nNOSr proteins were titrated with aliquots of $NADP^+$ at room temperature. The spectrum after every titration point was recorded 3 min after $NADP^+$ was added. Absorbance difference between 510 nm and 457 nm from the spectral shift was plotted versus $NADP^+$ concentration.

2.2.15 Fluorescence Spectroscopy

Bound flavins in NOS have intrinsic fluorescence mostly due to the FMN[112]. Flavin fluorescence of nNOSr, CL5 and CL5SS-BMOE was measured in a 1 ml quartz cuvette with 1 cm path length by a Hitachi model F-2500 spectrofluorometer. 2 μM nNOSr proteins in 40 mM Epps, pH 7.6 containing 3 μM CaM and 0.6 mM EDTA were used in this experiment. The emission intensity at 530 nm excited by irradiation at 457 nm was monitored versus time before or after adding 1 mM $CaCl_2$ and 3 mM EDTA.

2.3 Results and Discussion

2.3.1 Generation and Characterization of CL5 and CL5SS

The wild type nNOSr has 10 cysteine residues at position 744, 823, 921, 945, 1088, 1211, 1226, 1244, 1275,1284 and 1349[99]. Prior to engineering a Cys pair on the FMN-FAD interface, it is necessary to remove all other the reactive Cys on nNOSr. Previous Mass spec analysis of A555 labeled wild type identified 5 reactive Cys at position 744, 823, 921, 945 and 1275 (data not shown). They are not in the regulatory regions of nNOSr so they were changed to Ser. This nNOSr variant is referred to as CL5.

E816 and R1229 were selected for FAD/FMN domain cross-linking for two reasons. First, these two residues naturally form a salt bridge between the FAD and FMN domain, implying they are sterically suitable for cross-linking. Second, variant nNOSr with single mutations on E816 or R1228 have been studied previously[113, 114]. The results imply both E816 and R1229 are involved in the FMN domain-related conformational equilibrium. These data also help to predict the impacts of the E816C-R1226C double mutations on nNOSr function. The CL5 nNOSr with E816C R1229C double mutation is referred as locked-down nNOSr or CL5SS.

During the purification process we found both CL5 and CL5SS maintained a normal level of expression. The spectrum of CL5 almost overlaps with the spectrum of wild type nNOS, indicating normal flavin content and flavin environment in CL5 (Fig. 12). Fig 12 also shows that CL5 did not react with A555 dye, confirming it did not have

any remaining dye-reactive Cys. This result agrees well with our mass-spec analysis that identified reactive Cys groups.

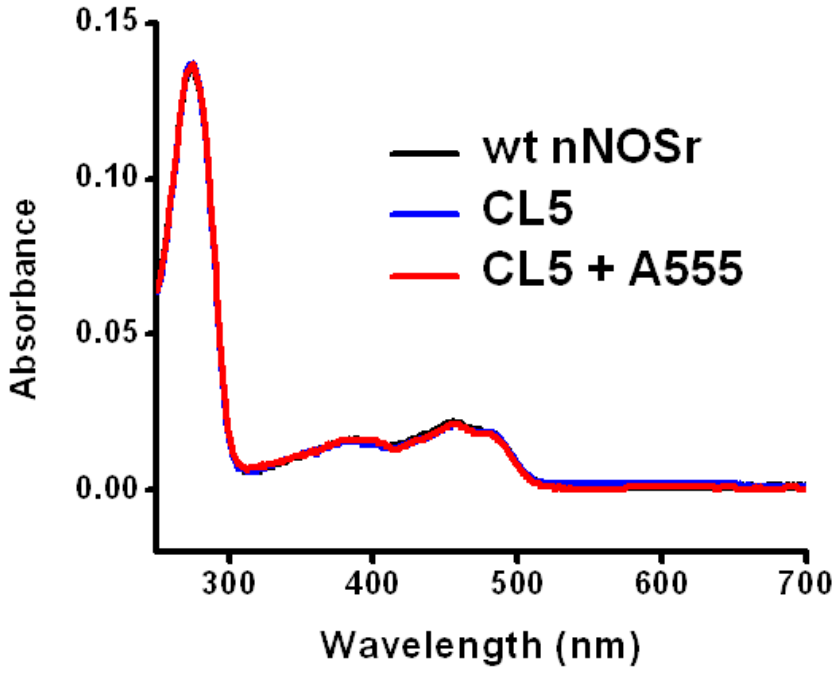

Fig. 12. **Spectra of nNOSr, CL5 and CL5SS**

2.3.2 Validation of Cross-linking of CL5SS

The direct cross-linking reaction of CL5SS by BMs generates side products including uncross-linked CL5SS with 2 bismaleimde groups on one CL5SS molecule as shown in Fig. 9. In order to get rid of such side products, a further separation step using GSH-sepharose to pull out the un-cross-linked nNOSr proteins was applied. To validate our cross-linking method, the percentage of free thiol groups and maleimide groups on

CL5SS cross-linked by BMs (CL5SS-BMs) was quantified. Fig. 13 indicates that < 5% reactive thiol groups remained on all CL5SS-BMs after final processing. CL5SS also had a very similar spectrum with wild type nNOSr, showing CL5SS has normal flavin content. After breaking all the disulfide bonds in CL5SS by incubation with TCEP, every CL5SS molecule had two reactive thiol groups. Also, the fluorescence intensities of 10 μM of CL5SS-BMs were lower than the most diluted dilute NEM standard (0.1μM), making it impossible to quantify the remaining maleimide on CL5SS-BMs. We can only estimate the remaining maleimide was less than 0.01 mol / mol nNOSr. These results show our protocol is robust and capable of generating nearly pure sample of cross-linked CL5SS.

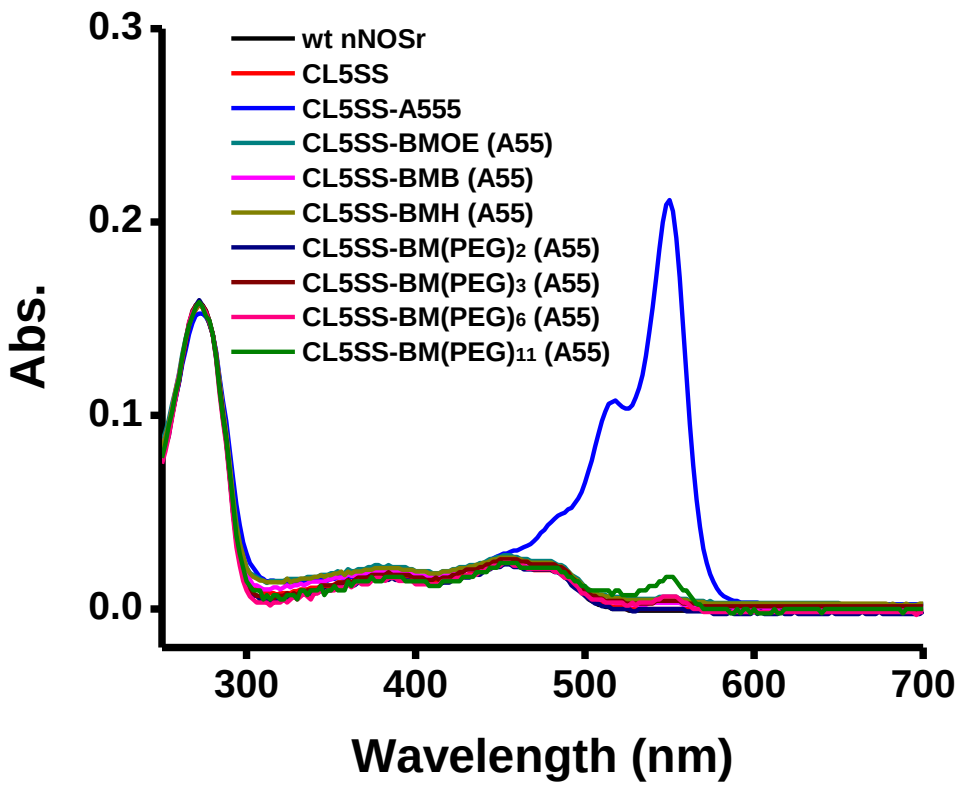

Fig. 13. **Normalized spectra of CL5SS-BMs after incubation with A555.** CL5SS-BMs were reacted with A555 dye and their spectra were compared with wild type nNOSr (negative control), CL5 (negative control) are CL5SS-A555 (positive control).

2.3.3 Steady-state Cytochrome *C* Activity of Cross-linked and DTT Treated CL5SS

Fig 14A shows CL5 has 84% of the activity compared to wild type nNOSr in presence of CaM, and has a 3 times elevated activity compared to wild type nNOSr in absence of CaM. This indicates the 5 Cys-Ser mutations do not impair the electron transfer though CaM-bounded nNOSr. The elevated activity under CaM-free state is commonly found in nNOSr variants with mutation(s) on its FMN or FNR surface[115]. It

is generally believed that such mutations partially remove the self-repression by altering the nNOSr conformation[114, 115]. The fact that relatively minor activity changes were found on CL5 compared to wild type nNOSr indicates that CL5 is a suitable template to engineer the locked-down nNOSr.

Cross-linking the FNR and FMN domains allow us to directly study the impact of FMN domain movement. Figure 14B and 14C shows the activity of disulfide bond cross-linked CL5SS before and after DTT treatment and BMOE cross-linked CL5SS. The results show that cross-linking of nNOSr on its FMN and FNR domain by both disulfide bond and BMOE results in a significant decrease of its cytochrome *c* reductase activity. Moreover, breaking the disulfide bond restored the activity of the disulfide bond cross-linked CL5SS. However, this data did not totally rule out the possibility that it was the nonspecific thiol group oxidation or the thiol maleimide modification, rather than the cross-linking itself, that caused such activity decrease. In order to test this, we examined the activity of two negative control groups under the same conditions. Negative control I was CL5 treated the same as CL5SS. CL5 does not have any reactive Cys thus cannot be cross-linked. This control can determine if the nonspecific thiol group oxidation would inhibit the nNOSr activity. Negative control II was an NEM reacted CL5SS. NEM is a mono-functional maleimide. It is capable of reacting with CL5SS but it cannot cross-link FMN domain with FNR domain. This control can determine if the addition of a maleimide group would inhibit the nNOSr activity. Normalized activities are shown in Fig. 13B. and Fig. 13C. Both of the two negative control groups maintained about 75% of initial activity.

The results confirm that the activity drop observed in locked-down CL5SS was due to the cross-linking between the FMN with FNA domain. Non-specific maleimide effects or simple thiol-maleimide modification did not repress nNOSr activity. The results also confirm the nNOSr is in a conformational equilibrium between an open and a closed conformation involving FMN domain motion and that the closed conformation is largely an inactive conformation.

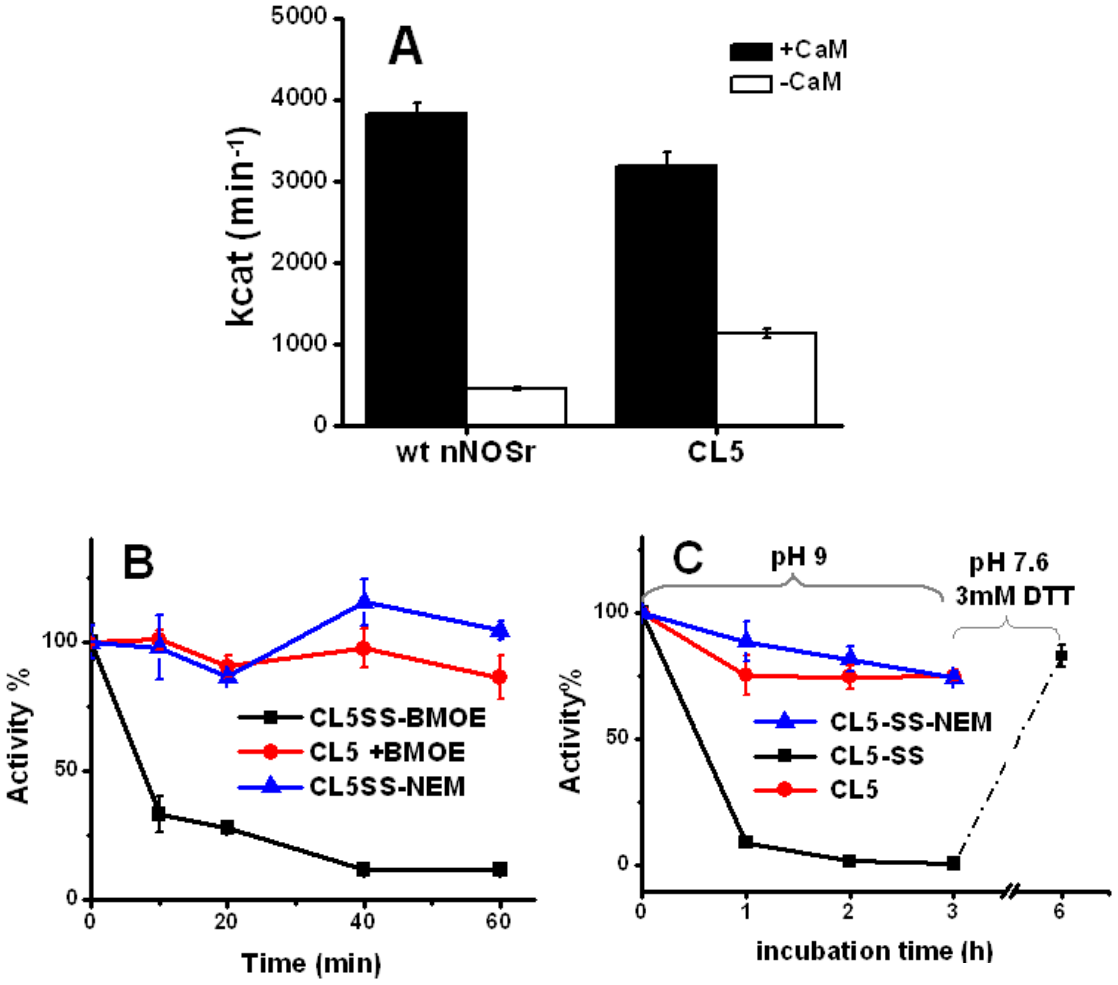

Fig. 14. **Effect of cross-linking on CL5SS**. A, steady-state cytochrome *c* reductase activity of wild type nNOSr and CL5 under CaM-bound and CaM-free condition; B, Activity of BMOE reacted CL5SS (■), CL5 (●) and CL5SS-NEM (▲)over time under CaM bound condition. C. activity of pH 9 or DTT treated CL5SS (■), CL5 (●) and CL5SS-NEM (▲) over time under CaM bound condition.

2.3.4 Cross-linker Length and Activity of CL5SS-BMs

The conclusion that the electron transfer in nNOSr is regulated by FMN domain motion raises another interesting question about how the flexibility of the FMN domain affects the nNOSr actitivity. In order to examine this relationship, we purchased a series of bis- maleimide cross-linkers with arm length ranging from 8 to 52 Å and then cross-linked CL5SS with these cross-linkers. Their steady state cytochrome *c* reductase activity under both CaM-free and CaM-bounded conditions had been measured. The results are shown in Fig 15.

The results show that the CL5SS-BMs with longer cross-linker have higher activity, implying that they support greater electron transfer though nNOSr by enabling nNOSr to adopt a more open conformation. However, the highest cytochrome *c* reductase activity observed under the CaM-bounded condition was still significantly lower than the activity of wild type nNOSr under the same condition. The low activity observed in CL5SS-BMs with long cross-linker might due to combined effects of several factors. First, the length of cross-linker might not reach that required for efficient electron transfer from FMN domain to cytochrome *c*. Also, the cross-linker might cause difficulty for FMN domain to get electrons from FAD due to steric hindrance, similar to the effect of the R1229E mutation on nNOSr[113]. The mechanism of such inhibitory effect requires further investigation.

The results in Fig. 15 also show that CL5SS cross-linked by the BMs almost lost the CaM response. Previous studies imply that CaM binding removes the self-repression on nNOSr by speeding the conformational transitions of nNOSr from closed

conformation to open conformation and also by altering the conformation distribution[100]. The CL5SS-BMs are likely stay in close conformation all the time regardless of CaM binding because the FMN and FAD domains are cross-linked. So it is not surprising that CaM has little effect on CL5SS-BMs.

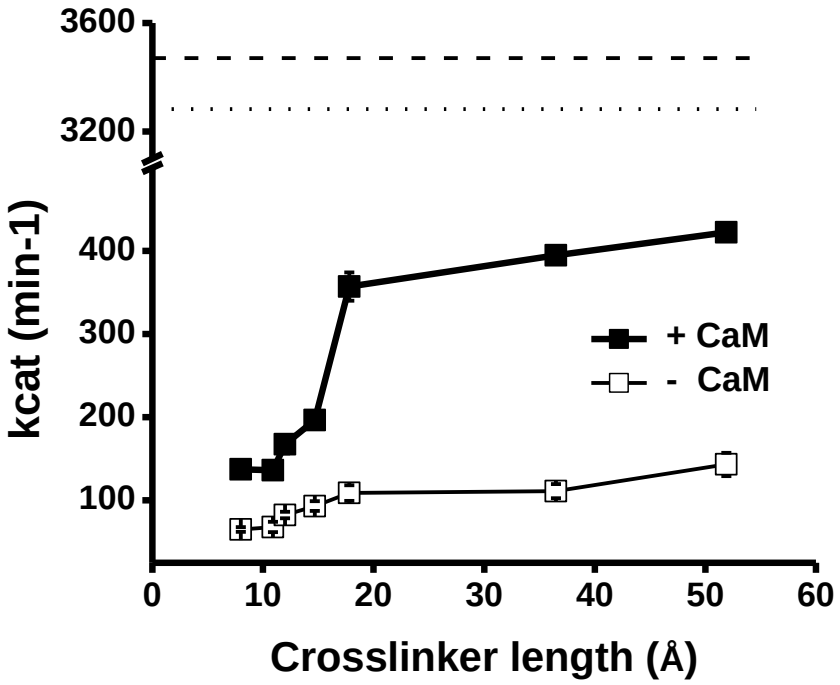

Fig. 15. **Rate of steady-state cytochrome *c* activity *versus* cross-linker length.** Activities were measured at room temperature in presence of (■) or in absence of (□) CaM as described in section 2.2.9. The dot line represents of the activity of CL5SS in present of CaM and the dash line represents the activity of CL5SS in absence of CaM. Values represent the mean and standard deviation of at least three independent measurements.

2.3.5 $NADP^+$ Binding Affinity Is not Affected by Cross-linking.

It is a common feature for oxidized NOSr enzyme that the nicotinamide ring of $NADP^+$ interact with the FAD isoalloxazine to form a charge-transfer complex, resulting in a shift of NOSr absorption spectrum[104]. The difference spectrum of nNOSr before and after $NADP^+$ binding is obtained by subtracting the spectrum of $NADP^+$ free nNOSr from $NADP^+$ bound nNOSr[104]. Here we compared the binding of $NADP^+$ in wild type nNOSr and CL5SS by this spectral shift. The spectral shifted of nNOSr proteins is shown in Fig. 16A. In this figure, the spectral shift of wild type nNOSr has a crest at 510 nm and a trough at 453 nm along with some modulation in the range of 400 nm to 700 nm, in well agreement with a previous report[104]. Similar spectral differences were obtained for both pH9 treated and DTT treated CL5SS. Their peak height at 510 nm and overall spectra are very similar with wild type nNOSr. The results show the $NADP^+$ binds in wild type nNOSr, cross-linked CL5SS or uncross-linked CL5SS in a similar manner, implying the cross-linking does not alter $NADP^+$ binding. To further study the binding between nNOSr proteins and $NADP^+$, nNOSr proteins at equal concentration were titrated with $NADP^+$ and the absorbance increase at 510 nm was plotted versus $NADP^+$ concentration (Fig. 16B). The result shows that both cross-linked and uncross-linked CL5SS also have similar titration curves, indicating that the cross-linking between FNR and FMN domains does not change the binding affinity of nNOSr with $NADP^+$.

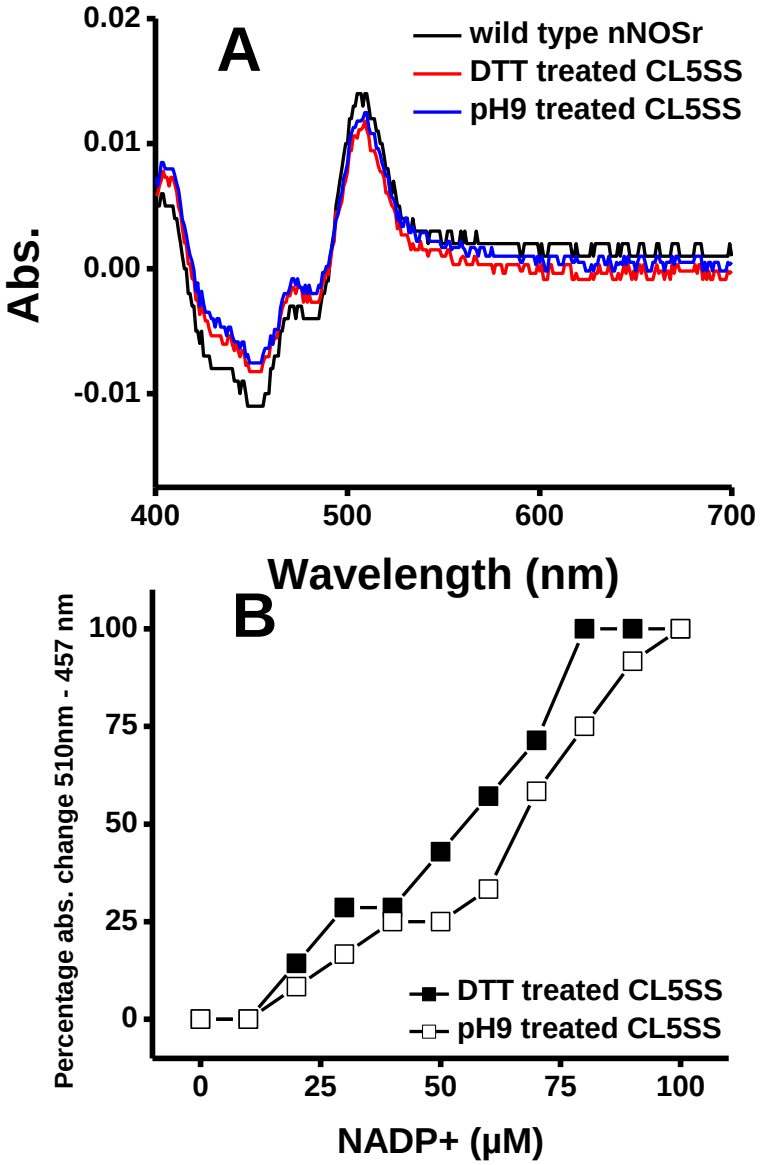

Fig. 16. **Titration of DTT treated CL5SS and pH 9 treated CL5SS with NADP$^+$.** *Panel A*, the difference spectra of wild type nNOSr, DTT treated CL5SS and pH 9 treated CL5SS before and after adding NADP$^+$; b, nNOSr proteins titrated by *Panel B*, each nNOSr protein (20 μM) was titrated with a NADP$^+$ solution. The difference between absorbance change at 510 nm and the absorbance change at 457 were recorded as described in section 2.2.14.

2.3.6 Flavin Reduction Kinetics

Flavin reduction kinetics study is used to examine the electron transfer through NOSr, especially the hydride transfer from NADPH to FAD domain and FAD-FMN inter domain electron transfer[111]. Here we investigated the flavin reduction kinetics of the CLSS-BMs and wild type nNOSr by rapid mixing a 10-fold molar access of NADPH with each nNOSr protein in the stopped-flow instrument. The spectral change of DTT-treated CL5SS and CL5SS-BMOE during this flavin reduction process was obtained and shown in Fig. 17. Their absorbance changes at 457 nm during the flavin reduction were shown in the insert of Fig. 17. This shows both cross-linked and uncross-linked CL5SS achieved the same extent of reduction, which is also similar with wild type nNOSr[111]. During our experiment, we observed an absorption increase at 600 nm with a sequential absorption decrease for both CL5SS-BMOE and DTT treated CL5SS (Fig.18). The results indicate that flavin semiquinone was first formed then decayed during the flavin reduction. The fitted semiquinone formation rate (k_f) and semiquinone decay rate (k_d) were also shown in Fig. 18. Similar phenomenon has been observed in other nNOS mutants[116]. In replica experiments, the absorbance change during the NADPH reduction of CL5SS proteins was monitored at 457 nm to obtain rate constants. The absorbance decrease at 457 nm represents the initial FAD reduction by NADPH and the subsequent reduction of FMN by $FADH_2$. The fitted kinetic parameters are listed and compared in Table I. We also did the two tailed test to compare the flavin reduction rates of DTT-treated CL5SS, which is primarily in open conformation, and cross-linked CL5SS. The rates which are statistically significant differed from the rates of DTT-

treated CLSS were labeled in Table I. The relationship between flavin reduction rates and cross-linker length was shown in Fig. 19. Flavin reduction traces of CL5SS-BMOE and DTT-treated CL5SS were normalized and compared in Fig. 20.

Under both CaM-free and CaM-bound states, the flavin reduction of wild type nNOSr is biphasic, with a fast phase k_1 reflecting the electron transfer from NADPH to FAD, and a slow phase k_2 reflecting the inter-flavin electron transfer from FAD to FMN and further reduction in flavins[111]. CaM binding increases both k_1 and k_2 of wild type nNOSr[111]. The kinetic traces at 457 nm for cross-linked CL5SS were also biphasic with a fast k_1 and slow k_2, and CaM did not alter either k_1 or k_2, indicating CL5SS loses the kinetic repression normally seen in absence of CaM[111]. This is expected results of mutation of E816 and R1229[113, 114]. The similarity of k_1 for both DTT-treated CL5SS and cross-linked CL5SSS indicates the cross-linking does not negatively affect the hydride transfer. In the meantime, an increased k_2 was observed in cross-linked CL5SS with relatively shorter linkers. Also the k_f and k_d of CL5SS-BMOE are faster than the k_f and k_d of DTT-treated CL5SS. The results indicate cross-linking favors the inter-flavin electron transfer in CL5SS. One possibility is that the BMOE connects the FMN and FAD domain in a conformation that facilitates the inter-flavin electron transfer. This conformation may be similar to that observed in the crystal structure of wild type nNOSr, which shows the FAD and FMN are close together in an orientation that could favor inter-flavin electron transfer[99]. The CL5SS-BMOE may stay in this conformation thus resulting in a larger k_2. Other CL5SS-BMs behave more like uncross-linked CL5SS as the cross-linker length increases. Together these results show that the cross-linking did not impair the hydride transfer and facilitates the inter-flavin electron transfer.

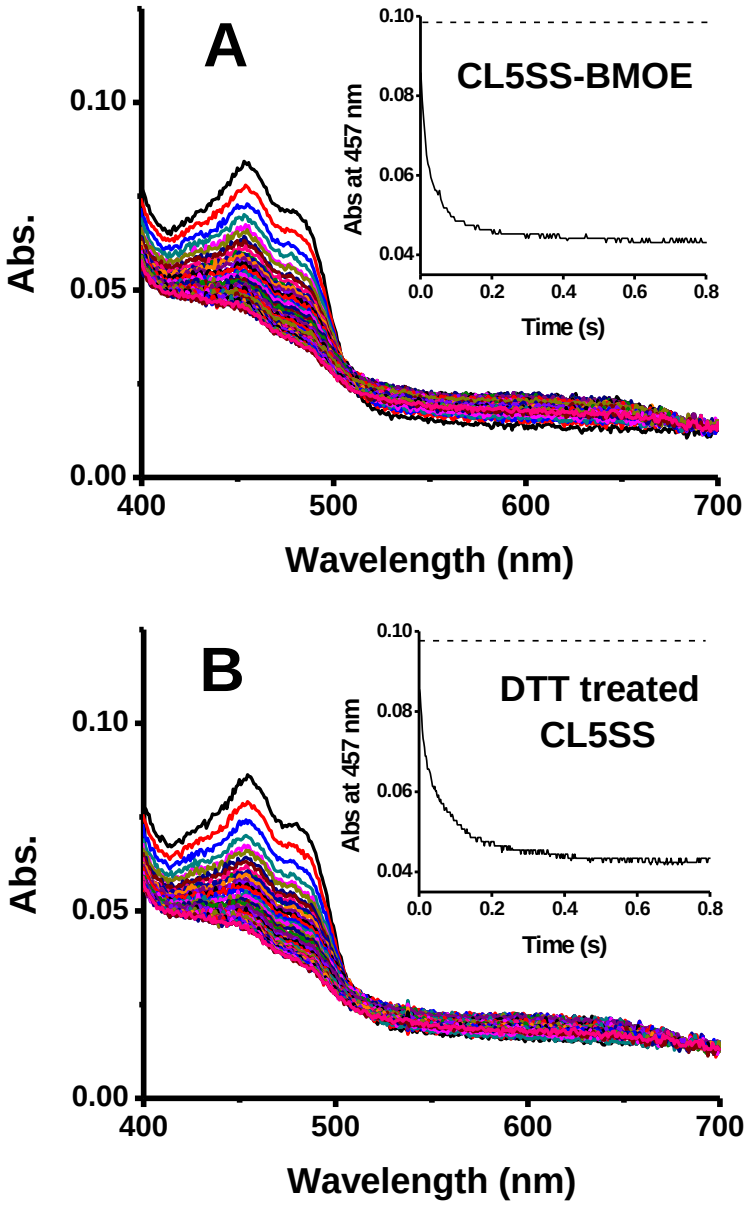

Fig. 17. **Spectral change of CL5SS-BMOE and DTT-treated CL5SS.** *Panel A,* spectral change of CL5SS-BMOE during flavin reduction. *Panel A insert,* absorption change of CL5SS-BMOE at 457 nm during flavin reduction. *Panel B,* spectral change of DTT treated CL5SS during flavin reduction. *Panel B insert,* absorption change of DTT treated CL5SS at 457 nm during flavin reduction.

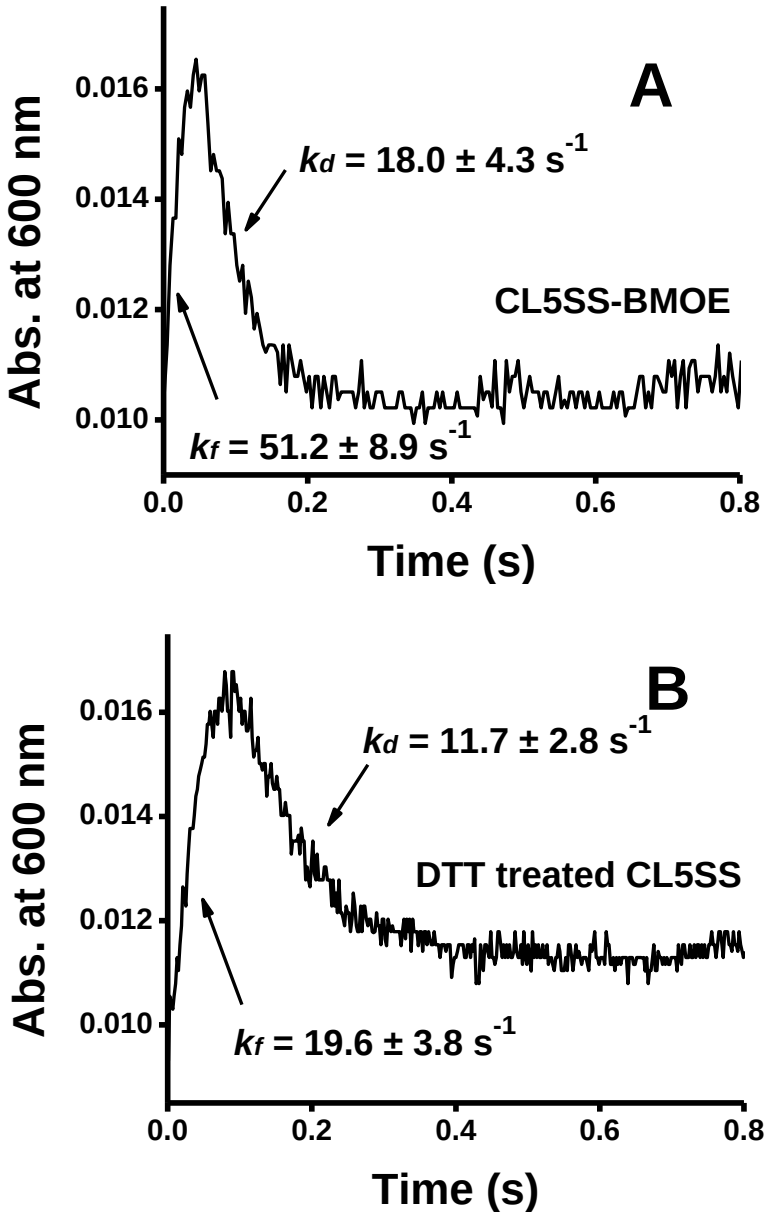

Fig. 18. **Absorption change of CL5SS-BMOE and DTT treated CL5SS at 600 nm.** *Panel A,* absorption change of CL5SS-BMOE at 600 nm during flavin reduction. *Panel B,* absorption change of DTT-treated CL5SS at 600 nm.

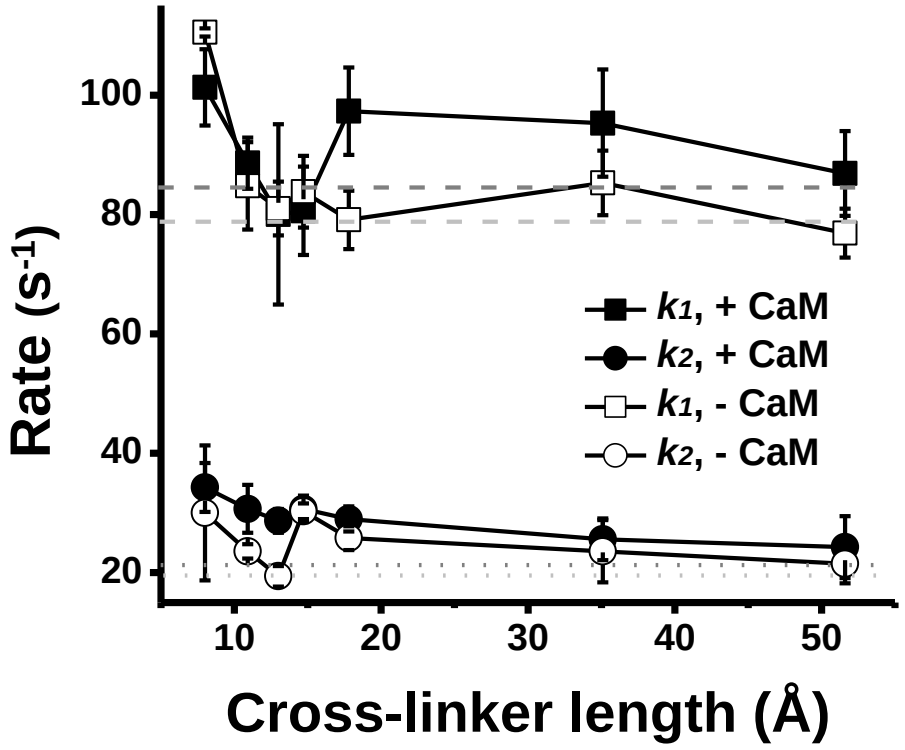

Fig. 19. **Flavin reduction rate *versus* cross-linker length.** The dark gray dash line (--) represents the k_1 for DTT-treated CL5SS in presences of CaM. The light gray dash line (--) represents the k_1 for DTT-treated CL5SS in absence of CaM. The dark gray dot line (⋯) represents the k_2 for DTT-treated CL5SS in presences of CaM. The light gray dot line (⋯) represents the k_2 for DTT-treated CL5SS in absence of CaM.

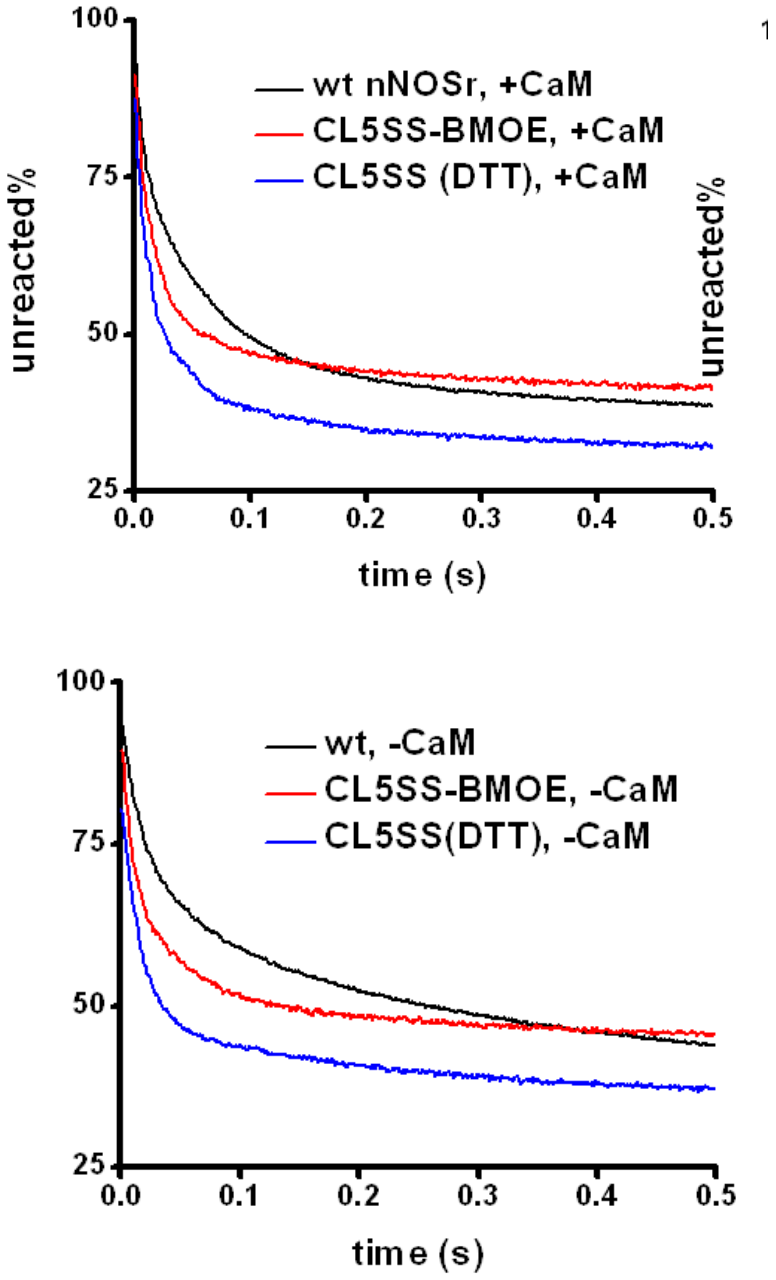

Fig. 20. N**ormalized kinetic trace of CL5SS-BMOE, DTT treated CL5SS and wild type nNOSr**

Table I. *Kinetic parameters of nNOSr protein flavin reduction.* Rates with ** are rates with p less than 0.01. Rates with * are rates with P less than 0.05 but more than 0.01.

	+CaM		-CaM	
Protien	*k1*	*k2*	*k1*	*k2*
	s^{-1}	s^{-1}	s^{-1}	s^{-1}
wt nNOSr	80.8 ± 2.2	12.1 ± 0.6	40.3 ± 7.7	3.1 ± 2.7
CL5SS (DTT)	84.9 ± 13.2	21.3 ± 4.2	79.5 ± 14.5	19.9 ± 3.0
CL5SS-BMOE	*101.3 ± 6.4	**34.3 ± 4.1	110.5 ± 0.7	*30.0 ± 11.3
CL5SS-BMB	88.6 ± 4.3	**30.7 ± 4.0	84.8 ± 7.3	*23.6 ± 1.2
CL5SS-BMH	80.0 ± 15.1	*28.7 ± 2.0	81.0 ± 4.5	19.4 ± 1.7
CL5SS-BM(PEG)2	80.6 ± 7.4	**30.7 ± 2.2	83.8 ± 6.0	**30.3 ± 1.3
CL5SS-BM(PEG)3	97.3 ± 7.3	*29.0 ± 2.1	79.1 ± 4.9	*25.8 ± 2.0
CL5SS-BM(PEG)6	95.3 ± 9.0	25.6 ± 3.5	85.3 ± 5.4	23.6 ± 5.2
CL5SS-BM(PEG)11	86.9 ± 7.1	24.3 ± 5.2	76.9 ± 4.1	21.5 ± 3.3

2.3.7 Cross-linking Shifts the K_{hq} Set Point of nNOSr

Reaction with excess cytochrome *c* is a direct way to study the conformational K_{hq} setpoints ([open-reactive]/[closed-unreactive]) of fully-reduced nNOSr proteins and their flavin semiquinone/hydroquinone cycling[99]. In this experiment, the fully-reduced (four electron reduced by photo reduction), NADPH bound nNOSr is mixed with 5-10 fold molar excess of cytochrome *c*[109]. Based on our model (Fig. 7.) and previous kinetic studies, nNOSr exists in active open or closed conformations that are in

equilibrium. It has been shown that, under this particular experimental setting that the fully-reduced nNOSr in an open conformation transfers an electron from FMNhq to cytochrome *c* with a rate of 225 s^{-1}, making the reaction between the open conformation and cytochrome *c* occur within the stopped-flow instrument mixing dead time, and so cannot be observed in our experiment [109]. In comparison, the model assumes that the nNOSr in closed conformation is not capable of directly reducing cytochrome *c* and only reduce cytochrome *c* after transforming into an open conformation[109]. This transformation depends on the conformational opening, which is slow enough to be observed by our instrument[109]. So, two different species of nNOSr contribute to the absorbance change within reduction of the first molar equivalent of cytochrome *c*. The absorbance change during the dead time, and from that time to the time point that one equivalent of cytochrome *c* is reduced, represents the distribution of open *versus* closed conformational states, giving an estimation of K_{hq}. Here we reacted excess cytochrome *c* with our locked-down CL5SS, DTT treated CL5SS and nNOSr wild type. The representative traces are shown in Fig. 21. The horizontal dash line represents the absorption increase for one equivalent of cytochrome *c to be* reduced. The vertical dash line represents the time it took to reduce one equivalent of cytochrome *c*. The solid horizontal line is the cytochrome *c* absorption baseline. The relationship between K_{hq} and cross-linker length is shown in Fig. 22.

In all the nNOSr proteins we observed same initial fast phase (absorbance gain in the dead time) and a slower linear phase. The activity of nNOSr proteins calculated from the tangents of the linear phase matches well with their steady state cytochrome *c* activity, suggesting a change from pre-steady state electron transfer to steady-state

electron transfer occurs quickly. This phenomenon has also been observed in other dual-flavin enzyme systems[109]. Data in Fig. 21 shows that the tested CL5SS proteins have different conformational equilibrium setpoints (K_{hq}). The zero time absorbance of reduced CL5SS-BMOE is very close to the absorbance of cytochrome *c* itself, showing NADPH-bound fully-reduced CL5SS-BMOE almost completely remains in the closed conformation. The time it took for CL5SS-BMOE to reduce one equivalent cytochrome *c* is longer than the CaM-free wild type nNOSr, suggesting the BMOE-cross-linking causing difficulty for FMNhq to donate electrons to cytochrome *c*. In contrast, the dead time absorbance change of the DTT-treated CL5SS-BMOE is very close to the absorbance for reducing one equivalent of cytochrome *c*, showing that the fully reduced CL5SS is almost completely open conformation even in the CaM-free state. The time required to reduce one equivalent cytochrome *c* is very close to the instrument dead time, also suggesting DTT treated CL5SS-BMOE stays in open conformation. Interestingly, CL5SS-BM$(PEG)_{11}$ has a relatively low cytochrome *c* activity but a high K_{hq} value, that indicates more than 60% of CL5SS-BM$(PEG)_{11}$ is in a reactive open conformation when fully reduced and bound with NADPH. The extended BM$(PEG)_{11}$ cross-linker is over 40 angstroms long and it is not surprising that the BM$(PEG)_{11}$ provides enough space for cytochrome *c* to get close enough to the FMN for electron transfer. Also, BM$(PEG)_{11}$ can rotate around its C-C and C-O bonds to create conformational diversity. However, the time it took to reduce one equivalent cytochrome *c* is still similar with CaM-free wild type nNOSr. This suggests that the CL5SS-BM$(PEG)_{11}$ has a lower activity than the wild type nNOSr. Moreover, and after donating the first electron, CL5SS-BM$(PEG)_{11}$ may have difficulty to continue donating electrons to cytochrome *c*. It is likely that the

$BM(PEG)_{11}$ cross-linker inhibits the FMN domain from getting back to FAD to form a closed structure thus causing a problem for electron transfer in *Ksq*. This is similar to the effect of mutation on residue R1229[113]. These data show that the cross-linker may impair electron transfer by a combined effect of preventing electron transfer from FMN to cytochrome *c*, and by preventing FMN domain dynamics and electron transfer.

Data in Fig. 21 and Fig. 22 show that fully-reduced, NADPH-bound CL5SS-BMH, CL5SS-$BM(PEG)_2$ and CL5SS-$BM(PEG)_3$ have a percentage of molecules in the open conformation that increases with cross-linker length. This implies that even in cross-linked form, the heme in cytochrome *c* may still get close enough to the FMN for electron transfer, and the longer cross-linkers allow the heme in cytochrome *c* to get closer to the FMN and thus favor electron transfer.

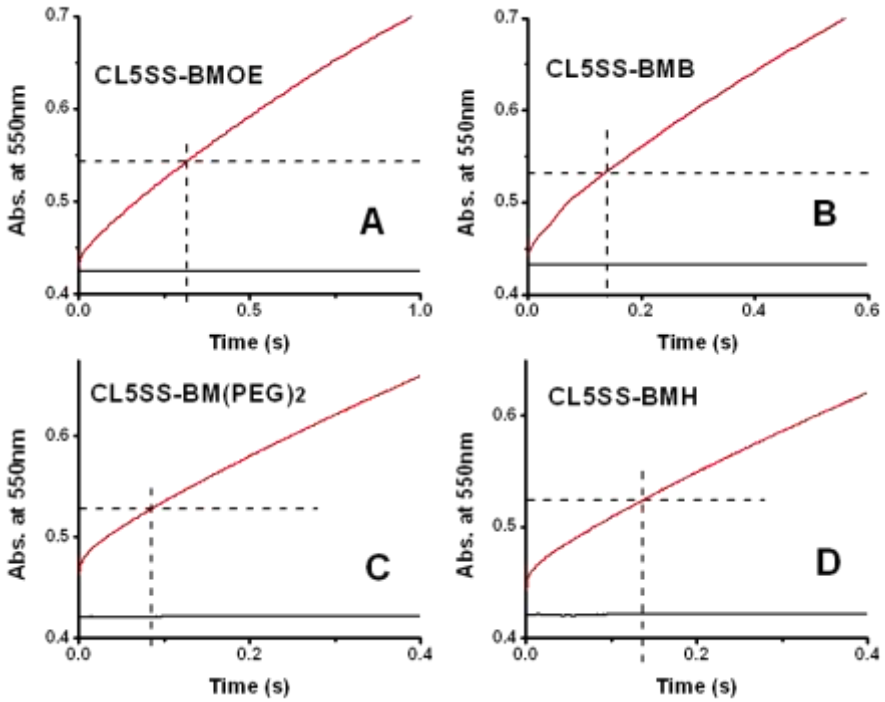

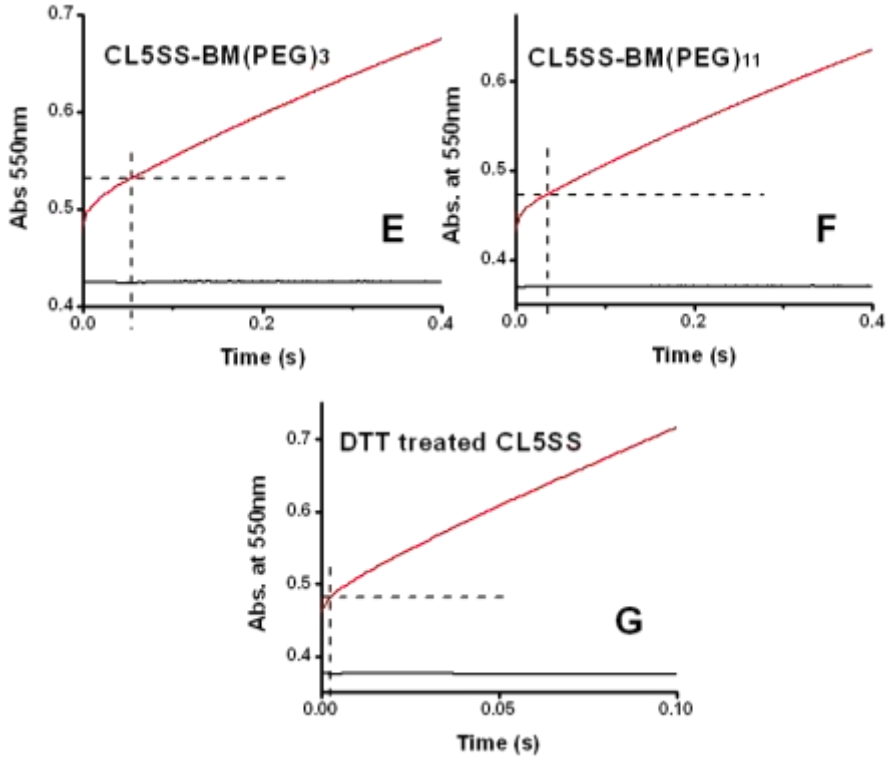

Fig. 21. **Pre-steady-state cytochrome *c* reduction traces of CL5SS proteins**. Solid horizontal line is the cytochrome *c* absorption baseline. Dash horizontal line is the absorbance of reducing 1 equivalent of cytochrome *c*. Vertical dash line is the time took to reduce 1 equivalent of cytochrome *c*. *Panel A*, pre-steady-state cytochrome *c* reduction traces of CL5SS-BMOE. *Panel B*, pre-steady-state cytochrome *c* reduction traces of CL5SS-BMB. *Panel C*, pre-steady-state cytochrome *c* reduction traces of CL5SS-BMH. *Panel D*, pre-steady-state cytochrome *c* reduction traces of CL5SS-BM(PEG)$_2$. *Panel E*, pre-steady-state cytochrome *c* reduction traces of CL5SS-BM(PEG)$_3$. *Panel F*, pre-steady-state cytochrome *c* reduction traces of CL5SS-BM(PEG)$_{11}$. *Panel G*, pre-steady-state cytochrome *c* reduction traces of DTT treated CL5SS.

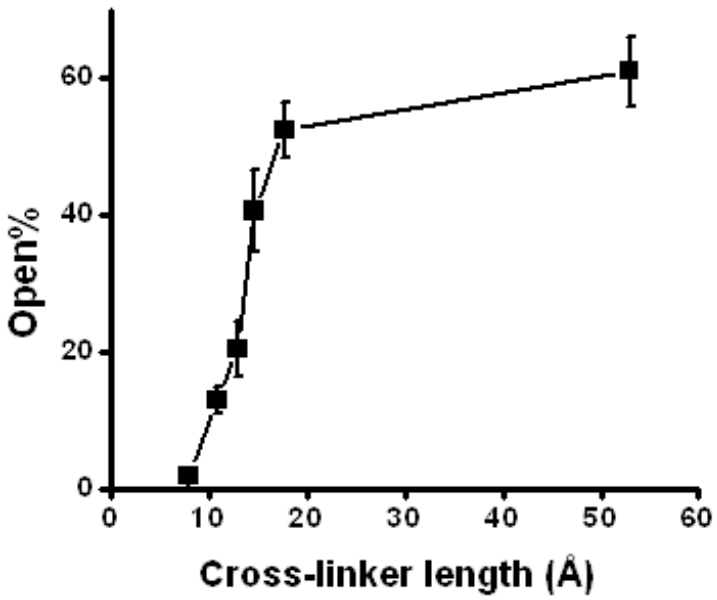

Fig. 22. **Cross-linker length *versus* K_{hq}.**

2.3.8 Flavin Fluorescence

Intrinsic flavin fluorescence of nNOSr has been observed previously and CaM binding increases the flavin fluorescence intensity of wild type nNOSr[104, 112]. Here we utilized the locked-down CL5SS to study the relationship between flavin fluorescence and conformation. In this experiment, we first induced CaM binding by adding Ca^{2+} to sample which contains nNOSr protein and CaM. Then we stripped CaM down from nNOSr protein by adding excess of EDTA. The flavin fluorescence of CL5SS-BMOE, DTT-treated CL5SS, pH9 treated CL5SS and wild type nNOSr during the experiment were monitored as shown in Fig. 23.

Results show that CL5SS-BMOE and wild type nNOSr have similar fluorescence intensity in CaM-free state. CaM binding caused an increase of fluorescence intensity of wild type nNOSr but only caused a small increase of fluorescence intensity of CL5SS-BMOE. The fluorescence intensity of the CaM-free DTT-treated CL5SS is similar to the fluorescence intensity of CaM-bound wild type nNOSr. Also, CaM binding had a small effect on its fluorescence intensity. Considering that the CL5SS-BMOE is in a closed conformation, while the DTT-treated CL5SS is primarily in open conformation, it is clear that conformation has a strong impact on flavin fluorescence, and that CaM binding changes wild type nNOSr from a closed conformation to an open conformation. In the CaM-free state, the flavins in wild type nNOSr are buried in the interior of the protein, as shown in the crystal structure. It is likely that CaM binding favors the FMN domain release and converts the flavins to an exposed state, resulting in a stronger fluorescence.

2.4 Conclusion

This chapter described our approach to study the structure - function relationship of nNOSr by locking down domains using cross-linkers of varying length. The engineered locked-down nNOSr proteins allowed us to study the property of nNOSr in its closed conformation and a series of partly open conformations. Our results directly support the existence of a conformational equilibrium of nNOSr between a closed conformation and an open conformation, which is dynamic and involves FMN domain motion. Our results also show that nNOSr in a closed conformation has a normal $NADP^+$ binding affinity and hydride transfer rate, and a slightly faster interflavin transfer rate, but has a impaired electron transfer rate to its substrate and an overall lowered activity. The flavin fluorescence changes confirmed the conformational behaviors. The

bismaleimide cross-linkers also proved to be useful tools to study the distance - activity relationship of FMN domain motion. The locked-down protein can be also applied to study other conformation-related regulatory elements in NOS including the CT and related residues[101, 103, 116].

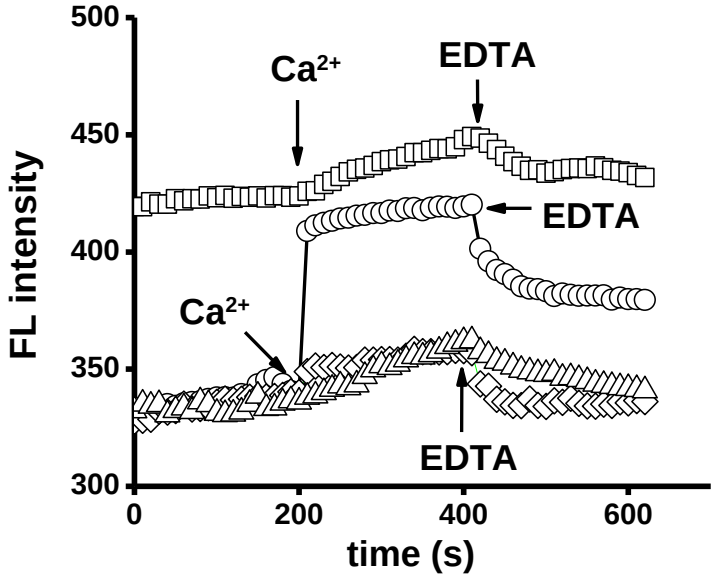

Fig. 23. **Flavin fluorescence of nNOSr proteins**. The flavin fluorescence of wild type nNOSr (○), DTT-treated CL5SS (□), pH-9 treated CL5SS (Δ) and CL5SS-BMOE (◊) were monitored before and after Ca^{2+} and EDTA as described in section 2.2.15.

CHAPTER III

DEVELOPMENT OF AN ASSAY QUANTIFYING NITRIC OXIDE SYNTHASE ACTIVITY OF BACTERIAL NITRIC OXIDE SYNTHASE AND CELL CYTOSOL

3.1 Introduction

3.1.1 Significance of NOS Activity Assay

Dedicated NO production by NOS is required for all NO-related functions[22, 37]. Over- or under- production of NO by NOS manifests in numerous human diseases and changes the bacterial lifespan[25, 40, 44]. The relationship to NO concentration makes the quantification of NO key for understanding its biological and physiological processes, and is a mainstay of NOS characterization. NOS activity measurements have proven invaluable in understanding NOS function, catalysis and regulation[37, 101, 103, 112]. It is also an indispensable tool for NOS inhibitor characterization and selection[117, 118].

3.1.2 Physiological Chemistry of NO

NO is a gaseous radical with very short half-life[119]. The NO produced by NOS is converted into more stable compounds immediately after being released by NOS[119]. The major downstream products for NO are the nitrite (NO^{2-}) and nitrate (NO^{3-})[119]. In buffer or other physiological fluids, NO is almost completely oxidized into nitrite[119]. The stepwise oxidation of NO by O_2 is shown below[119].

$$2NO + O_2 \rightarrow 2NO_2 \quad (1)$$

$$2NO + 2NO_2 \rightarrow 2N_2O_3 \quad (2)$$

$$2N_2O_3 + 2H_2O \rightarrow 4NO_2^- + 4H^+ \quad (3)$$

Although the oxidation of nitrite by oxygen is very slow in buffer[119], the produced nitrite in blood can be oxidized into more stable nitrate within several minutes[119]. One possible mechanism is the oxidation by certain oxyhemoproteins (P-$Fe^{2+}O_2$) such as oxyhemoglobin (oxyHb)[119]. The reactions are shown below:

$$2P\text{-}Fe^{2+}O_2 + 3NO_2^- + 2H^+ \rightarrow 2P\text{-}Fe^{3+} + 3NO_3^- + H_2O \quad (4)$$

or

$$4P\text{-}Fe^{2+}O_2 + 4\ NO_2^- + 4H^+ \rightarrow 4P\text{-}Fe^{3+} + 4\ NO_3^- + O_2 + 2H_2O \quad (5)$$

Another proposed mechanism is the direct oxidation of NO into nitrate by oxyhemoproteins before nitrite formation[119]. In this process, oxyhemoproteins are converted into methemoproteins[119].

$$P\text{-}Fe^{2+}O_2 + NO \rightarrow P\text{-}Fe^{3+} + NO_3^- \quad (6)$$

However, the mechanism of nitrate formation is not entirely clear till now and requires further investigation.

Besides being oxidized by oxygen, NO can react with superoxide species to generate RNS including peroxynitrite ($ONOO^-$) and peroxynitrous acid (ONOOH)[119]. Both peroxynitrite and peroxynitrous are strong oxidants and potentially involved in several pathological conditions[119]. The reaction was shown below.

$$O_2^- + NO \rightarrow ONOO^- + H^+ \leftrightarrow ONOOH \rightarrow NO_3^- + H^+ \quad (7)$$

Moreover, potent nitrating species nitrosoperoxycarbonate anion ($ONOOCO^{2-}$) can be produced in a non-enzymatic pathway from NO and O^{2-} in present of CO_2/HCO^{3-}[119]. The reaction is shown below.

$$NO + O_2^- \rightarrow ONOO^- + CO_2 \rightarrow ONOOCO_2^- \rightarrow NO_3^- + CO_2 \quad (8)$$

3.1.3 Assays Auantifying NO

Although directly quantification of the short-lived NO is technically difficult, quantification of the NO deviated compounds listed in section 3.1.2 is practical. Here we described the most commonly used methods allowing accurate quantification of NO.

3.1.3.1 Detecting the nitrite and nitrate using Griess assay

Griess assay is colorimetric nitrite assay. It is one of the most commonly used methods to determinate the NO production by quantifying the stable NO derivative nitrite and nitrate using sulfanilamide and N-alpha-naphthyl-ethylenediamin, which are referred to as Griess reagents[119]. The Griess reaction is a two-step reaction as shown in Fig. 24[119]. In this reaction, nitrite first reacts with the sulfanilamide to product a diazonium

ion. This diazonium ion then reacts with the azo dye reagent (N-alpha-naphthyl-ethylenediamin) producing a pink color compound with maximum absorbance at 540 nm, which is easily detected by UV-Vis spectrum[119]. Pre-reduction step is needed for the nitrate detection by Greiss assay because nitrate does not react with Griess reagents[119]. *Aspergillus* nitrate reductase is commonly used to reduce nitrate to nitrite[119]. Importantly, the NADPH in samples requires special attention because this inevitable component for NOS catalysis is a also strongly inhibits the Griess reaction[119]. Excess of lactate dehydrogenase (LDH) and pyruvate is commonly used to consume the excess NADPH in the samples before performing the Gress assay[119]. Potassium ferricyanide is an alternative of consuming NADPH[119]. Although the nitrite can be quantified directly using the absorption at 540 nm, a standard nitrite curve it is commonly used for its quantification[119].

The color product of Greiss reaction can be quantified by not only the UV-Vis spectrophotometer but also high throughput instrument such as a 96-well plate reader or a HPLC. Highly automated HPCL instruments, ENO-20 developed by EiCom is commercially available specially designed for nitrite/nitrate detection[119]. The nitrite and nitrate are first separated on a reverse phase column. After that the separated nitrate is reduced into nitrite by a reduction column packed with cadmium and reduced copper connected with the reverse phase column. These two separated peaks are then mixed with Greiss reagent and their peak areas are used to accurately quantify the nitrite and nitrate with a standard curve obtained from nitrite standards[119]. Ideally this system has nM level detection limit and small matrix effect since contaminations are separated with nitrite/nitrate by the reverse phase column[119].

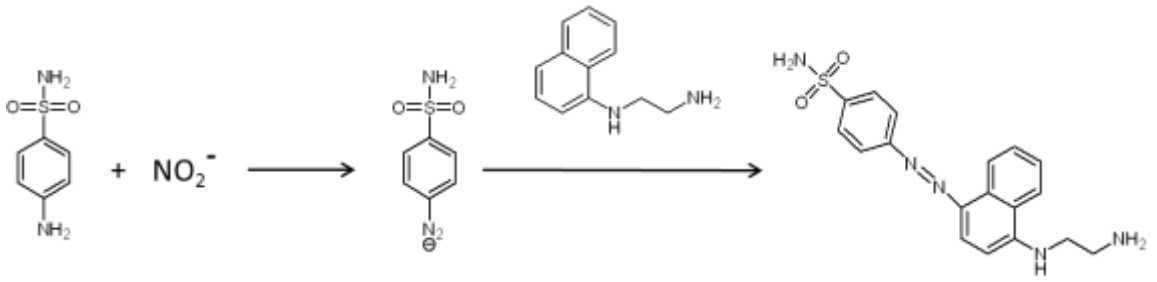

Fig. 24. **Scheme of Greiss reaction**

3.1.3.2 Fluorometric Assays

In order to detect trace amount of NO derived nitrite in biological samples, different fluorometric methods have been developed. Here we describe two of the most commonly used fluorometric assays.

The diaminonaphthalene assay

2,3-diaminonaphthalene (DAN) is an aromatic diamino compound with weak fluorescence[119]. However, the reaction between DAN and nitrite produces a highly fluorescent 2,3-naphthotriazole, which can be used directly for nitrite quantification[119]. The produced 2,3-naphthotriazole has very high quantum yield, making the detection limit of this assay as low as 10-30 nM[119]. Besides the amazing sensitivity, this assay is very specific since DAN is a very specific reactant for nitrite[119]. Moreover, DAN reacts fast with nitrite, which makes it a suitable NO indicator[119]. The high sensitivity

and specificity makes the diaminonaphthalene assay ideal for nitrite detection in biological samples, which has low nitrite concentration and contains various contaminants[119].

The Diaminofluoroscein-2 Assay

Similar to DAN, the relatively non-fluorescence compound diaminofluoroscein-2 (DAF-2) can react with nitrite formation a highly fluorescent triazole compound[119]. Different from DAN, the excitation wavelength of the resulting triazole compound locates in the visible light range, which makes it compatible with *in vivo* studies[119]. Moreover, this assay can be used to directly quantify the tiazole derivative produced by NO-derived nitrosation and oxidative nitrosylation in cell[119]. However, the specificity of DAF-2 is not as desirable as DAN. Previous study show except for nitrite, DAF-2 can react with nitroxyl and produces triazole compound, resulting a false positive result[119]. The auto fluorescence of DAF-2 also makes this assay unsuitable for low concentration detection[119]. The properties of DFA-2 limit the performance of this assay.

3.1.3.3 Oxyhemoglobin Assay

Instead of quantifying the NO derived compound such as nitrite and nitrate, the oxyhemoglobin (oxyHb) assay quantifies the methemoglobin (metHb) production as shown in equation (6). The oxyHb – metHb conversion can be characterized by an absorbance increase at 401 nm, which can be monitored directly by UV-Vis

spectrophotometer[114]. Compare to the Griess assay and the fluorometric assays, this assay offers advantage to monitor the real-time NO production because hemoglobin does not interfere NO production by NOS and absorbance change can be monitored in real-time by UV-Vis spectrophotometer[114]. This assay provides unique advantages to study the steady-state NO production by NOS within several minutes and has been widely used to study the kinetics of NOS[114].

3.1.4 Special Concerns about Bacterial NO Detection

Several attempts have been made to quantify the NO synthesis activity of bNOS. These assays, in general, require an external reductase partner for bNOS to facilitates an electron transfer chain for NO production since most bNOSs do not have a covalently attached reductase[80, 81, 120-122]. This makes the selection of external reductase partner the first priority for bNOS assay setup. The first tested reductase partner of bNOS is the reductase domain of nNOS and it has been showed that the nNOSr is a very poor electron donor for bNOS[80]. After that, study shows bacterial flavodoxin and flavodoxin reductase can act together as reductase partner for bsNOS with decent efficiency[120]. More recent studies discovered a more efficient bacterial flavodoxin reductase for bsNOS NO[117]. Although attempts have been made to identify the bona fide reductase partner proteins of bNOS, study suggests there is no dedicated reductase partner for bNOS[84]. This also implies each bNOS may have different optimal choice of reductase partner.

3.1.5 Special Concerns about NO Detection in Live Tissue

Due the complex matrix effect of biological samples, sample preparation is usually needed before conducting the quantification of the target NO derivatives[119]. It is extremely important not to artificially create NO derived contaminations during the sample preparation. Nitrite may metabolize quickly in biological samples including blood and cell culture by redox active metals such as thiols, resulting in formation of unstable nitroso/nitrosyl compounds, which will interfere the nitrite quantification[119]. It is important to preserve the sample integrity when collecting the sample. These unwanted reductions are commonly inhibited by perfusing sample with NEM and EDTA[119]. NEM blocks the thiols, prevents the formation of nitroso/nitrosyl compounds and EDTA chelates with metal ions and inhibits the transition metal catalyzed transnitrosation and degradation of endogenous RSNOs and nitrite[119].

Although these sample preparation methods increase the reliability of test, the analysis of blood samples can still be tricky. First, blood must be withdraw as rapidly as possible and be centrifuged immediately to separate red blood cells (RBCs) from the plasma to prevent hemolysis[119]. The blood withdrawal should take no more than 20 seconds otherwise hypoxia will be render and this will affect the steady state NO products[119]. Rapid perfusion of NEM/EDTA is required to inhibit the nitrite metabolism and minimize the hypoxia[119]. Usually the sample needs to be homogenized within 2 minutes and analyzed immediately afterwards[119]. Reduced ambient lighting conditions (<15 Lux) is need during sample preparation to minimize the photolysis of biological NO metabolites[119].

The analysis of plasma samples can also be problematic because the heparinized plasma may be precipitated by the acidic Griess reagent, making these samples difficult to analyze[119]. Addition of anticoagulant such as EDTA/DTPA may prevent this problem[119]. Also, pre-precipitation of heparin by protamine sulfate will in many cases allows the direct determination of nitrite in blood sample[119].

Comparing to blood, urinary samples are much easier for analysis due to its relatively smaller matrix effect[119]. The urine nitrite analysis is also a non-invasively method to quantify the *in vivo* NO metabolites level[119]. However, the tested nitrite level is a reflection the sum of endogenously product nitrite, dietary nitrite and nitrite produced by bacteria found in the gut[119]. Thus animals should either be fastened before collecting urine sample[119]. Also, it is import to include antibiotics in to prevent growth of bacteria in the collecting tubes to minimize the nitrite production by bacteria in sample[119].

3.1.6 PEGylation of Hb

Methoxypolyethylene glycol 5000 conjugated hemoglobin (MP4 or Hb-PEG) is initially developed as a vasodilatory hemoglobin based O_2 carrier (HBOC) to fit for the need of transfusion as a replacement of red cells[123]. Studies show Hb-PEG maintains a high oxygen binding affinity and does not cause apparent arterial blood pressure increase, which is the major problem of most of HBOCs[123]. Soon after that, the kinetics of NO association with PEGylated deoxyhemoglobin (deoxyHb-PEG) and NO oxidation by PEGylated oxyhemoglobin (oxyHb-PEG) have been studied[124]. The results show

PEGylation on hemoglobin does not altering NO association while slightly slows the NO oxidation rates, indicating PEGylation does not significantly change the chemistry property of the heme center in the hemoglobin[124].

3.1.7 Aims

While an assay for the direct quantification of nitric oxide, suitable for high through-put analysis for both purified proteins and cell cytosol has not yet been reported, we set out to develop an assay to address the following methodological hurdles: a) increase coupling of electron transfer from the orthologue flavodoxins to saNOS, b) improve detection and sensitivity by direct capture of NO produced by purified saNOS or cell cytosol containing NOS using oxyHb-PEG, and c) reduce assay time and workup procedures to enable large sample throughput.

3.2 Experiments

3.2.1 Materials

Methoxypolyethylene glycol 5000 maleimide (PEG-MAL5K) was obtained from Sigma. All other reagents and materials were obtained from Sigma or source previously elsewhere[120].

3.2.2 Expression and purification of iNOS, saNOS, FLDR and YkuN

pCWori vector containing both DNA of a wild type rat Δ65iNOS full length (AA65-1269) with a His_6 tag and rat calmodulin (CaM) were co-transformed into *E. coli* stand BL21 (DE3) for overexpression[125]. CaM was co-transformed to prevent full length iNOS from proteolysis in the CaM binding region[125]. Transformed *E. coli* cells were inoculated in 500 mL LB media at 37°C in presence of 100 mg/mL ampicillin and 100 mg/mL chloramphenicol with vigorous shaking (250 rpm) overnight. Eight 2 L flasks each containing 50 mL of overnight culture, 450 mL TB and the same antibiotics were used for expression. The cultures were grown at 37 °C with vigorous shaking. 1 mM IPTG and 1 mM δ-aminolevulinic acid was added to induce iNOSr expression when OD_{600} reached 0.8~1.0. Cultures were transferred to room temperature and grown for another 72 hrs with vigorous shaking (250 rpm). The cells were harvested by centrifuging at 5000 rpm for 30 min. The cell pellets were resuspended with minimum volume of 40 mM EPPS, 150 mM NaCl, 10% glycerol, pH 7.6 containing protease inhibitors, PMSF and lysosome. The resuspended cells were sonicated using a Branson digital sonifier on ice (3 × 35 s bursts on 35% power, interspaced by 1min). All of the following procedures were done at 4 °C unless indicated specifically. The lysate were centrifuged at 13000 rpm for 1 hr and the clear supernatant was loaded onto a gravity Ni^{2+}-nitrilotriaceteta (Ni-NTA) affinity column pre-equilibrated with 40 mM EPPS, 150 mM NaCl, 10% glycerol, pH 7.6. The column was washed with 200 ml of 40 mM EPPS, 500 mM NaCl, 10% glycerol, pH 7.6 containing 40 mM imidazole and eluted with 100 ml of 40 mM EPPS, 150 mM NaCl, 10% glycerol, pH 7.6 containing 160 mM imidazole. The eluted protein

was load onto another 2'5' ADP sepharose affinity column pre-equilibrated with 40 mM EPPS, 150 mM NaCl, 10% glycerol, pH 7.6. The column was washed with 200 ml of 40 mM EPPS, 500 mM NaCl, 10% glycerol, pH 7.6 and eluted with 40 ml of 40 mM EPPS, 150 mM NaCl, 10% glycerol, pH 7.6 containing 1 mM NADPH and 3 mM 2'(3')-AMP. Eluted full length iNOS was concentrated using a Millipore concentration unit with 50 kD cut off(EMD Millipore, MA) then dialyzed three times against 1 L of 40 mM EPPS, 150 mM NaCl, 10% glycerol, pH 7.6 with 1mM DTT. Concentrated iNOS was aliquoted and stored in -70°C. iNOS concentration was measured from ferrous-CO complex using an extinction coefficient of 76 mM^{-1} cm^{-1} at 444 nm[120].

saNOS DNA subcloned into pBAD vector from *S. aureus* chromosome using NcoI and EcoRI sites was a generous gift from Dr. Ivan Gusarov in New York University Medical School. Recombined pBAD-saNOS plasmid was transformed into *E. coli* strain BL21 (DE3) for protein expression. Transformant *E. coli* cells carrying pBAD-saNOS plasimd grew in 4 L of LB under 37°C with vigorous shaking (250 rpm) until OD600 reached 0.6~0.8 then induced with 2.5% arabinose and 1mM δ-aminolevulinic acid hydrochloride. Cultures were transferred to room temperature and grown for another 20 hrs with vigorous shaking. Cells were harvested by centrifuging at 5000 rpm for 30 min. Collected cell pellet was resuspended with minimum amount of 40 mM EPPS, 150 mM NaCl, 10% glycerol, pH 7.6 containing protease inhibitors, PMSF and lysosome. The resuspended cells were sonicated using a Branson digital sonifier on ice (5 × 35 s bursts on 35% power, interspaced by 1min). All of the following procedures were done at 4 °C unless indicated specifically. Disrupted cells were centrifuged at 13000 rpm for 1hr. The collected clear supernatant was directly loaded on to a gravity Q-sepharose column pre-

equilibrated with 40 mM EPPS, 150 mM NaCl, 10% glycerol, pH 7.6. The column was washed with 400 ml of 40 mM EPPS, 150 mM NaCl, 10% glycerol, pH 7.6 and bound saNOS was eluted with 100 ml of 40 mM EPPS, 1 M NaCl, 10% glycerol, pH 7.6. Eluted saNOS was concentrated using the Milipore centrifugal filter units with 30 kD cut off then dialyzed three times against 1 L of 40 mM EPPS, 150 mM NaCl, 10% glycerol, pH 7.6 with 1 mM DTT. saNOS concentration was measured from ferrous-CO complex using extinction coefficient 76 mM^{-1} cm^{-1} at 444nm [120].

B. subtilis flavodoxins (YkuN) subcloned into pET16b vector from *B. subtilis* chromosome using *Nco*I and *Bam*HI sites was a generous gift from Dr. Andrew Munro in University of Leicester, UK. Recombinant pETYkuN plasmid was transformed into *E. coli* BL21(DE3) strain for protein expression and the expressed protein was purified by a published method with modification[126]. Transformed *E. coli* cells carrying pETYkuN plasmid were cultured in 4 L of LB media in presence of 1 mM ampicillin media at 37°C with vigorous shaking (250 rpm). 0.5 mM IPTG was added to induce YkuN expression when OD_{600} reached 1.0. The cultures were grown at 37 °C for another 20 hrs with vigorous shaking (250 rpm). Cells were harvested by centrifuging at 5000 rpm for 30 min. The collected cell pellets were resuspended with minimum volume of 50 mM Tris-HCl, pH 7.2 containing protease inhibitors, PMSF and lysosome. The resuspended cells were then sonicated using a Branson digital sonifier on ice (5 × 35 s bursts on 35% power, interspaced by 1min). All of the following procedures were done at 4 °C unless indicated specifically. The lysates were centrifuged at 13000 rpm for 1 hr and the cleared blue supernatant was collected. Powdered ammonium sulfate was added slowly to the supernatant to give a final concentration 1.5 M with gently stirring. The precipitation was

removed by centrifugation at 13000 rpm for 1 hr and the clear supernatant was loaded onto a phenyl-sepharose column pre-equilibrated with 50mM Tris-HCl, 1.5 M ammonium sulfate pH 7.2. A linear gradient (1.5-0.5 M ammonium sulfate in 50mM Tris-HCl, pH 7.2) was applied on the phenyl-sepharose column to elute bound YkuN. The fractions with an A_{280}/A_{461} ratio equal to or less than 10:1 were retained. These fractions were pooled, concentrated then dialyzed against 50 mM Tris-HCl, pH 7.2 then loaded on a Q-Sepharose column pre-equilibrated with 50 mM Tris-HCl, pH 7.2. Bound YkuN was eluted by a liner salt gradient (50-500 mM KCl in 50 mM Tris-HCl, pH 7.2). Fractions with most intense yellow color were retained, pooled, concentrated using Milipore centrifugal filter units with 10 kD cut off then dialyzed against 50 mM Tris-HCl, pH 7.2 with 1 mM DTT for three times. The concentration of YkuN was measured using an extinction coefficient of 7.1 mM^{-1} cm^{-1}[120].

E. coli flavodoxins $NADP^+$ oxidoreductase (FLDR) subcloned into pCL21 vector using *Nco*I and *Bam*HI sites was a generous gift from Dr. Simon Daff in University of Leicester, UK. Recombinant pCLFLDR plasmid was transformed into *E. coli* BL21(DE3) strain for protein expression and the expressed protein was purified with a published method with modification[120]. Transformed *E. coli* cells carrying pCL21FLDR plasmid were cultured in 4 L LB media at 37°C with vigorous shaking (250 rpm) and 1 mM ampicillin. 1 mM IPTG was added to induce FLDR expression when OD_{600} reached 1.0. The cultures were grown at 37 °C for another 6 hrs with vigorous shaking (250 rpm). Harvest cells by centrifuging at 5000 rpm for 30 min. The collected cell pellets were resuspended with minimum amount of ice-cold 10 mM sodium phosphate, pH 7.5 containing protease inhibitors, PMSF and lysosome. The resuspended

cells were sonicated on ice using a Branson digital sonifier (5 × 30 s bursts on 35% power, interspaced by 1min). All of the following procedures were done at 4 °C unless indicated specifically. The lysate were centrifuged at 13000 rpm for 1 hr and the clear supernatant was loaded onto a Q-Sepharose column pre-equilibrated with 10 mM sodium phosphate, pH 7.5. Bound FLDR was eluted by a liner salt gradient (0-1 M NaCl in 10 mM sodium phosphate, pH 7.5). Fractions with most intense yellow color were retained and pooled then loaded on to an ADP Sepharose column pre-equilibrated with 10 mM sodium phosphate, 150 mM NaCl, pH 7.5. The bound FLDR was washed with 200 ml of 10 mM sodium phosphate, 150 mM NaCl, pH 7.5 then eluted with 100 ml of 10 mM sodium phosphate, 500 mM NaCl, pH 7.5. The eluted FLDR was concentrated using Milipore centrifugal filter units with 10 kD cut off then dialyzed against 1 L of 10 mM sodium phosphate, pH 7.5 with 1 mM DTT for 3 times. The concentration of FLDR was measured using an extinction coefficient of 10 mM^{-1} cm^{-1}[120].

3.2.3 Preparation of *E. coli* and Macrophage Cell Cytosol

Cell cytosol of *E. coli.* BL21(DE3) cells expressing iNOS was prepared using the method described previously[125]. Briefly, 50 ml culture of induced or un-induced *E. coli.* BL21(DE3) cells expressing iNOS was harvested by centrifuging at 5000 rpm for 30 min. All of the following procedures were done at 4 °C unless indicated specifically. Cell pellets were resuspended with minimum amount of 40 mM EPPS, 150 mM NaCl, 10% glycerol, pH 7.6 containing protease inhibitors, PMSF and lysosome. The resuspended cells were sonicated on ice using a Branson digital sonifier (5 × 35 s bursts on 35%

power, interspaced by 1min) then centrifuged at 13000 rpm for 1hr to collect the clear *E. coli* cell cytosol. For macrophage cytosol, RAW264.7 (ATCC, Rockville, MD) cells were cultured as described elsewhere[127]. Cells were induced by adding 25 µg/ml lipopolysaccharide (LPS) and 10 units/ml of interferon-γ (IFN- γ) followed by 18 hrs incubation at 37 °C and 5% CO_2 humidified incubator. After the induction, cells were quickly washed with phosphate buffered saline (PBS, 137 mM NaCl, 2.7 mM KCl, 10 mM Na_2HPO_4, 1.8 mM KH_2PO_4, pH 7.4) and lysed by 3 cycles of freeze and thaw in 40 mM EPPS, 150 mM NaCl, 10% glycerol pH 7.6 with protease inhibitors. Soluble supernatants after centrifuging lysates at 12000 rpm for 20 min at 4 ^oC were utilized for the assay. Uninduced macrophage cell cytosol was prepared using the same method.

3.2.4 Conjugation Hemoglobin (Hb) with Polyethylene Glycol (PEG)

Polyethylene glycol conjugated hemoglobin (PEGylated Hb or Hb-PEG) was prepared with the same method described by Vandegriff and Kluger[123, 128]. The conjugation process is shown in Fig. 25. Briefly, commercially available native bovine methemoglobin (metHb) was mixed with 10 equivalents of 2-iminothiolane (IMT) and 20 equivalents of MAL-PEG5K in phosphate buffered saline (PBS, 137 mM NaCl, 2.7 mM KCl, 10 mM Na_2HPO_4, 1.8 mM KH_2PO_4, pH 7.4) and kept at 4 °C overnight with gently stirring. Produced PEGylated metHb (metHb-PEG) was isolated by passing the resulting mixture through Sephadex G-25 PD10 column pre-equilibrated with PBS to eliminate unreacted IMT and Mal-PEG5K. PEGylated oxyhemoglobin (oxyHb-PEG) was prepared by adding excess amount of sodium dithionite (DITH) into the Hb-PEG solution then

passing the product through Sephadex G-25 PD10 gel filtration column pre-equilibrated with PBS[129]. Oxyhemoglobin (oxyHb) was made from metHb using then same method.

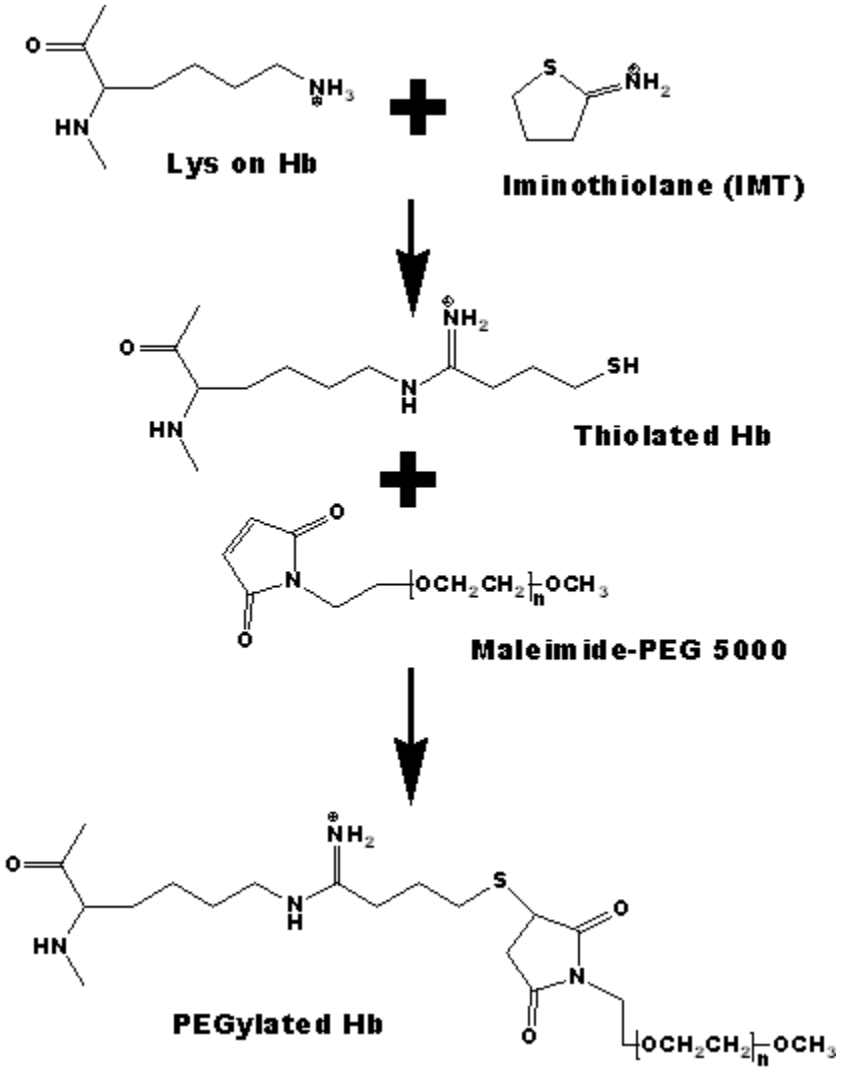

Fig. 25. **PEGylation Scheme of hemoglobin**

3.2.5 Gel-flitration Analysis of PEG-Hb

Hb-PEG and native Hb were analyzed using an analytical size-exclusion column (Superdex 200. 10 mm × 300 mm) on FLPC instrument (AKTA FPLC, Amersham Bioscience, NJ) to determine the size of PEG-Hb in buffer (40 mM EPPS, 150 mM NaCl, 10% glycerol pH 7.6). The effluent was monitored at 280 nm.

3.2.6 UV-Vis Analysis of PEG-Hb

UV-Vis spectrum of Hb-PEG and Hb were compared to determine their spectroscopic similarities. UV-visible spectra of PEG-Hb and Hb from 250 nm to 700 nm were obtained using a Shimadzu UV-2401 PC UV-Vis spectrophotometer.

3.2.7 Hb Reductase Activity of FLDR, YkuN, *E. coli* and Macrophage Cell Cytosol

Hb reductase assay quantifies the rate of metHb → oxyHb conversion. Hb reductase activity of FLDR, YkuN, *E. coli* and macrophage cell cytosol was examined to establish whether they could directly reduce metHb or metHb-PEG as a side reaction to NO formation (Fig. 26). Assay mixtures contained 40 mM EPPS, 250 mM NaCl, 10% glycerol, pH 7.6, 25 μM metHb or metHb-PEG with 1.5 μM FLDR, 4.5 μM YkuN or 10 μl uninduced *E. coli* or macrophage cell cytosol. The reactions were initiated by adding 100 μM NADPH and was monitored by following the absorbance at 401 nm by either UV-Vis spectrophotometer (for YkuN and FLDR) or 96-well plate reader (for cell cytosol). For plate reader experiments, one positive control reaction was run

simultaneously on both UV-Vis spectrophotometer and 96-well plate reader to correlate the slope calculated by 96-well plate reader with rate measured by UV-Vis spectrophotometer under the exact same experimental conditions. All the experiments were done at room temperature. An extinction coefficient of 38 mM^{-1} cm^{-1} was used to calculate Hb or Hb-PEG reduction rate for spectrophotometer assay[114]. Experiments were done in triplicates and results are shown as mean ± standard deviation.

3.2.8 Steady-state NO Synthase Assay of Purified iNOS, *E. coli* and Macrophage Cell Cytosol

The use of oxyhemoglobin assay (oxyHb assay) to determine mNOS activity has been reported previously [26, 30]. In this assay, large access of NADPH and oxyHb are used to initiate NO production by NOS to create a pseudo-zero order condition in the beginning of reaction. The produced NO oxidizes oxyHb into metHb resulting in a linear increase of absorbance at 401 nm in the beginning of reaction. The absorbance at 401 nm in is record by spectrophotometer along with time and its slope is calculated. The pseudo-zero order rate constant is calculated by dividing the slope of with an extinction coefficient of 38 mM^{-1} cm^{-1}[114]. The steady-state turnover number (*kcat*) is calculated by dividing the pseudo-first order rate constant with the concentration of enzyme used in the assay. In order to study the ability of oxyHb-PEG to support the oxyHb assay, both oxyHb-PEG and oxyHb were first used the oxyHb-PEG to determine the NO synthase activity of purified wild type iNOS. NO synthesis reactions containing 1 μM iNOS, 500 μM L-Arg, 4 μM H_4B, 0.2 mM DTT, 25 μM oxyHb or oxyHb-PEG, 150 units/ml SOD,

40 mM EPPS, 150 mM NaCl and 10% glycerol at pH 7.6 in cuvette were initiated by adding 100 μM NADPH at room temperature. The activity of iNOS in *E. coli* or macrophage cell cytosol were also quantified using both oxyHb and oxyHb-PEG as NO indicator by oxyHb assay with modifications. The assay was done under the same condition except the reactions were run in 96-well microplate on SpectraMax M2 plate reader (Molecular Devices, CA) instead of a cuvette. Slopes were obtained by fitting the initial velocities to linear equation using software SoftMax Pro 5.3. A cuvette reaction was run simultaneously to correlate the slope calculated by 96-well plate reader with rate measured by UV-Vis spectrophotometer under the exact same experimental conditions. Experiments were done at room temperature and performed in triplicate and the results were shown as mean ± standard deviation.

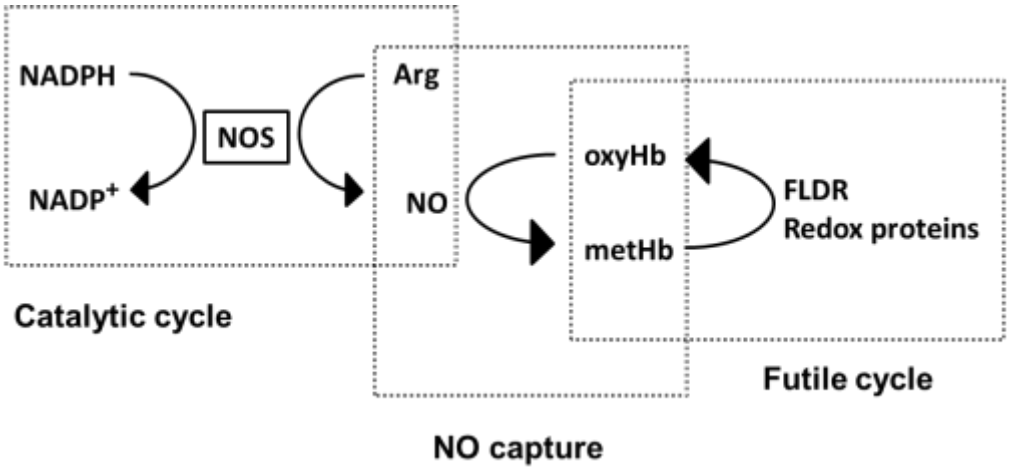

Fig. 26. **Electron transfer scheme in oxyHb assay system.** NO is produced in the catalytic cycle. The oxyHb react with NO in the NO capture cycle. The redox proteins react with metHb in the futile cycle.

3.2.9 Steady-state NO Synthase Assay and NADPH Oxidation Assay of saNOS

The ability of FLDR and YkuN as reductase partners has been studied in bsNOS systems previously[120]. Here we determined the NO synthase activity of saNOS in the three-component by the oxyHb assay reported previously with modifications[120]. Reactions were run in 96-well microplate on SpectraMax M2 plate reader (Molecular Devices, CA). Reaction mixtures contained 40 mM EPPS, 250 mM NaCl, 10% glycerol, various concentration of H_4B or H_4F, 0.2 mM DTT, 200 µM NOHA or 500 µM Arg, 150 units/ml SOD, 10 µM oxyHb-PEG, 1 µM saNOS, 1.5 µM FLDR and 4.5 µM YkuN. Reactions were initiated by adding 100 µM NADPH and absorbance at 401 nm was recorded. Slopes were obtained by fitting the initial velocities to a linear equation using software SoftMax Pro 5.3. A cuvette reaction was run simultaneously to correlate the slope obtained by 96-well plate reader with rate measured by UV-Vis spectrophotometer under the exact same experimental conditions. An extinction coefficient of 38 mM^{-1} cm^{-1} was used to calculate NO synthase rate measured by UV-Vis spectrophotometer. NADPH oxidation assay was described previously [120]. Briefly, reaction mixture containing 1 µM saNOS, 1.5 µM FLDR and 4.5 µM YkuN in cuvette was initiated by adding 100 µM NADPH at room temperature. The reactions were monitored by following the absorbance at 340 nm by spectrophotometer. Extinction coefficient of 6.22 mM^{-1} cm^{-1} at 340 nm was utilized to calculate the NADPH oxidation rate. Experiments were performed in triplicate and the results were shown as mean ± standard deviation.

3.2.10 Griess Assay Quantifying Nitrite Formation by saNOS and Cell Cytosol

Griess assay was used to quantify the nitrite production by iNOS in *E. coli* or macrophage cell cytosol and the results were compared with NO synthase activity quantified by oxyHb assay using Hb-PEG. Reactions were run in 96-well microplate on SpectraMax M2 plate reader (Molecular Devices, CA). Reaction mixtures contained 40 mM EPPS, 250 mM NaCl, 10% glycerol, 100 μM H_4F, 0.2 mM DTT, 500 μM NOHA, 150 units/ml SOD, 1 μM saNOS, 1.5 μM FLDR and 4.5 μM YkuN. The reactions were initiated by adding 100 μM NADPH at room temperature then run for 10, 20, 30, 40, 50 or 60 mins. Excess of NADPH was consumed by adding a quenching solution contains 10-units/ml lactate dehydrognease and 10 mM sodium pyruvate to stop further nitrite formation after reaction at these certain time points. Greiss reagent (a water solution containing 5 g/L sulfanilamide and 0.5 g/L N-(1-Naphthyl)-Ethylenediamine) was added into all wells immediately after 60 mins. Produced nitrite was quantified according to a standard curve obtained from standard nitrite solution prepared the same day of experiment.

3.2.11 K_m and K_i Determination

Plate reader oxyHb assay provides an efficient way to study the inhibitor kinetics for NOS. Here we characterized the Michaelis constant K_m of L-Arg and inhibitor constant (Ki) of L-N^G-monomethyl Arginine (L-NMMA) for both saNOS and iNOS. Briefly, various amount of L-Arg and L-NMMA were added into reaction mixture

containing either 1 μM iNOS, 150 units/ml SOD 4 μM H_4B, 0.2 mM DTT, 25 μM oxyHb-PEG, 40 mM EPPS, 150 mM NaCl, 10% glycerol or 1 μM saNOS, 1.5 μM FLDR, 4.5 μM YkuN, 150 units/ml SOD, 100uM H_4F, 0.2 mM DTT, 10 μM oxy Hb-PEG, 40 mM EPPS, 250 mM NaCl, 10% glycerol, pH 7.6 in each well of 96-well micro plate. Reactions were initiated by adding 100uM NADPH and absorbance at 401 nm was recorded by 96 well plate-reader. Slopes were obtained by fitting the initial velocities to linear equation. A cuvette reaction was run simultaneously to compare the performance of the 96-well plate reader assay under the exact same experimental conditions. An extinction coefficient of 38 mM^{-1} cm^{-1} was used to calculate NO synthase rate measured by UV-Vis spectrophotometer. *Km* of L-arg for iNOS and saNOS was calculated by fitting Lineweaver-Burk plot[130]. *Ki* of L-NMMA for iNOS and saNOS was calculated by fitting the following equation based on Michaelis-Menten mechanism for completive inhibitors:[131]

$$\frac{K'_m}{K_m} = \frac{[I]}{K_i} + 1$$

3.3 Results and Discussion

3.3.1 Characterization of Hb-PEG

PEGylataion is a robust way to increase the size of Hb while do not altering its O_2 binding affinity[123]. Here we characterized the Hb-PEG prepared in our own lab by size exclusion chromatograph, UV-Vis spectrophotometer and kinetic assay.

(i) Molecular weight analysis

Prepared Hb-PEG was analyzed by FPLC using a gel filtration Superdex 200 column. Hb-PEG eluted as a broad peak spanning molecular weights 79kD to 173kD with maximum UV absorption corresponding to a molecular weight of 128 kD (Fig. 27). The molecular weight of native Hb was calculated to be 62 kD using the same method. These results are in agreement with previous preparations of oxyHb-PEG reported by Kluger et al[128].

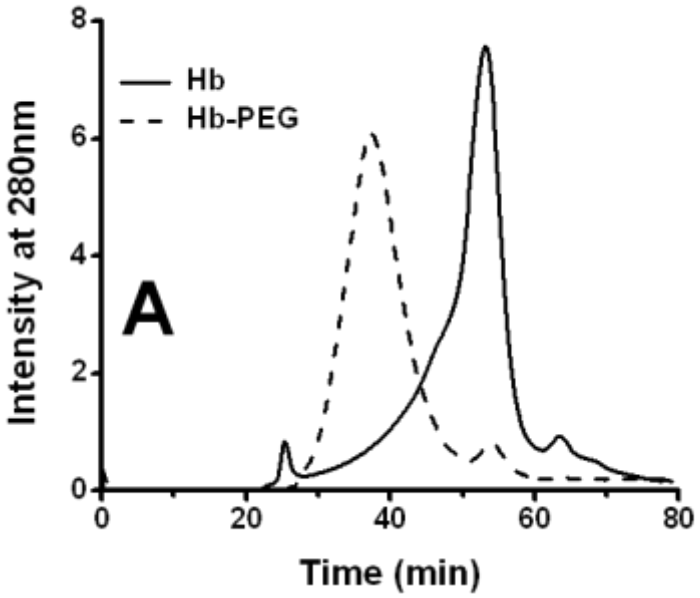

Fig. 27. **FPLC chromatography of PEG-Hb**

(ii)UV-Vis analysis

The spectrum of production after PEG-MAL5K conjugation Hb-PEG has a Soret peak at 405 nm and a charge-transfer band at 631 nm, essentially identical to those of native met-Hb, indicating the direct product is the PEGylated methemoglobin (metHb-PEG) as shown in Fig. 28[132]. Reduction with dithionite (DITH) followed by desalting using a G25-PD10 column produced a red shift of the absorption maxima with well-

defined bands appearing at 415 nm (Soret), 543 nm and 576 nm (Q-bands) along with disappearing of band at 613 nm. These spectral features are characteristic of oxyHb, suggesting such treatment turns metHb-PEG into PEGlyated oxyhemoglobin (oxyHb-PEG) and no significant perturbation of the heme center upon PEG binding[132]. The high similarity of the UV-visible spectra of native Hb and Hb-PEG in terms of absorption maxima and band intensity demonstrate no alterations of the heme center in either oxidation state and coordination environment, enabling the use of the same extinction coefficients for native Hb and Hb-PEG.

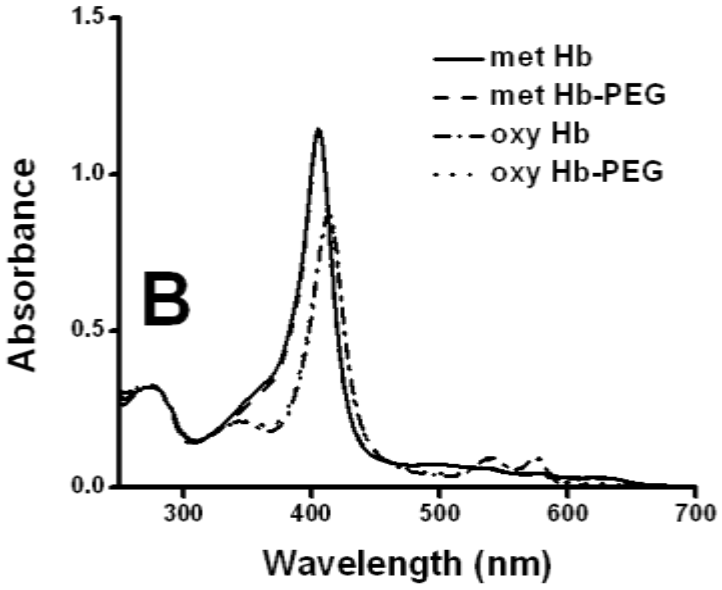

Fig. 28. **UV-Vis Spectrum of Hb and Hb-PEG**

(iii) Measurement of Mammalian iNOS Activity by oxyHb assay with oxyHb-PEG

In order to study the ability of oxyPEG-Hb to support the NO synthase assay, the activity of murine iNOS was examined using native oxyHb (control) and oxyHb-PEG

under the same experimental conditions. An extinction coefficient 38 mM^{-1} cm^{-1} was used to calculation iNOS NO synthase activity for both Hb and Hb-PEG groups based on the results described above. 4 μM H_4B and 500 μM L-Arg were used in the assay. The NO synthase activity of iNOS was 58.5 ± 3.6 min^{-1} with native oxyHb and 60.8 ± 2.4 min^{-1} with oxyHb-PEG. This shows that Hb bound to PEG is as proficient as the native Hb in capturing NO under these experimental conditions. The above results show we successfully conjugated MAL-PEG5000 with Hb and the oxyHb-PEG is a suitable substitute of oxyHb as NO indicator in the NO synthase assay.

3.3.2 A Futile Cycle Impairs the NO Detection in oxyHb Assay

The primary goal of this study was setting up an assay to directly quantify NO synthesis by either purified saNOS or cell cytosols to expand the usage of oxyHb assay and shorten the assay time. Most bNOS, including saNOS, lacks covalently attached reductase domain[25]. The identity and function of the reductase protein partners that drive NO synthesis in bacteria carrying a NOS protein are currently unknown, so external reductase partner protein is required in order to set up an in vitro assay to quantify the NO synthase activity of purified bNOS. Previous studies showed that flavoproteins YkuN and FLDR support NO synthesis by *Bacillus subtilis* NOS (bsNOS) with decent efficiency [120]. The high structural similarity between saNOS and bsNOS [87, 133] led us to hypothesize that the YkuN/FLDR pair could also support NO synthesis by saNOS. In order to test this hypothesis, we employed two types of assays commonly used to quantify mammalian NOS: 1) an indirect assay where the oxidation products of NO,

nitrite and nitrate are determined using the Griess reagent to quantify saNOS activity, or 2) a direct assay that uses oxyHb as a NO probe. The Griess assay is an end point assay that measures the final concentration of nitrite, the NO oxidation product, in the end of reaction. The oxyHb assay is a steady-state spectroscopic assay that monitors the absorbance change at the characterization wavelength of oxyHb-metHb (401nm) conversion during reaction. It measures the initial NO releasing rate, which can be done within a short period of time and exhibits greater sensitivity compared to end-product formation [28]. Our preliminary results show the YkuN/FLDR is capable of transferring electron to saNOS for NO production, but the produced NO was detectable only using the low sensitivity Griess assay but not the high sensitivity oxyHb assay (data not shown). Similarly, the NO synthase activity of cell cytosol determined by oxyHb with oxyHb is significantly lower activity than the activity determined by Griess assay (data not shown). This paradox suggests either a defective electron transfer between the reductase to the heme center in NOS or electron transfer from NO to the heme center in Hb when the assays were performed in the presence of native oxyHb. Taking in the consideration that both YkuN and FLDR are part of the electron transfer chain and many redox proteins exist in cell cytosol, we hypothesized that metHb, which is the NO oxidation product of oxyHb, could engage in redox cycling with the flavoproteins or other proteins contained in cell cytosol, derailing electrons from the metHb building up. Here we refer this redox cycle as futile cycle, as shown in the right part of Fig. 23. Also, NOS expressed by bacterial and mammalian cells co-exist with a variety of proteins could act as electron donor in cell cytosol, which potentially reduce metHb.

In order to test this hypothesis, we quantified the Hb reductase activity with both oxyHb and oxyHb-PEG. Fig. 29 shows the kinetic traces of metHb and metPEG-Hb reduced by the FLDR, YkuN, uninduced *E. coli* or macrophage cell cytosol. The results showed that FLDR alone reduced metHb with a rate 1.4 min^{-1}. This reduction rate increased to 1.6 min^{-1} when both FLDR and YkuN were present. YkuN does not have ability to directly reduce metHb. Uninduced *E. coli* and macrophage cell cytosol reduced metHb to the rate of 0.12 $\mu M^{-1}min^{-1}/\mu l$ cytosol and 0.35 $\mu M^{-1}min^{-1}/\mu l$ cytosol respectively. The results showed that the apparent incompatibility oxyHb with the saNOS/FLDR/YkuN system and cell cytosol was caused by this futile side reaction. More importantly, these unwanted reactions were eliminated by replacement of native oxyHb with oxyHb-PEG.

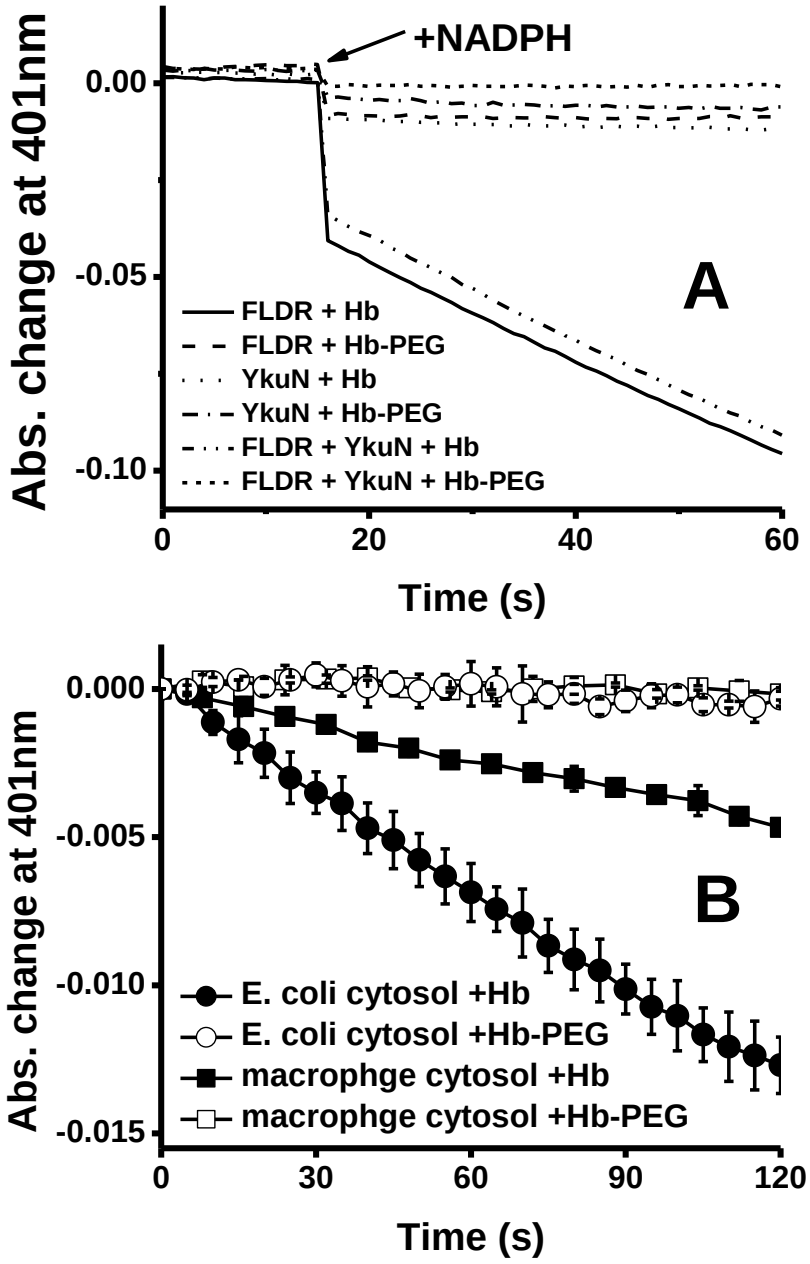

Fig. 29. **Hb reduction traces.** *Panel A,* Hb reduction traced by FLDR or YkuN. Panel B, Hb reduction traced by E. coli or macrophage cell cytosol

3.3.3 PEGylation on Hb Diminished the Futile Cycle

To further investigate the ability of Hb-PEG as NO indicator, we quantified the NO synthase activity of purified saNOS using both native oxyHb and oxyHb-PEG as NO indicator. 100 µM H_4B, 500 µM Arg and 20 µM oxyHb/oxyHb-PEG were used in the assay and the assays were run on both UV-Vis spectrophotometer and 96-well plate reader and their traces were shown in Fig. 30. The saNOS NO synthase activity quantified with oxyHb-PEG was 1.5 min^{-1} while no detectable activity was observed with oxyHb. This result directly proves oxyHb-PEG is a suitable NO indicator in the saNOS /YkuN/FLDR system. The fact that the saNOS NO synthase rate is similar to the FLDR reduction rate explains why no net absorbance gain at 401 nm was observed. On the other hand, the FLDR reduction rate is significant slower than the reported bsNOS NO synthase activity, explaining why oxyHb is compatible with bsNOS/YkuN/FLDR system.

Macrophage is the primary source producing iNOS in animal and *E. coli* is a universal host cell for NOS over-expression and purification[134]. Here we use the cytosol from these two cell types as examples to compare the ability of oxyHb and oxyHb-PEG in oxyHb assay for cell cytosol samples as NO indicator. Fig. 31 showed the kinetic traces of oxyHb and oxyHb-PEG as NO indicator measuring NO synthase activity of *E. coli* or macrophage cell cytosol. Nitrite formation rates of the same cytosol samples were quantified by Greiss assay and the rates were compared with the NO synthase rates in Table II.

Our Hb reductase activity measurements and NOS activity experiments confirmed these unidentified redox proteins contained in cell cytosol are capable of accepting

electrons from NADPH and drive oxyHb into futile cycle by transferring electrons directly to its heme center, similar to FLDR. PEGylation of Hb also successfully eliminates this futile cycle with these proteins. The identity of such proteins is unclear and requires further study. Quantification of NO instead of nitrite provides a more accurate NOS activity because nitrite is only a fraction of NO oxidation product.

Together, our results confirmed that two electron transfer pathways, a NO production pathway and a futile pathway, involved in the oxyHb assay. The NO production pathway results in an absorption increase at 401 nm while a futile pathway counteracts such absorption increase by reducing metHb back into oxyHb. Importantly, PEGylation on Hb diminishes the futile pathway, likely by limiting the direct interaction between hemoglobin and these redox proteins, making it a suitable NO indicator for both bacterial NOS and cell cytosol NOS activity quantification. The use of Hb-PEG in 96 well plate reader assay sharply shortens the assay time, greatly improved the assay through-put, making it a suitable way for cell cytosol NO synthase activity quantification as well. All following NO synthase activity measurements employ oxyHb-PEG as NO indicator and were done with 96-well plate-reader.

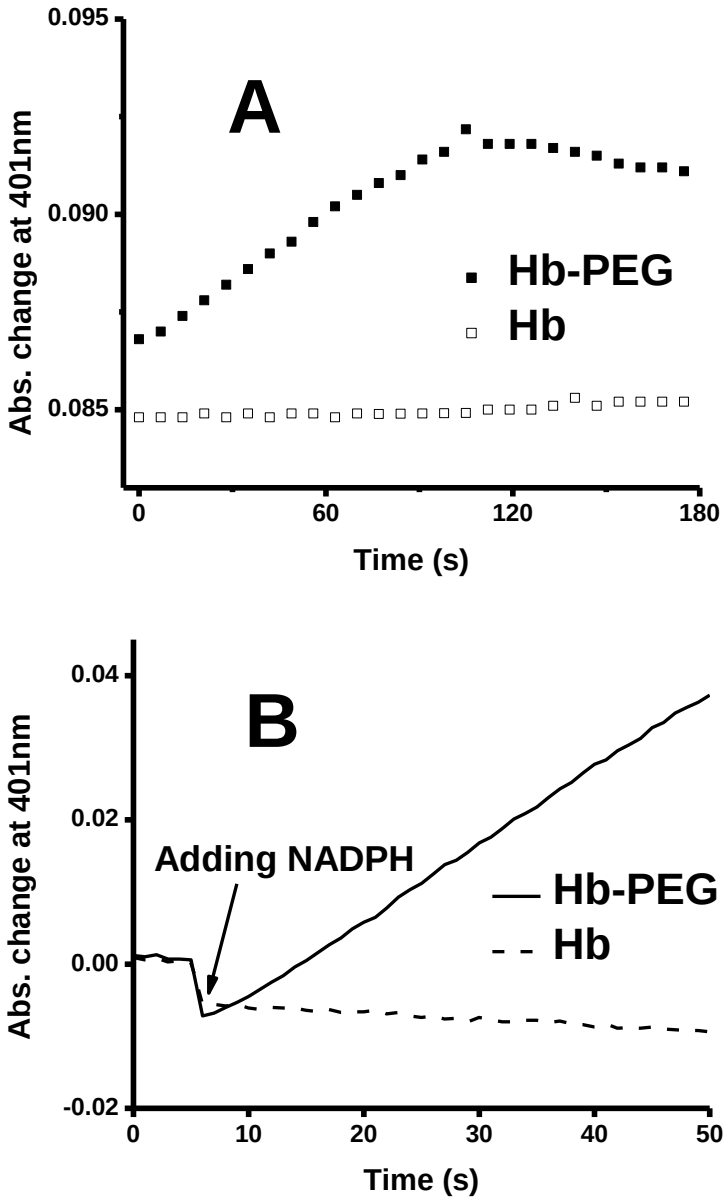

Fig. 30. **saNOS NO production trances using Hb/Hb-PEG.** *Panel A,* NO production traces monitored on a 96-well plate reader. Panel B, NO production traces monitored by UV-Vis spectrophotometer.

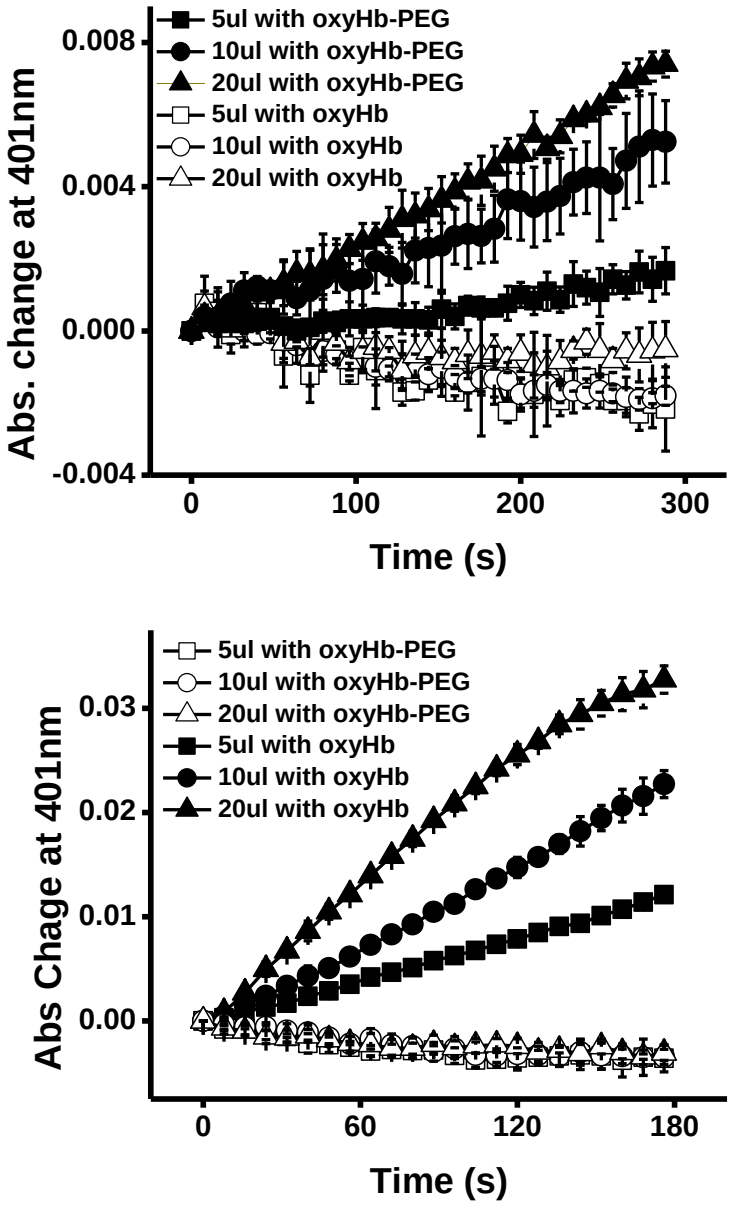

Fig. 31. **NO production traces of iNOS in cytosol using oxyHb and oxyHb-PEG.** *Upper panel,* the NO production traces of iNOS in macrophage cytosol. *Bottom panel,* the NO production traces of iNOS in *E. coli* cytosol.

Table II**.** *Comparison of NO production rates and nitrite formation rate by macrophage cell cytosol*

Sample Volume	Nitrite formation		NO production	
	$V\ (\mu M \cdot min^{-1})$	$k_{cat}\ (min^{-1})$	$V\ (\mu M \cdot min^{-1})$	$k_{cat}\ (min^{-1})$
5ul	0.18 ±0.02	48 ±5	0.20 ±0.01	53 ±3
10ul	0.37 ±0.01	49 ±3	0.42 ±0.02	56 ±5
20ul	0.86 ±0.02	57 ±5	0.97 ±0.02	64 ±5

3.3.4 **NO Synthase Activity and NADPH Oxidation Activity of saNOS**

The catalytic activity of NO synthesis and NADPH oxidation by saNOS were assessed under different conditions in order to further study the electron transfer through saNOS/YkuN/FLDR system. A summary of these kinetic parameters is presented in Table III. Our results show that saNOS, FLDR and YkuN are all indispensable component for saNOS NO production, system lacking any of the three shows little NO production. This shows saNOS needs an external electron donor for catalysis, which is expected. Reaction lacking saNOS shows little NO production but still maintains majority of NADPH oxidation, implying FLDR/YkuN act as reductase partner of saNOS together, which is similar with their function in bsNOS/FLDR/YkuN system reported previously[120]. Reaction lacking FLDR only has less than 10% NADPH oxidation activity while reaction lacking YkuN still has ~70%. These indicate electrons first

transfer from NADPH to FLRD then to FLDR as shown in Fig. 32. However, measurement of NADPH oxidation rates showed that the flavoprotein partners and saNOS is largely uncoupled with respect to NO synthesis compared to mammalian NOS, indicating FLDR/YkuN is not a very efficiently reductase partner for saNOS. This is not surprising, considering the fact that saNOS, FLDR and YkuN are all separated by solvent in the assay mixture instead of being covalently attached. Further, the FLDR and YkuN orthologs of *S. aureus* may not be the best structural fits to drive NO synthesis. Uncovering the native reductase partners of saNOS awaits further investigation. The result also indicates the NO synthesis by saNOS is the rate-limiting step during the electron transfer in the saNOS/YkuN/FLDR system under the experiment condition.

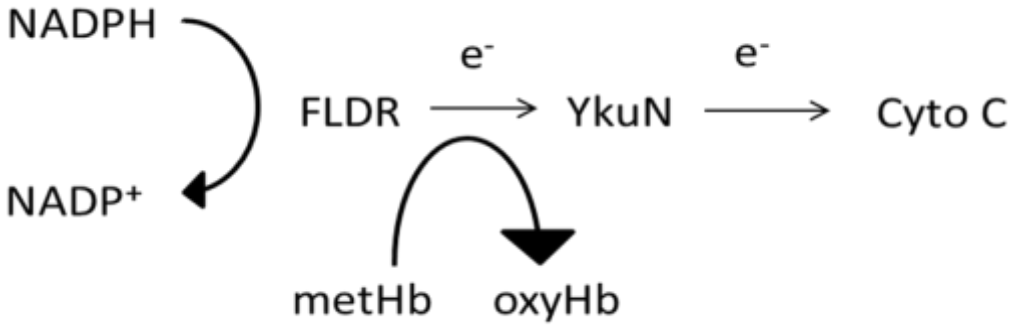

Fig. 32. **Electron transfer in the saNOS/YkuN/FLDR system.**

Table III. *Kinetic activities in the saNOS/YkuN/FLDR system*

FLDR	YkuN	saNOS	NO synthase	NADPH oxidation
			min^{-1}	min^{-1}
+	+	-	0	21.1 ±0.7
+	-	+	0.012 ±0.01	10.6 ±1.3
-	+	+	0.011 ±0.01	2.4 ±0.3
-	-	+	0	0
+	+	+	1.51 ±0.05	28.2 ±3.1

3.3.5 NO Synthase Activity Using Different Substrates and Cofactors

Unlike mammalian NOSs, bacterial NOS can utilize tetrahydrofolate (H_4F) to drive NO synthesis, in addition to H_4B [25]. H_4F has an identical pterin head with H_4B and an extended aromatic tail, which is not part of H_4B (Fig 31). Structural differences in the pterin binding pocket of mammalian and bacterial NOSs show that the extended aromatic tail of H_4F cannot be accommodated in the mammalian enzymes[25]. This is generally believed to be the reason why H_4F does not support NO synthesis in mammalian [25]. And interestingly, the bNOS activity quantified using H_4B is always different from the activity quantified using H_4F. This fine structural finding make bacterial NOS as great drug targets to fight infections caused by their pathogenic hosts, including *S. aureus*. Arg and NOHA are two substrates that NOSs use to produce NO. In

order to study the saNOS catalytic features and optimize the assay condition, we quantified saNOS NO synthase acitivity using different cofactors and substrates. Dose dependence curves of different cofactor-substrate combinations are shown in Fig. 33.

Our results show the pterin cofactor is an indispensible component for saNOS NO synthesis. We did not observe any detectable NO production without a pterin cofactor, indicating pterin involves directly in the saNOS catalysis, which is similar with its effect in mNOS catatlysis. The results also show H_4F was more proficient than H_4B in driving NO synthesis by saNOS. The H_4F's superiority to H_4B to support saNOS NO synthesis is surprising because it is generally believed that smaller cofactor H_4B has higher possibility getting into the binding pocket of saNOS. One possible explanation is that the aromatic tail of H_4F binds to specific structure elements in saNOS and favors electron transfer from H_4F to saNOS to drive substrate oxidation. Even at high concentrations of H_4B or H_4F saNOS did not reach its highest activity. This implies that the biopterin cofactor binds saNOS loosely, which agrees with the prediction from its crystal structure [25, 133]. Overall, the NO production in *S. aureus* is likely staying at very low level in order to maintain the homeostasis of bacterial since NO is toxic at higher concentration. Also, the NO level in bacteria is possibly regulated by the bio-availability of H_4F. Of the two substrates tested, NOHA was 2-fold more effective than L-Arg in supporting NO synthesis. This is reminiscent of the behavior of mammalian NOSs and suggests that in saNOS, L-Arg must undergo two cycles of oxidation to produce NO, just as required in mammalian NO synthesis.

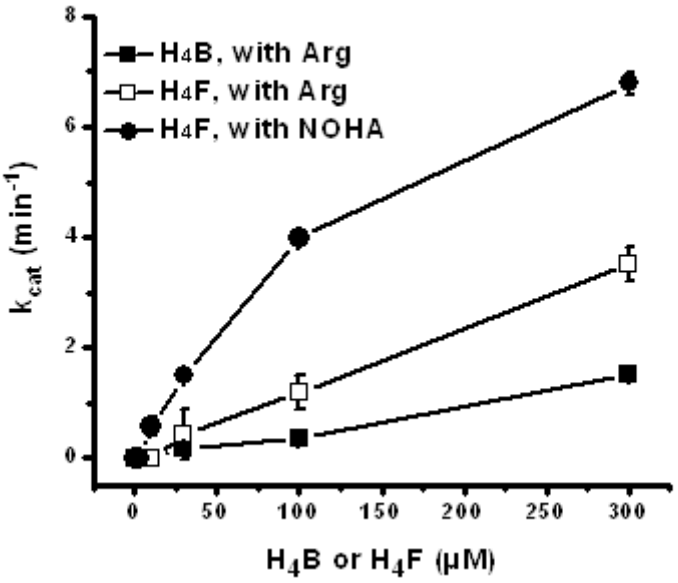

Fig. 33. A**ctivity of saNOS with different cofactors and substrates.**

3.3.6 K_m of Arg and K_i of L-MMA

K_m of Arg and K_i of L-MMA for iNOS measured by our assay set well agreement with published values as shown in Fig. 33[118]. The measured *Km* of Arg for saNOS is one fold larger than that of iNOS, implying Arg binding pocket on saNOS does not favor Arg binding as much as iNOS. The smaller size of Arg binding pocket on saNOS than iNOS may be the cause of this difference. The fact that *Ki* of L-MMA for saNOS is ~9 fold larger than that of iNOS further proved that the binding Arg binding pocket on saNOS and iNOS differs. The structure basis for such difference requires more study. The fact that L-MMA is a better inhibitor for iNOS than saNOS also suggested that inhibitors designed based on NOS substrate is not like to have good selectivity.

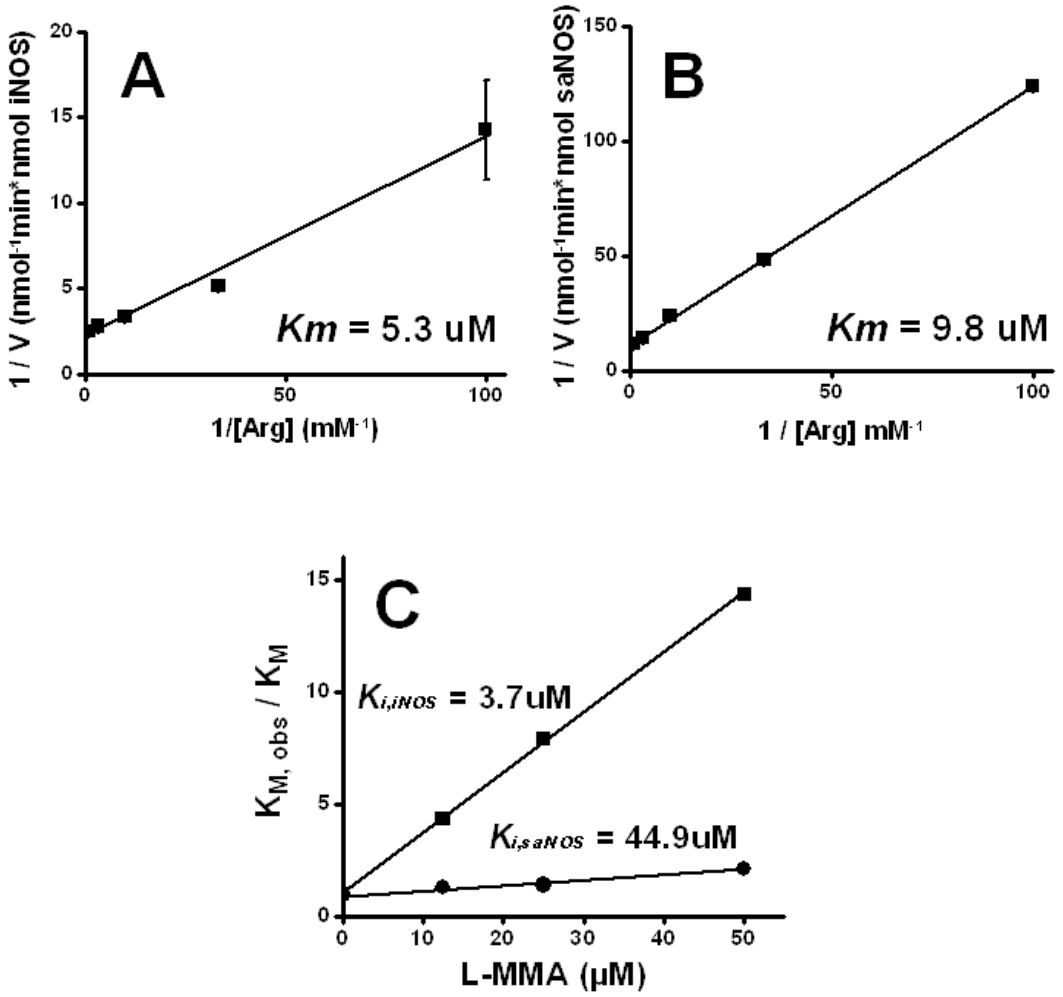

Fig. 34. **Determination of K_m of L-Arg and K_i of L-NMMA.** *Panel A,* Lineweaver-Burk plot determining K_m of L-Arg for iNOS. *Panel B,* Lineweaver-Burk plot determining K_m of L-Arg for saNOS. *Panel C,* determining K_i of L-NMMA for iNOS and saNOS.

3.4. Conclusions

This is the first study to present a direct measurement of the NO synthesis activity of *S. aureus* NOS and the cell cytosols. We developed a rapid, inexpensive 96-well plate reader assay that employs Hb modified with PEG5000 to optimize electron transfer toward NO synthesis. This assay utilizes FLDR and YkuN as reductase partners to saNOS, which have been proven to support NO synthesis in other systems such as bsNOS. No special component was needed for assay with cell cytosols except that oxyHb-PEG is used instead of oxyHb. This Hb-PEG based assay allowed us to uncover unique features of saNOS including the dose-dependence and preference for tetrahydrofolate over tetrahydrobiopterin, the NO synthesis rates with natural substrates L-Arg and NOHA. This assay was also used to study the kinetics of well-established mammalian NOS inhibitor, L-MMA, for both saNOS and iNOS. From a mechanistic standpoint our assay revealed that saNOS is largely uncoupled, with NADPH oxidation rates comparable to the NO synthesis pathway. The structural basis of the bias between tetrahydrofolate over tetrahydrobiopterin for saNOS is still unclear and requires further investigation. The usage of tetrahydrofolate over tetrahydrobiopterin for saNOS makes it an outstanding candidate for drug design. On the contrary, the facts that substrate (L-arg) binds to iNOS and bNOS with similar affinity, and substrate analog (L-NMMA) inhibits iNOS with higher potency than saNOS, makes L-arg an unsuitable template for selective inhibitor design. We anticipate that this assay will facilitate the study of 1) NOS expression and regulation in mammalian or bacterial cell, 2) function of other bacterial NOSs and 3) screening of potential drugs to target their host pathogenic microorganisms.

CHAPTER IV

SELECTION OF *STAPHYLOCOCCUS AUREUS* NITRIC OXIDE SYNTHASE INHIBITORS

4.1 Introduction

4.1.1 *Staphylococcus aureus*

Staphylococcus aureus, discovered in 1880 by Dr. Alexander Ogstom, is a Gram-positive, catalase-positive and oxidase-negative facultative anaerobe with approximately 1 µm diameter[135]. The cell division of *S. aureus* takes place simultaneously in different planes, making them aggregate into grape-like clusters[135]. The golden color observed in *S. aureus* colonies is a result of several carotenoids present in its cell cytosol[135]. External supply of nutrients including many amino acids and vitamins B is needed of the

growth of *S. aureus*[135]. *S. aureus* endogenously produces coagulants, which catalyze the conversion of fibrinogen to fibrin in plasma, causing plasma coagulation[135]. This feature has been used to distinguish *S. aureus* with other bacteria in the same genus[135].

Staphylococcus aureus is a widespread and versatile micro-organism[136-138]. Study shows approximately 30% of the healthy individuals are persistently inhabited by *S. aureus* in their skin, mucous membrane and particularly in the anterior nares[138]. Although being nonpathogenic sometimes, *S. aureus* is one of the leading causes of hospital- and community- acquired bacterial infections[135]. It can cause various level of infection from mild skin, soft tissue and lower respiratory tracts infections to lethal pneumonia, bacteremia, osteomyelitis, endocarditis and sepsis[136]. Besides multiple levels of infection, *S. aureus* is related with toxin-mediated diseases including toxic shock syndrome, scalded skin syndrome and *staphylococcal* foodborne diseases (SFD)[137]. Hospital patients with health care risk factor are particularly venerable to *S. aureus* infections due to their compromised immune system and medical treatments involving catheter or injections[135]. In the meantime, health individuals are not risky free since many community-associated *S. aureus* can infect people without any prime heath care risky factors[135].

S. aureus is equipped with a great variety of virulence factors that allow it to invade human self-defending system[135]. It is also capable of developing resistance to almost all antibiotics[135, 139]. Historically, penicillin is initially developed as antibiotics to kill *S. aureus*, but a penicillin resistant *S. aureus* strain was found two years after the discovery of penicillin[139]. After that methicillin was used to fight *S. aureus*

but methicillin-resistant *S. aureus* was reported within one year after the discovery of methicillin[139]. Vancomycin is currently used to treat *S. aureus* infections and *S. aureus* strain with reduced vancomycin susceptibilities has already been reported[139]. These unique features make *S. aureus* a major public health threat and one of the most extensively studied bacteria[139].

4.1.2 saNOS as a Drug Target

S. aureus is a one of the bacterial species that express a nitric oxide synthase similar protein (saNOS)[133]. It has been confirmed that saNOS is capable of endogenously utilizing L-Arginine for NO production[25]. Gusarov *et al.* first found that the endogenous NO produced by saNOS could directly react with some antibiotics to detoxify them or induce catalase production to reduce the intracellular oxidative stress level, protecting saNOS from a wide spectrum of antibiotics[97]. They also showed short-term exposure of NO to the nos gene knocked-out *S. aureus* (Δnos) could protect it from aminoglycoside toxicity by limiting the aminoglycoside intake[97]. In the meantime, it has been shown that methicillin-resistant *Staphylococcus aureus* (MRSA) becomes more susceptible to oxidative stress and host cathelicidin antimicrobial peptides (produced in human neutrophil and capable of killing MRSA) after the removal of nos gene[140]. However, the Δnos strains surprisingly obtained resistance to aminoglycosides, suggesting the relationship between saNOS and its antibiotic resistance is more complex than the simple protecting effect of NO[140]. Mouse model study confirmed that MRSA with saNOS mutation is less virulent and has a decreased survival

rate[140]. These data indicate that saNOS plays an important role in the innate immune of *S. aureus*, suggesting saNOS can be a potential drug target[140, 141]. It will be very valuable to develop specific saNOS inhibitor to decrease the virulence of *S. aureus*, making *S. aureus* vulnerable to human immune system, or making *S. aureus* more susceptible to other commonly used antibiotics.

4.1.3. bNOS Inhibitor Development

There are two major issues for saNOS inhibitor design or selection, to which special attentions need to be paid. The first issue is, by what way(s), we can inhibit saNOS activity. Although saNOS catalysis is a multiple-step process, inhibitor affecting the less essential steps is unlikely to be a potent inhibitor. The facts that saNOS does not have an attached reductase and it is not likely to have a specific reductase partner make it less practical to inhibit saNOS activity by interrupting electron transfer from the reductase partner to saNOS. This leaves us almost no other options but directly inhibition of saNOS[84]. The second issue is how to make inhibitors only specific to saNOS while not interfering the function of mNOS. NO produced by mNOS involves in several important biological functions including blood pressure regulation and immune response thus avoiding inhibition of mNOS is important for saNOS inhibitors design.

Several mNOS inhibitors derived from L-arginine were tested initially in bacterial NOS system[117]. These inhibitors compete with L-Arg for the NOS binding site, but do not support NOS catalysis, and thus repress NOS. However, none of these inhibitors show potent inhibition or any selectivity toward bNOS. The low potency and poor

selectivity of these L-Arg derivatives are not unexpected since the L-Arg binding pocket of mNOS and bNOS are similar[25]. Moreover, some of the L-Arg based inhibitors have several serious *in vivo* side effects including hypertension and decreased cardio output and may cause mortality in some cases, making them an less favorable bNOS inhibitor candidate[142].

Different from blindly selecting inhibitors from current NOS inhibitor library, designing bNOS inhibitors targeting the unique bNOS structures has been proved to be a better strategy[143, 144]. Comparing to mNOS, bNOS is unique in the way that bNOS lacks the N-terminal hook thus has more exposed pterin binding site which can accommodate the relatively bigger cofactor H_4F while mNOS cannot. Structure inhibitor design targeting the bNOS ptering binding site is attractive since it is possible to design a selective inhibitor only bind the bNOS. The Poulos group in Northwestern University designed and synthesized a series of compounds exploiting the unique bsNOS pterin binding side and evaluated their potential as bsNOS inhibitors[144]. Crystal structures of inhibitors bounded bsNOS indicate these inhibitors partially accommodate ptern binding sites and interact with the bsNOS heme, suggesting these inhibitors are selective against bsNOS[145]. However, the potencies of these inhibitors are generally poor and kinetic studies show many of them only weakly interact with bsNOS[145]. Although potent and selective inhibitor is not identified, studies about these compounds provide a structural framework for designing better bsNOS inhibitors[145].

4.1.4 DHFR Inhibitors as saNOS Inhibitors

Dihydrofolate reductase (DHFR) is an enzyme that reduces dihydrofolic acid to tetrahydrofolic acid in a NADPH dependent way[146]. This enzyme plays an important role in folate biosynthesis and it is essential for the *de novo* synthesis of purines, thymidylic acid and several aminio acid[146, 147]. DHFR is a major drug target for parasitic protozoa including plasmodium[147]. However, barely any clinically used human DHFR inhibitors including trimethoprim (TMP) and pyrimethamine (PYR) are effective against the DHFR of *Cryptosporidium hominis*, which is a class B biodefense pathogen causing cryptosporidiosis[147]. In order to develop effective and selective inhibitors for *Cryptosporidium hominis* DHFR (ChDHFR), Anderson *et al.* first identified the structure features of ChDHFR causing the bias against human DHFR inhibitors then designed and tested a series of trimethoprim derivatives exploiting a unique binding pocket in ChDHFR[147]. Several of the designed inhibitors are very potent against ChDHFR while do not significantly affect the human DHFR activity[147-150].

Although original designed as ChDHFR inhibitors, the structural features of these trimethoprim derivatives made us think about the possibility of using them as bNOS inhibitors. The 2,4-diaminopyrimidine structure shared by these compounds are structurally similar with the biopterin ring of H_4B and H_4F, suggesting this 2,4-diaminopyrimidine head may bind to NOS on the pterin binding site. The extended phenyl group tail on these DHFR inhibitors may not fit the mNOS H_4B binding pocket but possibly fit the binding pocket of bNOS with a binding pattern similar to the unique bNOS cofactor H_4F, providing selectivity against bNOS.

4.1.5 Aims

While selective inhibitors for saNOS have not yet been reported, we would like to evaluate several DHFR inhibitors as saNOS inhibitosr. We also would like to find the relationship between the inhibitor structure and its potency/selectivity as saNOS inhibitor.

4.2 Experiments

4.2.1 Materials

The tested TMP derived DHFR inhibitors are generous gifts from Dr. Dennis Wright, University of Connecticut. PEGylated oxyhemoglobin was prepared with method described in section 3.2.4. All other reagents and materials were obtained from Sigma or source reported elsewhere [120].

4.2.2 Protein Expression and Purification

saNOS, *B. Subtitlis* flavodoxin YkuN, *E. coli* flavodoxin $NADP^+$ oxidoreducase FLDR and full length rat iNOS were purified with the methods described in section 3.2.7. iNOS and saNOS concentration were measured from ferrous-CO complex using extinction coefficient 76 $mM^{-1}\,cm^{-1}$ at 444 nm[120]. FLDR and YkuN concentration were

measured using an extinction coefficient of 7.1 mM^{-1} $cm^{-1}$and 10 mM^{-1} cm^{-1} respectively[120].

4.2.3 Hemoglobin Reductase Activity of FLDR and Cytochrome *C* Reductase Activity of YkuN

DHFR inhibitors' effects on FLDR/YkuN enzyme system was measured by hemoglobin reductase assay and cytochrome c reductase assay shown in Fig 35. Previous study in section 3.2.7 shows that FLDR could directly reduce hemoglobin. So we quantified the hemoglobin reductase activity of FLDR in presence of selected DHFR inhibitors to study the impact of these inhibitors on the electron transfer from FLDR to its electron accepter. Similarly, YkuN can receive electrons from NADPH directly or FLDR and reduce cytochrome *c* as indicated in section 3.3.4. We quantified the cytochrome *c* reductase activity of YkuN in presence of selected DHFR inhibitors to study the impact of these inhibitors on the electron transfer from YkuN to its electron accepter.

The Hb reductase assay was done as described in section 3.2.7 with modifications. The assay was done on 96-well microplate on SpectraMax M2 plate reader (Molecular Devices, CA) with each well containing 25 µM metHb and 1 µM of FLDR in 40 mM EPPS, 250 mM NaCl, 10% glycerol, pH 7.6 buffer with 20 µM inhibitors. Reaction was initiated by 100 µM NADPH and absorbance at 401 nm in each well was monitored over time. Slopes of the recorded traces were obtained by fitting the initial velocities to a linear equation using software SoftMax Pro 5.3. A cuvette reaction was run simultaneously to correlate the slope calculated by 96-well plate reader with rate

measured by UV-Vis spectrophotometer under the exact same experimental conditions. An extinction coefficient of 38 mM^{-1} cm^{-1} was used to calculate the hemoglobin reduction rate measured by UV-Vis spectrophotometer. The cytochrome *c* reductase assay was done on 96-well microplate on SpectraMax M2 plate reader (Molecular Devices, CA) with each well containing 4.5 µM YkuN and 50 µM cytochrome *c* in 40 mM EPPS, 250 mM NaCl, 10% glycerol, pH 7.6 buffer with 20 µM inhibitors. Reaction was initiated by 100 µM NADPH and absorbance at 550nm in each well was monitored along with time. Slopes of the recorded traces were obtained by fitting the initial velocities to a linear equation using software SoftMax Pro 5.3. A cuvette reaction was run simultaneously to correlate the slope calculated by 96-well plate reader with rate measured by UV-Vis spectrophotometer under the exact same experimental conditions. An extinction coefficient of 21 mM^{-1} cm^{-1} was used to calculate the cytochrome *c* reduction rate measured by UV-Vis spectrophotometer. Experiments were done at room temperature and performed in triplicate and the results were shown as mean ± standard deviation.

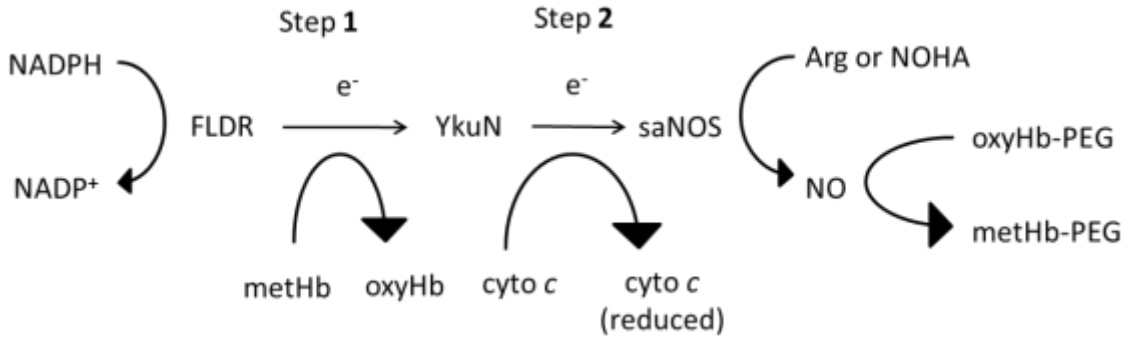

Fig. 35. **Scheme of Hb reductase activity and YkuN cytochrome *c* activity**

4.2.4 IC50 Determination and IC50 Index of Selected Inhibitors

The IC50s of selected DHFR inhibitors, TMP and 4-amino-H_4B on saNOS was obtained from the dose dependent curves after inhibitor addition. Origin Lab 8 were used to fit these curves using a dose dependent equation to calculate the IC50 of inhibitors [151]. The NO synthase activities of purified saNOS were quantified using the oxyHb assay described in section 3.2.9. 100 μM H_4F and 200 μM NOHA were used in the assay to achieve desirable saNOS activity.

The IC50 index of selected DHFR inhibitors were obtained by plotted the concentration of selected inhibitors vs. both saNOS and iNOS NO synthase activity. The NO synthase activities of purified full length iNOS were quantified using the oxyHb assay described in section 3.2.8. The IC50 index were plotted using percentage activity setting the activity in absence of inhibitors as 100%[81].

4.2.5 Determination of V_{max} of saNOS, K_m of H_4F and K_i of Selected Inhibitors

Dose dependence of H_4F on saNOS activity in presence of 20μM DHFR inhibitors was obtained using saNOS NO synthesis assay described in 3.2.8. The K_m of H_4F and V_{max} were obtained by fitting the dose-dependent curves with Lineweaver-Burk equation[130]. K'_m of H_4F in presence of different amounts of UCP121A and UCP111F26M were obtained with the same method. Competitive inhibition constant K_i of UCP121A and UCP111F26M for saNOS was calculated by fitting the following equation based on Michaelis-Menten mechanism for completive inhibitors[118]:

$$\frac{K'_m}{K_m} = \frac{[I]}{K_i} + 1$$

4.3 Results and Discussion

4.3.1 Structure Comparison of Inhibitors and H_4F

The structure and of chosen DHFR inhibitor, common mNOS cofactor H_4B, bNOS cofactor H_4F and mNOS inhibitor 4-Amino-(6R)-5,6,7,8-tetrahydro-L-biopterin dihydrochloride (4-amino-H_4B) are listed and compared in Fig. 36.

H_4F is an unique bNOS cofactor sharing the same structure with common mNOS cofactor H_4B except that H_4F has an extended glutamyl p-amino benzoic acid side chain (pABA side chain). Although crystal structure of H_4F bound saNOS has not yet been resolved, it is predicted that the 3,4 amino groups of H_4F bind to the saNOS heme carboxylate by hydrogen bond based on the structure of H_4F bounded bsNOS (Protein Data Bank (PDB) code: 1M7Z). This is similar to the interaction between H_4B with iNOS. On the other hand, the crystal structure of H_4B bound iNOS (Protein Data Bank Code (PBD) code: 1NOD) reveals the H_4B side chain clashes with the N-terminal hook of iNOS, implying that the pABA side chain of H_4F would not fit the mNOS pterin binding pocket. Different from iNOS, the pABA side chain of H_4F fits the binding pocked on bsNOS since bsNOS lacks the N-terminal hook. This difference explains why only the bNOSs are capable of getting electron from H_4F[25]. Considering the facts that (1) H_4F shares same biopterin ring with H_4F, (2) biopterin is an indispensable part for NOS catalysis and (3) H_4F is a preferred cofactor for saNOS than H_4B as shown in

section 3.3.5; we predict that the pABA side chain of H_4F is helping H_4F interacting with saNOS and it may be the key to create cofactor analogs which can specifically binds saNOS.

Inspired by this prediction, we found that the DHFR inhibitors based on TMP template might be good saNOS inhibitor. They do not have any reducing functional groups thus are not capable of transferring electrons to saNOS. The chosen DHFR inhibitors are derivatives of TMP and they are made of three different structural components, a 2,4-diaminopyrimidine head, a triple bond linker and an extended aromatic tail. The 2,4-diaminopyrimidine head is structurally similar with the pterin ring of H_4F thus potentially allowing these DHFR inhibitors to bind saNOS. The aromatic tail on DHFR inhibitors is structurally similar the pABA side chain on H_4F. It provides steric hindrance preventing these inhibitors from binding mNOS and potential strengthens the interaction between these inhibitors and saNOS. These selected DHFR inhibitors differ in two ways, (1) the R group on 6 position of 2,4-diaminopyrimidine ring (2) the structure of the aromotic tail. These modifications alter the binding properties of inhibitors and may result is a potent and specific saNOS inhibitor.

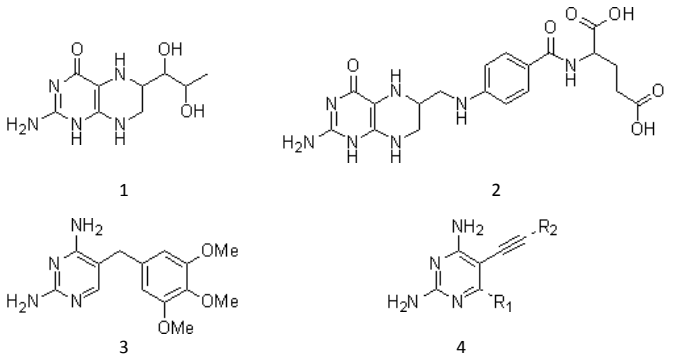

Inhibitor	R_1	R_2
UCP113D	--CH_3	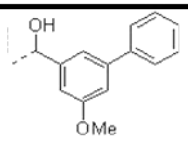
UCP111F26M	--CH_3	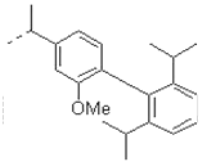
UCP121A	--\	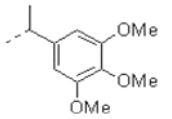
UCP1006	--\	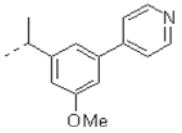
UCP1007	--CH_3	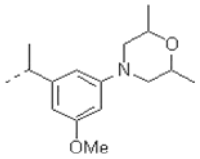
UCP111B	--CH_3	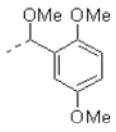

Fig. 36. **Structure of H4B (1), H4F(2), TMP(3), selected DHFR inhibitors(4)**

4.3.2 Effects of DHFR Inhibitor on YkuN and FLDR

The saNOS NO synthesis in the saNOS/YkuN/FLDR system involves several electron transfer steps as shown in Fig. 35. Before testing the potency of selected inhibitors, it is essential to figure out if these inhibitors affect the FLDR (step 1) and YkuN (step 2) used in the assay as reductase partner for saNOS. Here we employed the Hb reductase assay and cytochrome *c* reductase assay to study the impact of selected inhibitors on step 1 and 2. The Hb reductase activity of FLDR and cytochrome *c* reductase activity of YkuN were shown in Fig. 37. The results show all selected inhibitors have negligible effect on YkuN (electron transfer step 2) and FLDR (electron transfer step 1). Electron transfer from NADPH directly to flavodoxin YkuN without flavodoxin reductase is generally unfavored thus slow YkuN cytochrome c reduction rate was observed.

4.3.3 Effects of DHFR Inhibitors on saNOS.

The dose dependent curves of selected DHFR inhibitors and TMP were shown in Fig. 38 and their IC50 were listed in Table IV. Among the tested inhibitors, UCP121A and UCP111F26M showed surprisingly high potency while UCP111B showed no effect on saNOS NO synthesis. Other inhibitors showed potency similar to the parent compound TMP. The results show that except for UCP111B, all selected DHFR inhibitors inhibit saNOS activity by directly affecting the saNOS catalysis. The R group on the 6 position on the 2,4-diaminopyrimidine head does not seem to have determining

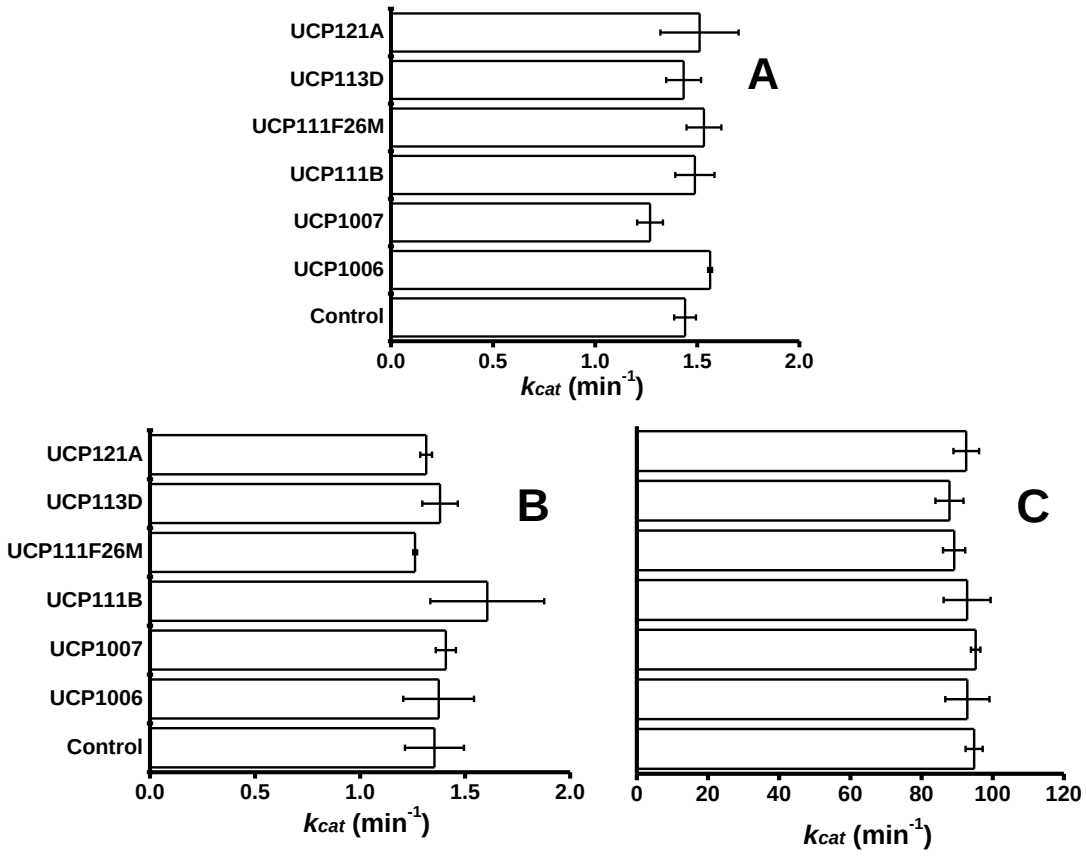

Fig. 37. **Effects of inhibitors on FLDR and YkuN.** *Panel A,* the Hb reductase activity of FLDR in presence of 15 µM inhibitors. *Panel B,* the cytochrome *c* reductase activity of YkuN in presence of 15 µM inhibitors. *Panel C,* the cytochrome *c* reductase activity of YkuN+FLDR in presence of 15 µM inhibitors. The control represents the activities in absence of inhibitors.

effect on the inhibition potency. The most potent inhibitors, UCP121A and UCP111F26M have different R_1 and the IC_{50} of inhibitors with the same R_1 differ significantly. Opposite to the effect to R_1, the aromatic tail structure R_2 drastically changes the IC_{50} of the inhibitors. One unique structure of the most potent inhibitor UCP111F26M is the two isopropyl groups on its aromatic tail. These two isopropyl arms may help the inhibitor stays in specific conformation which stabilizes the inhibitor-saNOS complex. The methoxy group on UCP121A may also has similar effect However, further study is need to elucidate the structure-potency relationship of these TMP based inhibitors.

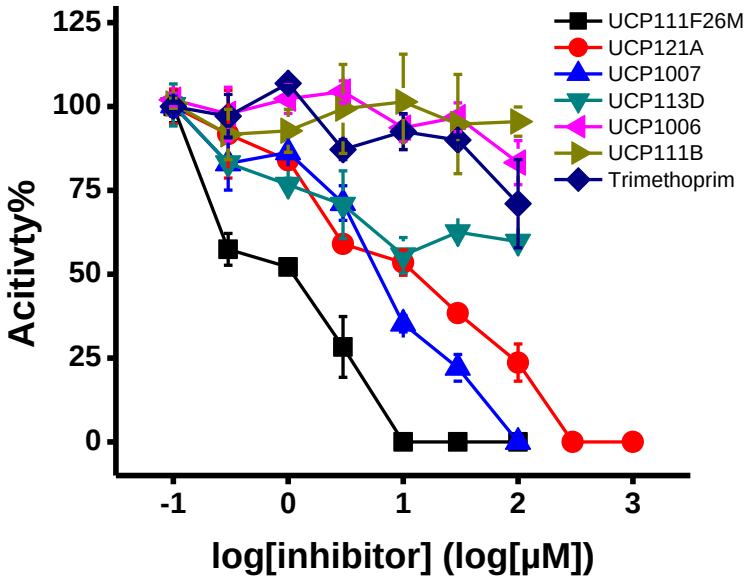

Fig. 38. **IC50 determination of selected inhibitors**

Table IV. *IC50 of selected inhibitors*

Inhibitor	***IC_{50} (μM)***
Trimethoprim	N/A
UCP111F26M	4.4 ± 2.1
UCP121A	36 ± 5.5
UCP1007	56 ± 9.7
UCP113D	369 ± 42
UCP1006	N/A
UCP111B	N/A

4.3.4 Selectivity of Tested Inhibitors

NO produced by iNOS in animal is important for the immune response so we need an inhibitor which can selectively inhibit the saNOS activity while left the iNOS activity intact. Here we studied the selectivity of the chosen DHFR inhibiters by comparing their effect on both iNOS and saNOS. The well-known iNOS inhibitor 4-amino-H_4B was used as a control. Results in Fig. 39A showed iNOS NO synthase activity remained almost unchanged in present of 15μM DHFR inhibitors, which is 5 times of H_4B used in the assay. As comparison, 15μM 4-amino-H4B inhibits almost all iNOS NO synthase activity. This result implies, the effective concentration for saNOS (15μM), DHFR inhibitors do not change iNOS NO synthase activity. Moreover, the IC50 index of UCP121A and UCP111F26M were shown in Fig 39B. This proves directly that the UCP121A and UCP111F26M are highly selective inhibitors for saNOS. The results

also prove our hypothesis that the aromatic tail on the DHFR inhibitor preventing them from binding to iNOS. The modification on the tail seems does not change their selectivity since the tested inhibitors has little effect on the iNOS activity under the experiment condition.

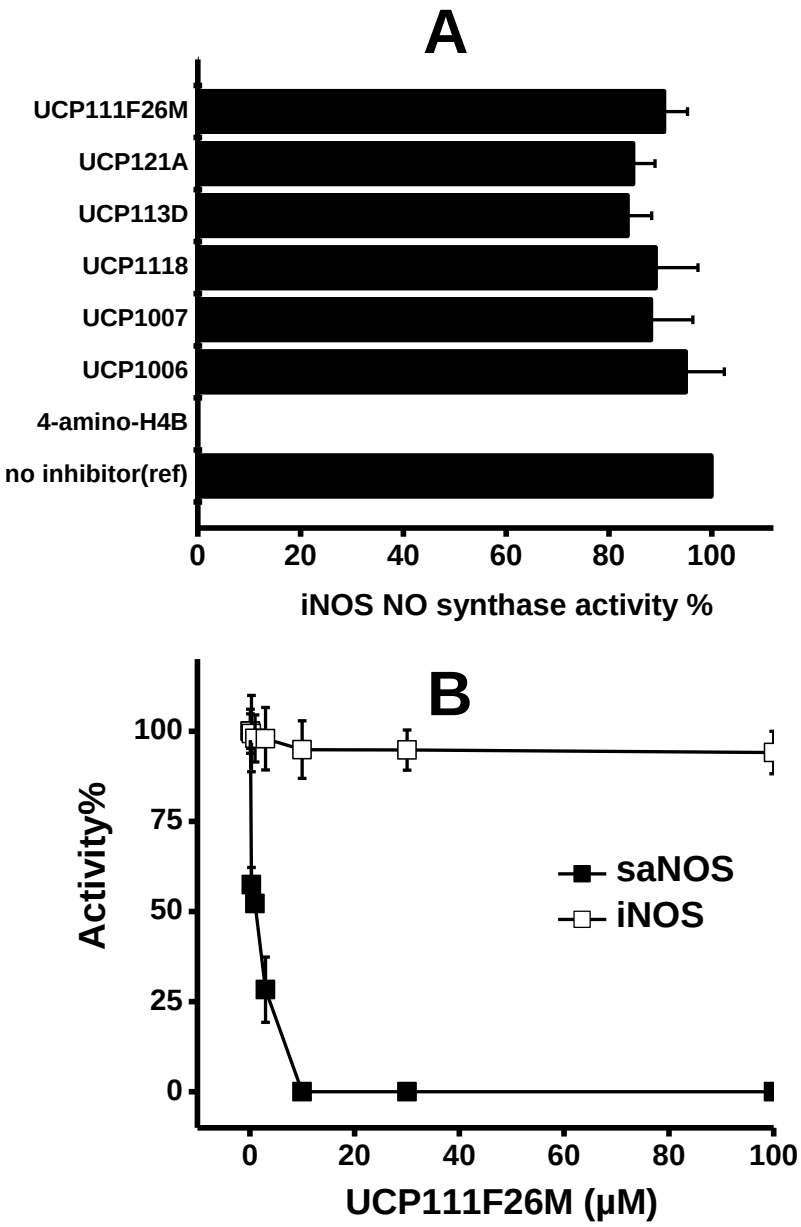

Fig. 39. **IC50 index determination**. *Panel A,* inhibitor's effect on iNOS. Activity of iNOS were measured in presence of 15 μM inhibitors. The dash line represents the activity of iNOS in absence of inhibitor. *Panel B,* IC50 index of UCP111F26M.

4.3.5 The Selected DHFR Inhibitors Are Competitive Inhibitors for H_4F

The inhibitory mechanism of these DHFR inhibitors is another important question in this study. In order to elucidate their inhibition mechanism, we obtained the dose-response curves of H_4F on saNOS activity in presence of a set amount of DHFR inhibitors to test if they are competitive inhibitor of H_4F since they were designed as H_4F analogs.

The double reciprocal analysis results were shown in Fig. 40. The Calculated apparent $K_{m.}$ *(*$K_{m.\ app}$*)* of H_4F and V_{max} for saNOS were listed in Table V. The V_{max} of saNOS in presence of all tested compound are all very close to V_{max} computed from H_4F dose dependent curve without inhibitors. This clearly showed the selected DHFR inhibitors are competitive inhibitors of H_4F. This proves DHFR inhibitors share the same binding site with H_4F. Considering the structure similarity between H_4F and DFHR inhibitors and the fact that the aromatic tail on the DHFR inhibitor alters the *Km* of inhibitor, it is implied that both the 2,4-diaminopyrimidine head and the aromatic tail on DHFR inhibitors interact with saNOS. Thus modification on either part will change its affinity to saNOS. The *Ki* of the two most potent inhibitors, UCP111F26M and UCP121A were obtained by plotting the $K_{m\ app}$ *versus* inhibitor concentration used for the corresponding $K_{m\ app}$ calculation (Fig. 41.) The small values of K_i for UCP111F26M also suggests it is a potent inhibitor.

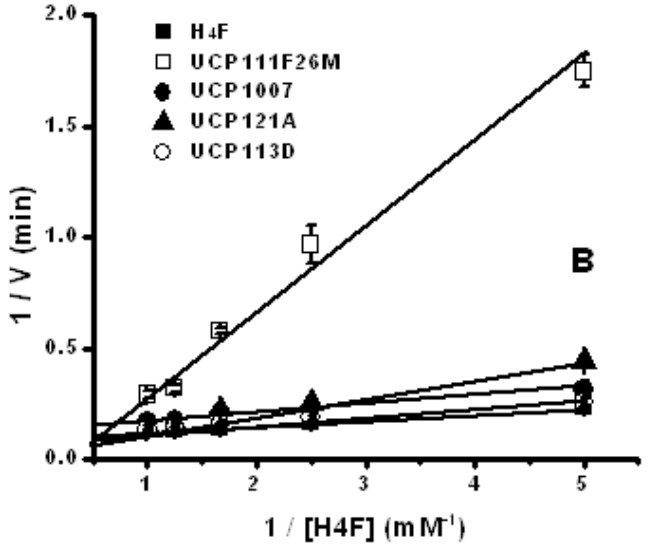

Fig. 40. ***K_m*** **and** ***V_{max}*** **determination using Lineweaver-Burk plot.**

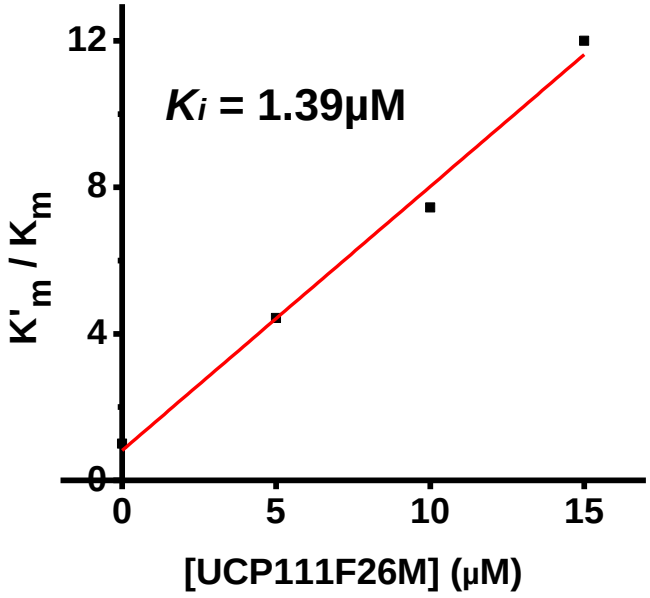

Fig. 41. ***K_i*** **determinations of UCP111F26M for saNOS**

Table V. *V_{max} and K_m determination of H_4F in absence and presence of DHFR inhibitors*

Inhibitors	$V_{max}(min^{-1})$	$K_m(mM^{-1}min^{-2})$
No inhibitors (H_4F only)	9.035056017	0.193892302
UCP111F26M	7.499625019	1.567046648
UCP1007	7.150518413	0.242259564
UCP121A	9.284189026	0.632346115
UCP113D	10.20824826	0.364638628

4.4 Conclusions

Facile inhibition of saNOS catalysis expands our understanding about saNOS and gives us a reliable way to specifically inhibit saNOS while not interfering with iNOS activity. These DHFR inhibitors resemble the structure of saNOS cofactor H_4F and specifically interacts with the saNOS and do not interfere other component enzymes used in assay. These inhibitors compete binding sites with saNOS cofactor H4F thus inhibit saNOS activity. The inhibition properties of DHFR inhibitors particularly suggested that H4F competitor development is a feasible away to develop selective saNOS inhibitor. The K_m differences of different inhibitors suggested that R group in the inhibitor tail provide specificity to the binding site on the saNOS. However, the actual impacts of each individual functional group on the aromatic tail still needs to be further studied. It will be interesting to crystallize the DHFR inhibitor bounded saNOS or do point mutations on these residues to further identify the cofactor binding site or structure feature on saNOS

causing specific binding between saNOS and DHFR inhibitors. This will further help us to design more selective and effective saNOS inhibitor. Also, it would be interesting to test these DHFR inhibitors on other bNOS system to figure out if this is a common feature for all bacterial NOS.

CHAPTER V

GENERAL DISCUSSION

5.1 Summary of Data

The data presented in Chapter 2 seeks to understand the electron transfer mechanism of nNOSr, while the data present in Chapter 3 and 4 seeks to setting up a robust approach to quantify saNOS activity and using this assay to evaluate the saNOS inhibitor. The major finds of the works are summarized as follows:

The study about nNOSr reveals the nNOSr electron is regulated conformationally by FMN domain motion. In electron transfer through nNOSr, FMN shuttles electron from FAD to its electron accepter. Constraining of the FMN domain motion severally impairs the electron transfer through nNOSr. FMNhq and FMNsq is also in equilibrium during the nNOSr electron transfer and this FMNhq/FMNsq equilibrium is related with the nNOSr conformational opening-closing.

In another separated research project focusing on bacterial drug selection, we found the PEGylated hemoglobin is a suitable NO indicator preventing the hemoglobin going to the futile cycle during oxyhemoglobin assay and can be used directly quantifying the NO production by cell cytosol. The assay using PEGylated hemoglobin as NO indicator and YkuN/FLDR as external reductase partner also successfully quantified the saNOS activity. With the help of this assay, we tested 6 potential saNOS inhibitors, which structurally similar with H_4F and found two of the tested compounds were very potent against saNOS while do not significantly interrupted iNOS, providing a good template for future selective saNOS inhibitor design.

5.2 Experimental Limitations

Due the technical difficulties of generating a full length cys-lite NOS, the electron transfer studies were first done with the reductase domain only using artificial electron acceptor cytochrome *c*, leaving a knowledge gap between the conformation equilibrium of NOSr and the NO synthase activity of NOSoxy. How this conformation equilibrium affects the NO synthesis, heme reduction and other behaviors of NOSoxy remains unknown. Although cytochrome *c* is a good electron acceptor of nNOSr, the faster electron transfer from nNOSr to cytochrome *c* made all intermediates, which may be important in the electron transfer from nNOSr to nNOSoxy invisible and undetectable by our experimental approaches. Also, we are not able to get a fully cytochrome *c* reduction trace by our stopped-flow instrument since we cannot monitor the absorbance change within the instrument dead time, resulting in an incomplete information and only an

estimated K_{hq} value. Although the data we extract from stopped-flow experiment is sufficient to confirm our hypothesis, we still lack the ability to study kinetics faster than 200 s^{-1}.

On the other hand, whether there are better reductase partner for saNOS remains unknown, leaving the possibility that FLDR/YkuN may not be an optimal reductase partner of saNOS. The activity of saNOS quantified by our assay is generally slow, it would be better if we can identify more efficient reductase partner for saNOS, which will give us a larger window to study the effect of inhibitor on saNOS activity. Also, due to the security requirements of our lab, currently we are not allowed to conduct experiments testing these inhibitors with *S. aureus.* So the real effect of these inhibitors on *S. aureus* remains unclear.

5.3 Future Directions

Different facets of the nNOS conformation can be studied using the locked down version of NOS. One priority is generating a full length cys-lite nNOS to study the impact of nNOSr conformation on nNOS overall catalysis. Function of other regulatory elements within the reductase can also be studied using other locked down nNOSr, such as studying the function of CT using a CT-FMN locked down nNOSr or CT-FNR locked down nNOSr. Also, this approach can apply to other NOS isoforms and other protein systems. Single molecule FRED approaches can be used to get more precise information about distance in our locked down NOS, providing more information which cannot be obtained by our current kinetic approaches.

For the saNOS selection, more efficient reductase may be needed for setting up a better *in vitro* assay. Flavindoxin and flavindoxin oxidoreductase from other bacteria may be good candidates. More importantly, test with live *S. aureus* bacteria is critical for this study. Study with behaviors of *S. aureus* in response to inhibitor may lead us to find other virulence factor of *S. aureus* or helping us to reveal the mechanism of how *S. aureus* develop antibiotics resistance. Last but not least, structure based design of more potent and selective inhibitor can benefit great this research and also *S. aureus* related clinical researches.

References

1. Koppenol, W.H., *The basic chemistry of nitrogen monoxide and peroxynitrite.* Free Radical Biology and Medicine, 1998. **25**(4–5): p. 385-391.
2. Patel, R.P., et al., *Biological aspects of reactive nitrogen species.* Biochimica et Biophysica Acta (BBA) - Bioenergetics, 1999. **1411**(2–3): p. 385-400.
3. Alderton, W.K., C.E. Cooper, and R.G. Knowles, *Nitric oxide synthases: structure, function and inhibition.* Biochem J, 2001. **357**(Pt 3): p. 593-615.
4. Barbato, J.E. and E. Tzeng, *Nitric oxide and arterial disease.* Journal of Vascular Surgery, 2004. **40**(1): p. 187-193.
5. Griffith, O.W. and D.J. Stuehr, *Nitric oxide synthases: properties and catalytic mechanism.* Annu Rev Physiol, 1995. **57**: p. 707-36.
6. Knott, A.B. and E. Bossy-Wetzel, *Nitric oxide in health and disease of the nervous system.* Antioxid Redox Signal, 2009. **11**(3): p. 541-54.
7. Lipton, S.A., *Physiology: Nitric oxide and respiration.* Nature, 2001. **413**(6852): p. 118-121.
8. Nott, A. and A. Riccio, *Nitric oxide-mediated epigenetic mechanisms in developing neurons.* Cell Cycle, 2009. **8**(5): p. 725-30.
9. Pfeiffer, S., B. Mayer, and B. Hemmens, *Nitric Oxide: Chemical Puzzles Posed by a Biological Messenger.* Angewandte Chemie International Edition, 1999. **38**(12): p. 1714-1731.
10. Yun, H.Y., V.L. Dawson, and T.M. Dawson, *Neurobiology of nitric oxide.* Crit Rev Neurobiol, 1996. **10**(3-4): p. 291-316.

11. Bellamy, T.C. and J. Garthwaite, *Pharmacology of the nitric oxide receptor, soluble guanylyl cyclase, in cerebellar cells.* Br J Pharmacol, 2002. **136**(1): p. 95-103.

12. Brandish, P.E., W. Buechler, and M.A. Marletta, *Regeneration of the ferrous heme of soluble guanylate cyclase from the nitric oxide complex: acceleration by thiols and oxyhemoglobin.* Biochemistry, 1998. **37**(48): p. 16898-907.

13. Martin, E., et al., *Soluble guanylyl cyclase: the nitric oxide receptor.* Methods Enzymol, 2005. **396**: p. 478-92.

14. Zhao, Y., P.M. Vanhoutte, and S.W. Leung, *Vascular nitric oxide: Beyond eNOS.* J Pharmacol Sci, 2015. **129**(2): p. 83-94.

15. Kroncke, K.D., *Nitrosative stress and transcription.* Biol Chem, 2003. **384**(10-11): p. 1365-77.

16. Iovine, N.M., et al., *Reactive Nitrogen Species Contribute to Innate Host Defense against Campylobacter jejuni.* Infection and Immunity, 2008. **76**(3): p. 986-993.

17. Pauly, N., et al., *Reactive oxygen and nitrogen species and glutathione: key players in the legume-Rhizobium symbiosis.* J Exp Bot, 2006. **57**(8): p. 1769-76.

18. Stuehr, D.J., *Mammalian nitric oxide synthases.* Biochim Biophys Acta, 1999. **1411**(2-3): p. 217-30.

19. Knowles, R.G. and S. Moncada, *Nitric oxide synthases in mammals.* Biochemical Journal, 1994. **298**(Pt 2): p. 249-258.

20. Zhou, L. and D.-Y. Zhu, *Neuronal nitric oxide synthase: Structure, subcellular localization, regulation, and clinical implications.* Nitric Oxide, 2009. **20**(4): p. 223-230.

21. Kröncke, K.D., K. Fehsel, and V. Kolb-Bachofen, *Inducible nitric oxide synthase in human diseases.* Clinical and Experimental Immunology, 1998. **113**(2): p. 147-156.

22. Jin, R.C. and J. Loscalzo, *Vascular nitric oxide: formation and function.* Journal of blood medicine, 2010. **1**: p. 147-162.

23. Chatterjee, A. and J.D. Catravas, *ENDOTHELIAL NITRIC OXIDE (NO) AND ITS PATHOPHYSIOLOGIC REGULATION.* Vascular pharmacology, 2008. **49**(4-6): p. 134-140.

24. Kopincová, J., A. Púzserová, and I. Bernátová, *Biochemical aspects of nitric oxide synthase feedback regulation by nitric oxide.* Interdisciplinary Toxicology, 2011. **4**(2): p. 63-68.

25. Crane, B.R., J. Sudhamsu, and B.A. Patel, *Bacterial nitric oxide synthases.* Annu Rev Biochem, 2010. **79**: p. 445-70.

26. Stuehr, D.J., *Structure-function aspects in the nitric oxide synthases.* Annu Rev Pharmacol Toxicol, 1997. **37**: p. 339-59.

27. Tejero, J., et al., *A bridging interaction allows calmodulin to activate NO synthase through a bi-modal mechanism.* J Biol Chem, 2010. **285**(34): p. 25941-9.

28. Hannibal, L., et al., *Dissecting structural and electronic effects in inducible nitric oxide synthase.* Biochem J, 2015. **467**(1): p. 153-65.

29. Haque, M.M., et al., *Charge-pairing interactions control the conformational setpoint and motions of the FMN domain in neuronal nitric oxide synthase.* Biochem J, 2013. **450**(3): p. 607-17.

30. Crane, B.R., et al., *The Structure of Nitric Oxide Synthase Oxygenase Domain and Inhibitor Complexes.* Science, 1997. **278**(5337): p. 425-431.

31. Zhang, J., et al., *Crystal structure of the FAD/NADPH-binding domain of rat neuronal nitric-oxide synthase. Comparisons with NADPH-cytochrome P450 oxidoreductase.* J Biol Chem, 2001. **276**(40): p. 37506-13.

32. Raman, C.S., et al., *Crystal structure of constitutive endothelial nitric oxide synthase: a paradigm for pterin function involving a novel metal center.* Cell, 1998. **95**(7): p. 939-50.

33. Doukov, T., et al., *Single crystal structural and absorption spectral characterizations of nitric oxide synthase complexed with N(ω)-hydroxy-L-arginine and diatomic ligands.* Biochemistry, 2009. **48**(43): p. 10246-10254.

34. Tejero, J. and D. Stuehr, *Tetrahydrobiopterin in nitric oxide synthase.* IUBMB Life, 2013. **65**(4): p. 358-65.

35. Stuehr, D.J., J. Tejero, and M.M. Haque, *Structural and mechanistic aspects of flavoproteins: electron transfer through the nitric oxide synthase flavoprotein domain.* Febs j, 2009. **276**(15): p. 3959-74.

36. Page, C.C., C.C. Moser, and P.L. Dutton, *Mechanism for electron transfer within and between proteins.* Current Opinion in Chemical Biology, 2003. **7**(5): p. 551-556.

37. Stuehr, D.J., et al., *Update on mechanism and catalytic regulation in the NO synthases.* J Biol Chem, 2004. **279**(35): p. 36167-70.

38. Porasuphatana, S., et al., *Involvement of the perferryl complex of nitric oxide synthase in the catalysis of secondary free radical formation.* Biochim Biophys Acta, 2001. **1526**(1): p. 95-104.

39. Schwarz, P.M., H. Kleinert, and U. Forstermann, *Potential functional significance of brain-type and muscle-type nitric oxide synthase I expressed in adventitia and media of rat aorta.* Arterioscler Thromb Vasc Biol, 1999. **19**(11): p. 2584-90.

40. van Praag, H., et al., *Functional neurogenesis in the adult hippocampus.* Nature, 2002. **415**(6875): p. 1030-4.

41. Romero-Grimaldi, C., B. Moreno-Lopez, and C. Estrada, *Age-dependent effect of nitric oxide on subventricular zone and olfactory bulb neural precursor proliferation.* J Comp Neurol, 2008. **506**(2): p. 339-46.

42. Islam, A.T., A. Kuraoka, and M. Kawabuchi, *Morphological basis of nitric oxide production and its correlation with the polysialylated precursor cells in the dentate gyrus of the adult guinea pig hippocampus.* Anat Sci Int, 2003. **78**(2): p. 98-103.

43. Matarredona, E.R., et al., *Nitric oxide synthesis inhibition increases proliferation of neural precursors isolated from the postnatal mouse subventricular zone.* Brain Res, 2004. **995**(2): p. 274-84.

44. Zhu, X.J., et al., *Neuronal nitric oxide synthase-derived nitric oxide inhibits neurogenesis in the adult dentate gyrus by down-regulating cyclic AMP response element binding protein phosphorylation.* Neuroscience, 2006. **141**(2): p. 827-36.

45. Packer, M.A., et al., *Nitric oxide negatively regulates mammalian adult neurogenesis.* Proc Natl Acad Sci U S A, 2003. **100**(16): p. 9566-71.

46. Blackshaw, S., et al., *Species, strain and developmental variations in hippocampal neuronal and endothelial nitric oxide synthase clarify discrepancies in nitric oxide-dependent synaptic plasticity.* Neuroscience, 2003. **119**(4): p. 979-90.

47. Haley, J.E., G.L. Wilcox, and P.F. Chapman, *The role of nitric oxide in hippocampal long-term potentiation.* Neuron, 1992. **8**(2): p. 211-6.

48. Bohme, G.A., et al., *Altered synaptic plasticity and memory formation in nitric oxide synthase inhibitor-treated rats.* Proc Natl Acad Sci U S A, 1993. **90**(19): p. 9191-4.

49. Rickard, N.S. and M.E. Gibbs, *Effects of nitric oxide inhibition on avoidance learning in the chick are lateralized and localized.* Neurobiol Learn Mem, 2003. **79**(3): p. 252-6.

50. Holscher, C., et al., *7-Nitro indazole, a selective neuronal nitric oxide synthase inhibitor in vivo, impairs spatial learning in the rat.* Learn Mem, 1996. **2**(6): p. 267-78.

51. Weitzdoerfer, R., et al., *Neuronal nitric oxide synthase knock-out mice show impaired cognitive performance.* Nitric Oxide, 2004. **10**(3): p. 130-40.

52. Kirchner, L., et al., *Impaired cognitive performance in neuronal nitric oxide synthase knockout mice is associated with hippocampal protein derangements.* Nitric Oxide, 2004. **11**(4): p. 316-30.

53. Sattler, R. and M. Tymianski, *Molecular mechanisms of calcium-dependent excitotoxicity.* J Mol Med (Berl), 2000. **78**(1): p. 3-13.

54. Arundine, M. and M. Tymianski, *Molecular mechanisms of calcium-dependent neurodegeneration in excitotoxicity.* Cell Calcium, 2003. **34**(4-5): p. 325-37.

55. Eliasson, M.J., et al., *Neuronal nitric oxide synthase activation and peroxynitrite formation in ischemic stroke linked to neural damage.* J Neurosci, 1999. **19**(14): p. 5910-8.

56. Oka, M., et al., *Involvement of peroxynitrite and hydroxyradical generated from nitric oxide in hypoxia/reoxygenation injury in rat cerebrocortical slices.* Neuropharmacology, 2000. **39**(7): p. 1319-30.

57. Dawson, V.L., et al., *Resistance to neurotoxicity in cortical cultures from neuronal nitric oxide synthase-deficient mice.* J Neurosci, 1996. **16**(8): p. 2479-87.

58. Manji, H.K., W.C. Drevets, and D.S. Charney, *The cellular neurobiology of depression.* Nat Med, 2001. **7**(5): p. 541-7.

59. Angulo, J., et al., *Differential effects of serotonin reuptake inhibitors on erectile responses, NO-production, and neuronal NO synthase expression in rat corpus cavernosum tissue.* Br J Pharmacol, 2001. **134**(6): p. 1190-4.

60. Harvey, B.H., et al., *Increased hippocampal nitric oxide synthase activity and stress responsiveness after imipramine discontinuation: role of 5HT 2A/C-receptors.* Metab Brain Dis, 2006. **21**(2-3): p. 211-20.

61. Yildiz, F., et al., *Antidepressant-like effect of 7-nitroindazole in the forced swimming test in rats.* Psychopharmacology (Berl), 2000. **149**(1): p. 41-4.

62. Zhou, Q.G., et al., *Neuronal nitric oxide synthase contributes to chronic stress-induced depression by suppressing hippocampal neurogenesis.* J Neurochem, 2007. **103**(5): p. 1843-54.

63. Burns, R.S., et al., *A primate model of parkinsonism: selective destruction of dopaminergic neurons in the pars compacta of the substantia nigra by N-methyl-4-phenyl-1,2,3,6-tetrahydropyridine.* Proc Natl Acad Sci U S A, 1983. **80**(14): p. 4546-50.

64. Kuhn, K., et al., *The mouse MPTP model: gene expression changes in dopaminergic neurons.* Eur J Neurosci, 2003. **17**(1): p. 1-12.

65. Matthews, R.T., et al., *MPP+ induced substantia nigra degeneration is attenuated in nNOS knockout mice.* Neurobiol Dis, 1997. **4**(2): p. 114-21.

66. Kurosaki, R., et al., *Role of nitric oxide synthase against MPTP neurotoxicity in mice.* Neurol Res, 2002. **24**(7): p. 655-62.

67. Gatto, E.M., et al., *Overexpression of neutrophil neuronal nitric oxide synthase in Parkinson's disease.* Nitric Oxide, 2000. **4**(5): p. 534-9.

68. Selkoe, D.J., *Alzheimer's disease: genes, proteins, and therapy.* Physiol Rev, 2001. **81**(2): p. 741-66.

69. Tran, M.H., et al., *Tyrosine nitration of a synaptic protein synaptophysin contributes to amyloid beta-peptide-induced cholinergic dysfunction.* Mol Psychiatry, 2003. **8**(4): p. 407-12.

70. Malinski, T., *Nitric oxide and nitroxidative stress in Alzheimer's disease.* J Alzheimers Dis, 2007. **11**(2): p. 207-18.

71. Simic, G., et al., *nNOS expression in reactive astrocytes correlates with increased cell death related DNA damage in the hippocampus and entorhinal cortex in Alzheimer's disease.* Exp Neurol, 2000. **165**(1): p. 12-26.

72. Thorns, V., L. Hansen, and E. Masliah, *nNOS expressing neurons in the entorhinal cortex and hippocampus are affected in patients with Alzheimer's disease.* Exp Neurol, 1998. **150**(1): p. 14-20.

73. Luth, H.J., et al., *Expression of endothelial and inducible NOS-isoforms is increased in Alzheimer's disease, in APP23 transgenic mice and after experimental brain lesion in rat: evidence for an induction by amyloid pathology.* Brain Res, 2001. **913**(1): p. 57-67.

74. Barbaree, J.M. and W.J. Payne, *Products of denitrification by a marine bacterium as revealed by gas chromatography.* Marine Biology, 1967. **1**(2): p. 136-139.

75. Kelly, D.P. and A.P. Wood, *Confirmation of Thiobacillus denitrificans as a species of the genus Thiobacillus, in the beta-subclass of the Proteobacteria, with strain NCIMB 9548 as the type strain.* Int J Syst Evol Microbiol, 2000. **50 Pt 2**: p. 547-50.

76. Lam, Y. and D.J.D. Nicholas, *A nitrate reductase from Micrococcus denitrificans.* Biochimica et Biophysica Acta (BBA) - Enzymology, 1969. **178**(2): p. 225-234.

77. Baumann, B., et al., *Dynamics of denitrification activity of Paracoccus denitrificans in continuous culture during aerobic-anaerobic changes.* Journal of Bacteriology, 1996. **178**(15): p. 4367-4374.

78. Lenhart, J.S., et al., *DNA Repair and Genome Maintenance in Bacillus subtilis.* Microbiology and Molecular Biology Reviews : MMBR, 2012. **76**(3): p. 530-564.

79. White, O., et al., *Genome sequence of the radioresistant bacterium Deinococcus radiodurans R1.* Science, 1999. **286**(5444): p. 1571-7.

80. Adak, S., et al., *Cloning, expression, and characterization of a nitric oxide synthase protein from Deinococcus radiodurans.* Proc Natl Acad Sci U S A, 2002. **99**(1): p. 107-12.

81. Adak, S., K.S. Aulak, and D.J. Stuehr, *Direct evidence for nitric oxide production by a nitric-oxide synthase-like protein from Bacillus subtilis.* J Biol Chem, 2002. **277**(18): p. 16167-71.

82. Reece, S.Y., J.J. Woodward, and M.A. Marletta, *Synthesis of nitric oxide by the NOS-like protein from deinococcus radiodurans: a direct role for tetrahydrofolate.* Biochemistry, 2009. **48**(23): p. 5483-91.

83. Johnson, E.G., et al., *Plant-pathogenic Streptomyces species produce nitric oxide synthase-derived nitric oxide in response to host signals.* Chem Biol, 2008. **15**(1): p. 43-50.

84. Gusarov, I., et al., *Bacterial nitric-oxide synthases operate without a dedicated redox partner.* J Biol Chem, 2008. **283**(19): p. 13140-7.

85. Shatalin, K., et al., *Bacillus anthracis-derived nitric oxide is essential for pathogen virulence and survival in macrophages.* Proc Natl Acad Sci U S A, 2008. **105**(3): p. 1009-13.

86. Patel, B.A., et al., *Endogenous nitric oxide regulates the recovery of the radiation-resistant bacterium Deinococcus radiodurans from exposure to UV light.* Proc Natl Acad Sci U S A, 2009. **106**(43): p. 18183-8.

87. Pant, K., et al., *Structure of a nitric oxide synthase heme protein from Bacillus subtilis.* Biochemistry, 2002. **41**(37): p. 11071-9.

88. Bird, L.E., et al., *Crystal Structure of SANOS, a Bacterial Nitric Oxide Synthase Oxygenase Protein from Staphylococcus aureus.* Structure, 2002. **10**(12): p. 1687-1696.

89. Sudhamsu, J. and B.R. Crane, *Structure and reactivity of a thermostable prokaryotic nitric-oxide synthase that forms a long-lived oxy-heme complex.* J Biol Chem, 2006. **281**(14): p. 9623-32.

90. Schneiker, S., et al., *Complete genome sequence of the myxobacterium Sorangium cellulosum.* Nat Biotechnol, 2007. **25**(11): p. 1281-9.

91. Agapie, T., et al., *NO formation by a catalytically self-sufficient bacterial nitric oxide synthase from Sorangium cellulosum.* Proc Natl Acad Sci U S A, 2009. **106**(38): p. 16221-6.

92. Kers, J.A., et al., *Nitration of a peptide phytotoxin by bacterial nitric oxide synthase.* Nature, 2004. **429**(6987): p. 79-82.

93. Healy, F.G., et al., *The txtAB genes of the plant pathogen Streptomyces acidiscabies encode a peptide synthetase required for phytotoxin thaxtomin A production and pathogenicity.* Mol Microbiol, 2000. **38**(4): p. 794-804.

94. Cox, M.M. and J.R. Battista, *Deinococcus radiodurans [mdash] the consummate survivor.* Nat Rev Micro, 2005. **3**(11): p. 882-892.

95. Battista, J.R., *Against all odds: the survival strategies of Deinococcus radiodurans.* Annu Rev Microbiol, 1997. **51**: p. 203-24.

96. Buddha, M.R., K.M. Keery, and B.R. Crane, *An unusual tryptophanyl tRNA synthetase interacts with nitric oxide synthase in Deinococcus radiodurans.* Proc Natl Acad Sci U S A, 2004. **101**(45): p. 15881-6.

97. Gusarov, I., et al., *Endogenous nitric oxide protects bacteria against a wide spectrum of antibiotics.* Science, 2009. **325**(5946): p. 1380-4.

98. Gusarov, I. and E. Nudler, *NO-mediated cytoprotection: instant adaptation to oxidative stress in bacteria.* Proc Natl Acad Sci U S A, 2005. **102**(39): p. 13855-60.

99. Garcin, E.D., et al., *Structural basis for isozyme-specific regulation of electron transfer in nitric-oxide synthase.* J Biol Chem, 2004. **279**(36): p. 37918-27.

100. He, Y., et al., *Single-molecule spectroscopy reveals how calmodulin activates NO synthase by controlling its conformational fluctuation dynamics.* Proc Natl Acad Sci U S A, 2015. **112**(38): p. 11835-40.

101. Tiso, M., et al., *C-terminal tail residue Arg1400 enables NADPH to regulate electron transfer in neuronal nitric-oxide synthase.* J Biol Chem, 2005. **280**(47): p. 39208-19.

102. Tiso, M., et al., *Versatile regulation of neuronal nitric oxide synthase by specific regions of its C-terminal tail.* Biochemistry, 2007. **46**(50): p. 14418-28.

103. Adak, S., et al., *Neuronal nitric-oxide synthase mutant (Ser-1412 --> Asp) demonstrates surprising connections between heme reduction, NO complex formation, and catalysis.* J Biol Chem, 2001. **276**(2): p. 1244-52.

104. Konas, D.W., et al., *The FAD-shielding residue Phe1395 regulates neuronal nitric-oxide synthase catalysis by controlling NADP+ affinity and a*

conformational equilibrium within the flavoprotein domain. J Biol Chem, 2004. **279**(34): p. 35412-25.

105. Konas, D.W., et al., *Role of Asp1393 in catalysis, flavin reduction, NADP(H) binding, FAD thermodynamics, and regulation of the nNOS flavoprotein.* Biochemistry, 2006. **45**(41): p. 12596-609.

106. Panda, K., et al., *A conserved aspartate (Asp-1393) regulates NADPH reduction of neuronal nitric-oxide synthase: implications for catalysis.* J Biol Chem, 2004. **279**(18): p. 18323-33.

107. Ellis, J., et al., *Domain motion in cytochrome P450 reductase: conformational equilibria revealed by NMR and small-angle x-ray scattering.* J Biol Chem, 2009. **284**(52): p. 36628-37.

108. Xia, C., et al., *Conformational changes of NADPH-cytochrome P450 oxidoreductase are essential for catalysis and cofactor binding.* J Biol Chem, 2011. **286**(18): p. 16246-60.

109. Haque, M.M., et al., *Distinct conformational behaviors of four mammalian dual-flavin reductases (cytochrome P450 reductase, methionine synthase reductase, neuronal nitric oxide synthase, endothelial nitric oxide synthase) determine their unique catalytic profiles.* Febs j, 2014. **281**(23): p. 5325-40.

110. Haque, M.M., et al., *Thermodynamic characterization of five key kinetic parameters that define neuronal nitric oxide synthase catalysis.* Febs j, 2013. **280**(18): p. 4439-53.

111. Haque, M.M., et al., *Control of electron transfer and catalysis in neuronal nitric-oxide synthase (nNOS) by a hinge connecting its FMN and FAD-NADPH domains.* J Biol Chem, 2012. **287**(36): p. 30105-16.

112. Adak, S., et al., *Role of reductase domain cluster 1 acidic residues in neuronal nitric-oxide synthase. Characterization of the FMN-FREE enzyme.* J Biol Chem, 1999. **274**(32): p. 22313-20.

113. Welland, A., et al., *Importance of the domain-domain interface to the catalytic action of the NO synthase reductase domain.* Biochemistry, 2008. **47**(37): p. 9771-80.

114. Tejero, J., et al., *Surface charges and regulation of FMN to heme electron transfer in nitric-oxide synthase.* J Biol Chem, 2010. **285**(35): p. 27232-40.

115. Panda, K., et al., *Surface charge interactions of the FMN module govern catalysis by nitric-oxide synthase.* J Biol Chem, 2006. **281**(48): p. 36819-27.

116. Guan, Z.W., et al., *Lys842 in neuronal nitric-oxide synthase enables the autoinhibitory insert to antagonize calmodulin binding, increase FMN shielding, and suppress interflavin electron transfer.* J Biol Chem, 2010. **285**(5): p. 3064-75.

117. Holden, J.K., N. Lim, and T.L. Poulos, *Identification of Redox Partners and Development of a Novel Chimeric Bacterial Nitric Oxide Synthase for Structure Activity Analyses.* Journal of Biological Chemistry, 2014. **289**(42): p. 29437-29445.

118. Stuehr, D.J., *Enzymes of the l-Arginine to Nitric Oxide Pathway.* The Journal of Nutrition, 2004. **134**(10): p. 2748S-2751S.

119. Bryan, N.S. and M.B. Grisham, *Methods to detect nitric oxide and its metabolites in biological samples.* Free Radic Biol Med, 2007. **43**(5): p. 645-57.

120. Wang, Z.Q., et al., *Bacterial flavodoxins support nitric oxide production by Bacillus subtilis nitric-oxide synthase.* J Biol Chem, 2007. **282**(4): p. 2196-202.

121. Chen, Y. and J.P. Rosazza, *A bacterial nitric oxide synthase from a Nocardia species.* Biochem Biophys Res Commun, 1994. **203**(2): p. 1251-8.

122. Choi, W.S., et al., *Identification of nitric oxide synthase in Staphylococcus aureus.* Biochem Biophys Res Commun, 1997. **237**(3): p. 554-8.

123. Vandegriff, K.D., et al., *MP4, a new nonvasoactive PEG-Hb conjugate.* Transfusion, 2003. **43**(4): p. 509-16.

124. Hu, T., et al., *Influence of the chemistry of conjugation of poly(ethylene glycol) to Hb on the oxygen-binding and solution properties of the PEG-Hb conjugate.* Biochem J, 2005. **392**(Pt 3): p. 555-64.

125. Wang, Z.-Q., C.-C. Wei, and D.J. Stuehr, *How does a valine residue that modulates heme-NO binding kinetics in inducible NO synthase regulate enzyme catalysis?* Journal of Inorganic Biochemistry, 2010. **104**(3): p. 349-356.

126. Lawson, R.J., et al., *Expression and characterization of the two flavodoxin proteins of Bacillus subtilis, YkuN and YkuP: biophysical properties and interactions with cytochrome P450 BioI.* Biochemistry, 2004. **43**(39): p. 12390-409.

127. Chakravarti, R. and D.J. Stuehr, *Thioredoxin-1 regulates cellular heme insertion by controlling S-nitrosation of glyceraldehyde-3-phosphate dehydrogenase.* J Biol Chem, 2012. **287**(20): p. 16179-86.

128. Lui, F.E., P. Dong, and R. Kluger, *Polyethylene glycol conjugation enhances the nitrite reductase activity of native and cross-linked hemoglobin.* Biochemistry, 2008. **47**(40): p. 10773-80.

129. Salter, M. and R. Knowles, *Assay of NOS Activity by the Measurement of Conversion of Oxyhemoglobin to Methemoglobin by NO,* in *Nitric Oxide Protocols,* M. Titheradge, Editor. 1998, Humana Press. p. 61-65.

130. Stuehr, D.J., et al., *N omega-hydroxy-L-arginine is an intermediate in the biosynthesis of nitric oxide from L-arginine.* J Biol Chem, 1991. **266**(10): p. 6259-63.

131. Ascenzi, P., M.G. Ascenzi, and G. Amiconi, *Enzyme competitive inhibition. Graphical determination of Ki and presentation of data in comparative studies.* Biochemical Education, 1987. **15**(3): p. 134-135.

132. Zijlstra, W.G. and A. Buursma, *Spectrophotometry of Hemoglobin: Absorption Spectra of Bovine Oxyhemoglobin, Deoxyhemoglobin, Carboxyhemoglobin, and Methemoglobin.* Comparative Biochemistry and Physiology Part B: Biochemistry and Molecular Biology, 1997. **118**(4): p. 743-749.

133. Bird, L.E., et al., *Crystal structure of SANOS, a bacterial nitric oxide synthase oxygenase protein from Staphylococcus aureus.* Structure, 2002. **10**(12): p. 1687-96.

134. Chakravarti, R., et al., *Novel insights in mammalian catalase heme maturation: Effect of NO and thioredoxin-1.* Free Radic Biol Med, 2015. **82**: p. 105-13.

135. Plata, K., A.E. Rosato, and G. Wegrzyn, *Staphylococcus aureus as an infectious agent: overview of biochemistry and molecular genetics of its pathogenicity.* Acta Biochim Pol, 2009. **56**(4): p. 597-612.

136. Chang, V.S., et al., *Antibiotic Resistance in the Treatment of Staphylococcus aureus Keratitis: a 20-Year Review.* Cornea, 2015. **34**(6): p. 698-703.

137. Knox, J., A.C. Uhlemann, and F.D. Lowy, *Staphylococcus aureus infections: transmission within households and the community.* Trends Microbiol, 2015. **23**(7): p. 437-44.

138. Rao, Q., et al., *Staphylococcus aureus ST121: a globally disseminated hypervirulent clone.* J Med Microbiol, 2015. **64**(12): p. 1462-73.

139. Chambers, H.F. and F.R. Deleo, *Waves of resistance: Staphylococcus aureus in the antibiotic era.* Nat Rev Microbiol, 2009. **7**(9): p. 629-41.

140. van Sorge, N.M., et al., *Methicillin-resistant Staphylococcus aureus bacterial nitric-oxide synthase affects antibiotic sensitivity and skin abscess development.* J Biol Chem, 2013. **288**(9): p. 6417-26.

141. Holden, J.K., et al., *Nitric Oxide Synthase as a Target for Methicillin-Resistant Staphylococcus aureus.* Chem Biol, 2015. **22**(6): p. 785-92.

142. Vitecek, J., et al., *Arginine-based inhibitors of nitric oxide synthase: therapeutic potential and challenges.* Mediators Inflamm, 2012. **2012**: p. 318087.

143. Holden, J.K., et al., *Structure-Based Design of Bacterial Nitric Oxide Synthase Inhibitors.* Journal of Medicinal Chemistry, 2015. **58**(2): p. 994-1004.

144. Holden, J.K., et al., *Structural and biological studies on bacterial nitric oxide synthase inhibitors.* Proc Natl Acad Sci U S A, 2013. **110**(45): p. 18127-31.

145. Holden, J.K., et al., *Inhibitor Bound Crystal Structures of Bacterial Nitric Oxide Synthase.* Biochemistry, 2015. **54**(26): p. 4075-82.

146. Arora, K. and C.L. Brooks, 3rd, *Multiple intermediates, diverse conformations, and cooperative conformational changes underlie the catalytic hydride transfer reaction of dihydrofolate reductase.* Top Curr Chem, 2013. **337**: p. 165-87.

147. Popov, V.M., et al., *Analysis of complexes of inhibitors with Cryptosporidium hominis DHFR leads to a new trimethoprim derivative.* Bioorg Med Chem Lett, 2006. **16**(16): p. 4366-70.

148. Liu, J., et al., *The crystal structure of Candida glabrata dihydrofolate reductase drives new inhibitor design toward efficacious antifungal agents.* Chemistry & biology, 2008. **15**(9): p. 990-996.

149. Pelphrey, P.M., et al., *Highly efficient ligands for dihydrofolate reductase from Cryptosporidium hominis and Toxoplasma gondii inspired by structural analysis.* J Med Chem, 2007. **50**(5): p. 940-50.

150. Bolstad, D.B., et al., *Structure-based approach to the development of potent and selective inhibitors of dihydrofolate reductase from cryptosporidium.* J Med Chem, 2008. **51**(21): p. 6839-52.

151. Yung-Chi, C. and W.H. Prusoff, *Relationship between the inhibition constant (KI) and the concentration of inhibitor which causes 50 per cent inhibition (I50) of an enzymatic reaction.* Biochemical Pharmacology, 1973. **22**(23): p. 3099-3108.